Journal of Mathematical Imaging and Vision
https://doi.org/10.1007/s10851-017-0778-5

Fast-Marching Methods for Curvature Penalized Shortest Paths

Jean-Marie Mirebeau[1]

Received: 19 June 2017 / Accepted: 30 November 2017

Abstract
We introduce numerical schemes for computing distances and shortest paths with respect to several planar paths models, featuring curvature penalization and data-driven velocity: the Dubins car, the Euler/Mumford elastica, and a two variants of the Reeds–Shepp car. For that purpose, we design monotone and causal discretizations of the associated Hamilton–Jacobi–Bellman PDEs, posed on the three-dimensional domain $\mathbb{R}^2 \times \mathbb{S}^1$. Our discretizations involve sparse, adaptive and anisotropic stencils on a cartesian grid, built using techniques from lattice geometry. A convergence proof is provided, in the setting of discontinuous viscosity solutions. The discretized problems are solvable in a single pass using a variant of the fast-marching algorithm. Numerical experiments illustrate the applications of our schemes in motion planning and image segmentation.

Keywords Fast-marching algorithm · Reeds–Shepp car · Euler–Mumford elastica · Dubins car · Hamilton–Jacobi equation · Viscosity solution · Voronoi reduction of quadratic forms

1 Introduction

In this paper, we develop numerical schemes for computing distance maps and globally minimal paths with respect to data-driven costs depending on the local path position, orientation, and curvature. We address a variety of models including two variants of the Reeds–Shepp car [21,46], the Euler–Mumford elastica [14,23], and the Dubins car [22]. Their qualitative features differ widely: depending on the model, minimal paths may or may not be smooth, and the associated distance may or may not be continuous. For that purpose, we discretize generalized eikonal equations, also called first-order static Hamilton–Jacobi–Bellman PDEs, with a unified approach relying on a tool from lattice geometry named Voronoi's first reduction of quadratic forms, also considered in [36]. Our discretizations are monotone and causal, hence can be solved using the fast-marching algorithm/dynamic programming principle, with complexity $\mathcal{O}(N \ln N)$ where N is the number of points in the discrete domain. Numerical experiments, presented in Sect. 5 and in [32], illustrate the potential applications of our methods in motion planning control problems and medical image segmentation tasks.

In the models of interest to us, the cost of a smooth path $\mathbf{x} : [0, T] \to \mathbb{R}^2$, parametrized at unit speed, takes the form

$$\int_0^T \alpha(\mathbf{x}(s), \dot{\mathbf{x}}(s))\, \mathcal{C}(|\ddot{\mathbf{x}}(s)|)\, \mathrm{d}s. \tag{1}$$

One of the considered models, the Reeds–Shepp model *with reverse gear*, also applies to piecewise smooth paths with cusps, whose total cost is the sum of the costs of the smooth sections. Our objective is to numerically compute globally minimal paths for this energy, constrained to a subdomain, with prescribed endpoints and tangents at these endpoints, and regarding the terminal time T as a free parameter. We denoted by $\alpha : \mathbb{R}^2 \times \mathbb{S}^1 \to]0, \infty[$ a continuous cost function, depending on the path position and orientation, and usually data driven in applications. The path curvature, $|\ddot{\mathbf{x}}(s)|$ in (1), denoted by κ in (2), is penalized using a second cost function $\mathcal{C} : \mathbb{R} \to \mathbb{R}_+$, for which we consider the following three instantiations:

$$\mathcal{C}^{\mathrm{RS}}(\kappa) := \sqrt{1 + |\xi\kappa|^2},$$
$$\mathcal{C}^{\mathrm{EM}}(\kappa) := 1 + |\xi\kappa|^2, \qquad \mathcal{C}^{\mathrm{D}}(\kappa) := \begin{cases} 1 & \text{if } |\xi\kappa| \leq 1, \\ +\infty & \text{otherwise.} \end{cases} \tag{2}$$

This work was partly supported by ANR research Grant MAGA, ANR-16-CE40-0014.

✉ Jean-Marie Mirebeau
jean-marie.mirebeau@math.u-psud.fr

[1] University Paris-Sud, CNRS, University Paris-Saclay, 91405 Orsay, France

Published online: 13 December 2017

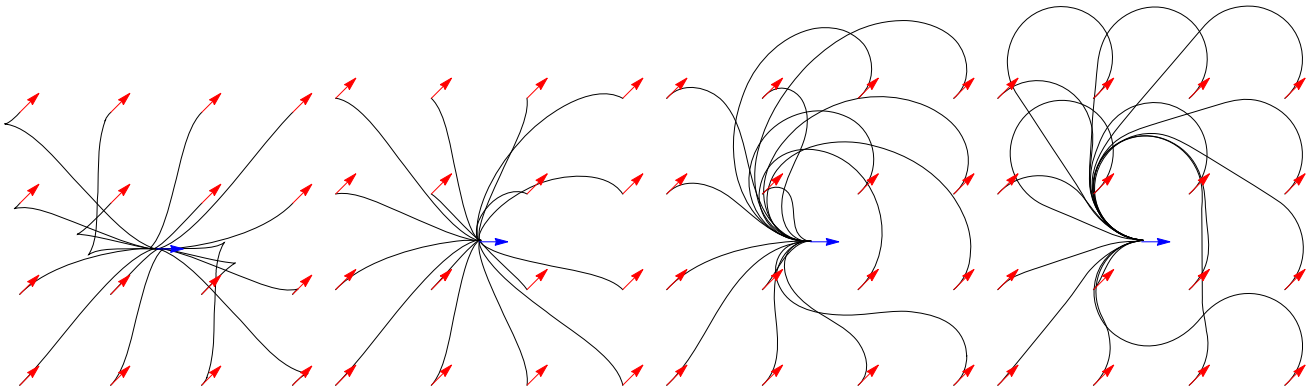

Fig. 1 Globally minimal paths for the Reeds–Shepp reversible model ($\xi = 0.3$), Reeds–Shepp forward model ($\xi = 0.3$), Euler–Mumford elastica model ($\xi = 0.2$), and Dubins model ($\xi = 0.2$), with uniform cost $\alpha \equiv 1$. Seed point $(1/2, 1/2, 0) \in \mathbb{R}^2 \times \mathbb{S}^1$, tip points $(k/3, l/3, \pi/4)$, $k, l \in \{0, \cdots, 3\}$. (Results obtained using our numerical schemes, see Sect. 2, with relaxation parameter $\varepsilon = 0.1$, and angular resolution $2\pi/60$)

The costs $\mathcal{C}^{\mathrm{RS}}$, $\mathcal{C}^{\mathrm{EM}}$ and $\mathcal{C}^{\mathrm{D}}$ correspond, respectively, to the Reeds–Shepp car, the Euler–Mumford elastica, and the Dubins car models. The parameter $\xi > 0$ has the dimension of a length and should be interpreted as a typical radius of curvature. Our approach easily extends to models where $\xi : \mathbb{R}^2 \times \mathbb{S}^1 \to]0, \infty[$ is a continuous and positive function of the path position and orientation, similarly to the cost α. The Reeds–Shepp car (with or without reverse gear), the Euler–Mumford elastica and the Dubins car are classical path models involving increasingly strong penalizations of curvature. Their qualitative properties are strikingly distinct, as illustrated in Fig. 1 and discussed below.

- The Reeds–Shepp cost $\mathcal{C}^{\mathrm{RS}}(\kappa) = \sqrt{1 + |\xi\kappa|^2}$ is used to model slow vehicles, typically wheelchairs. Following [21], we consider two models based on this cost, referred to as the *Reeds–Shepp reversible* (RS±, as originally considered in [46]) and *Reeds–Shepp forward* (RS+) models, and where the vehicle, respectively, may, or may not, shift into reverse gear. Minimal paths for the reversible and forward models distinguish themselves by the presence of *cusps* and of *in-place rotations* of the path orientation, respectively, see Fig. 1. The latter happen at the path endpoints and sometimes at the corners of obstacles, and are admissible since the curvature cost $\mathcal{C}^{\mathrm{RS}}(\kappa)$ only grows linearly asymptotically as $\kappa \to \infty$. See [21] for a discussion and the description of a semi-lagrangian PDE discretization of the Reeds–Shepp models, which is different from the one considered in this paper.[1]
  The special case $\alpha \equiv 1$ of a constant cost has been extensively studied by analytic means. In particular, an optimal synthesis of minimal paths is presented in [48] for the Reeds–Shepp reversible model. In addition, [7,20] study in detail the endpoint configurations for which the minimal path for the Reeds–Shepp reversible model is *cuspless* (such paths are smooth, and are also minimal for the Reeds–Shepp forward model).
- The Euler–Mumford cost $\mathcal{C}^{\mathrm{EM}} = 1 + |\xi\kappa|^2$ has the physical interpretation of the bending energy of an elastic bar [23], when the data-driven cost is identically constant $\alpha \equiv 1$ and the terminal time T is fixed. The relevance of this model for image processing and segmentation was first outlined in [39]. Contrary to earlier works of the author [13,16], the PDE discretization introduced in this paper for this model obeys a causality property which makes the fast-marching algorithm applicable.
- The Dubins cost $\mathcal{C}^{\mathrm{D}}$ penalizes euclidean path length only, unless curvature exceeds the threshold ξ^{-1}, in which case the path is rejected, see (2). Minimal (relaxed) paths for this cost are known, when $\alpha \equiv 1$, to be concatenations of straight lines and of circular segments of radius ξ. This description is used in [3] to design exact polynomial time solvers for the minimal Dubins path problem, in the presence of smooth obstacles. In contrast, our PDE approach is approximate by nature, but it can accommodate non-constant costs α, and can easily be extended to variants of the model involving, e.g., position dependent bounds on the radius of curvature or additional state variables.

In the rest of Introduction, we present the classical mathematical theory underlying the addressed problems, fixing in the process important notation for the rest of the paper, and provide additional motivation for our work. More precisely, we show in Sect. 1.1 how the second-order planar path models of interest (1) can be cast as a first-order path

[1] The Reeds–Shepp models are in this paper mostly discussed for comparison with the Euler–Mumford and Dubins models, since our numerical results in the Reeds–Shepp case are actually quite similar to [21], despite the distinct discretization.

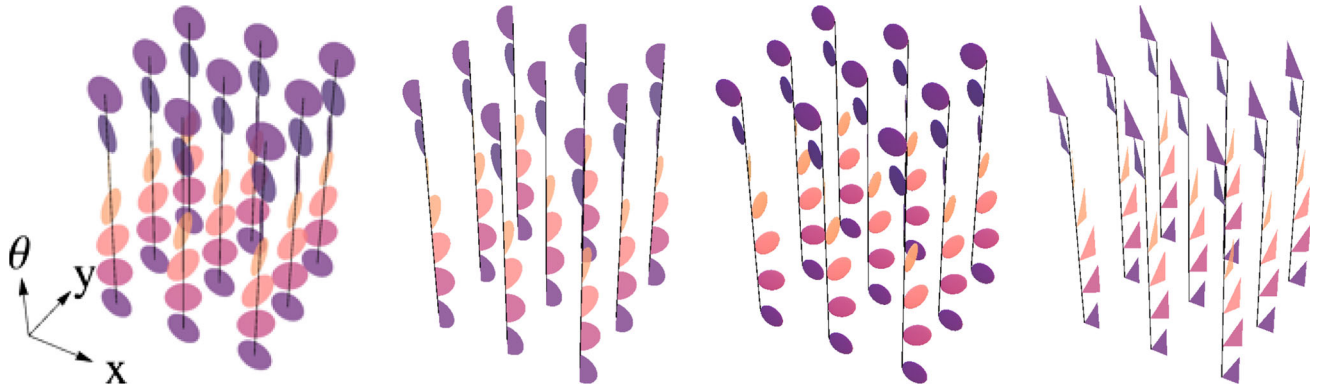

Fig. 2 Control sets of the Reeds–Shepp reversible, Reeds–Shepp forward, Euler–Mumford and Dubins models, see (4). All have empty interior, reflecting the non-holonomy of the models

model in a three-dimensional domain equipped with a singular metric. We then discuss in Sect. 1.2 the exit time optimal control problem and the corresponding static Hamilton–Jacobi–Bellman (HJB) Partial Differential Equation (PDE). We describe in Sect. 1.3 some potential applications, in the field of medical image processing, of the numerical methods developed in this paper. We finally present in Sect. 1.4 the paper outline and list of contributions.

1.1 Dimension Lifting in An Orientation Domain

Our implementation of curvature penalization requires to lift paths into the configuration space $\mathbb{M} := \mathbb{R}^2 \times \mathbb{S}^1$ of positions and orientations. Other strategies have been proposed in the literature, see Remark 1.1. We use the identification $\mathbb{S}^1 \cong \mathbb{R}/(2\pi\mathbb{Z})$ of the unit circle with a periodic interval, and denote points of the configuration space by $\mathbf{p} = (\mathbf{x}, \theta) \in \mathbb{M}$. The tangent space to $\mathbb{M}$ is independent of the base point and denoted $\mathbb{E} := \mathbb{R}^2 \times \mathbb{R}$. Vectors are denoted $\dot{\mathbf{p}} = (\dot{\mathbf{x}}, \dot{\theta}) \in \mathbb{E}$, and co-vectors $\hat{\mathbf{p}} = (\hat{\mathbf{x}}, \hat{\theta}) \in \mathbb{E}^*$. The unit vector of orientation $\theta \in \mathbb{S}^1$ is denoted $\mathbf{n}(\theta) := (\cos\theta, \sin\theta)$.

A (local) metric on $\mathbb{M}$ is a function $\mathcal{F} : \mathbb{M} \times \mathbb{E} \to [0, \infty]$, which is convex and 1-homogeneous in its second argument. Three metrics $\mathcal{F} = \mathcal{F}^{\mathrm{RS}+}, \mathcal{F}^{\mathrm{EM}}, \mathcal{F}^{\mathrm{D}}$ are defined by homogenization of the cost functions $\mathcal{C} = \mathcal{C}^{\mathrm{RS}}, \mathcal{C}^{\mathrm{EM}}, \mathcal{C}^{\mathrm{D}}$ as follows: for all $\mathbf{p} = (\mathbf{x}, \theta) \in \mathbb{M}$ and all $\dot{\mathbf{p}} = (\dot{\mathbf{x}}, \dot{\theta}) \in \mathbb{E}$

$$\mathcal{F}_{\mathbf{p}}(\dot{\mathbf{p}}) := \begin{cases} \|\dot{\mathbf{x}}\| \, \mathcal{C}(|\dot{\theta}|/\|\dot{\mathbf{x}}\|) & \text{if } \dot{\mathbf{x}} = \|\dot{\mathbf{x}}\|\mathbf{n}(\theta), \\ +\infty & \text{otherwise,} \end{cases} \tag{3}$$

with the additional convention that $\mathcal{F}_{\mathbf{p}}(0) = 0$, and that $\mathcal{F}_{\mathbf{p}}((0, \dot{\theta})) = \lim_{\lambda \downarrow 0} \lambda \, \mathcal{C}(|\dot{\theta}|/\lambda)$. A fourth metric $\mathcal{F}^{\mathrm{RS}\pm}$, corresponding to the Reeds–Shepp model *with* reverse gear, is defined like $\mathcal{F}^{\mathrm{RS}+}$ up to the constraint which is replaced with the unsigned collinearity requirement $\dot{\mathbf{x}} = \langle \dot{\mathbf{x}}, \mathbf{n}(\theta) \rangle \mathbf{n}(\theta)$. We prove in Appendix B that (3) does indeed define a convex lower semi-continuous function w.r.t. $\dot{\mathbf{p}}$, as this is not entirely obvious from the definition. The "unit balls" in each tangent space w.r.t. the local metric are referred to as the *control sets*. Their graphical representation, see Fig. 2, provides important geometric intuition and is called Tissot's indicatrix. The control sets are denoted $\mathcal{B}(\mathbf{p}) \subseteq \mathbb{E}$, and defined for all $\mathbf{p} \in \overline{\Omega}$ by

$$\mathcal{B}(\mathbf{p}) := \{\dot{\mathbf{p}} \in \mathbb{E};\ \mathcal{F}_{\mathbf{p}}(\dot{\mathbf{p}}) \leq 1\}. \tag{4}$$

The length of a Lispchitz path $\gamma : [0, 1] \to \mathbb{R}^2 \times \mathbb{S}^1$, w.r.t. a metric $\mathcal{F}$, is defined as

$$\mathrm{length}_{\mathcal{F}}(\gamma) := \int_0^1 \alpha(\gamma(t)) \, \mathcal{F}_{\gamma(t)}(\dot{\gamma}(t)) \, \mathrm{d}t, \quad \text{where} \quad \dot{\gamma}(t) := \frac{\mathrm{d}}{\mathrm{d}t}\gamma(t), \tag{5}$$

and where $\alpha : \mathbb{M} \to]0, \infty[$ is a continuous cost function, previously mentioned and fixed throughout this paper. A *bounded* domain $\Omega \subseteq \mathbb{M}$ is also fixed throughout the paper, and to each (local) metric $\mathcal{F}$ is associated a quasi-distance $d_{\mathcal{F}}$ defined for all $\mathbf{p}, \mathbf{q} \in \overline{\Omega}$ by

$$d_{\mathcal{F}}(\mathbf{p}, \mathbf{q}) := \inf\{\mathrm{length}_{\mathcal{F}}(\gamma);\ \gamma \in \mathrm{Lip}([0, 1], \overline{\Omega}), \ \gamma(0) = \mathbf{p},\ \gamma(1) = \mathbf{q}\}. \tag{6}$$

Note that one may have $d_{\mathcal{F}}(\mathbf{p}, \mathbf{q}) \neq d_{\mathcal{F}}(\mathbf{q}, \mathbf{p})$ (lack of symmetry), or $d_{\mathcal{F}}(\mathbf{p}, \mathbf{q}) = \infty$ (lack or global controllability), or $\lim_{\mathbf{q} \to \mathbf{p}} d_{\mathcal{F}}(\mathbf{p}, \mathbf{q}) \neq 0$ (lack of local controllability). For the metrics $\mathcal{F}^{\mathrm{RS}+}, \mathcal{F}^{\mathrm{RS}\pm}, \mathcal{F}^{\mathrm{EM}}$ and $\mathcal{F}^{\mathrm{D}}$ considered in this paper, the infimum (6) is attained whenever $d_{\mathcal{F}}(\mathbf{p}, \mathbf{q}) < \infty$, see Appendix A of [13] or Appendix A of [21].

Remark 1.1 (Alternative approaches to curvature penalized minimal paths) To the knowledge of the author, two alternative methods have been proposed to compute curvature penalized minimal paths via dynamic programming. Paths are approximated in [53] with collections of non-superposable

short splines, each determined by three or four control points with integer coordinates, and the cost assigned to a path is the sum of the costs of the spline approximants. No convergence analysis is presented, and the numerical results do not address the models considered in this paper. The author remains doubtful that this method is appropriate for models whose minimal paths feature singularities such as cusps (Reeds–Shepp reversible) or in-place rotations (Reeds–Shepp forward), or are subject to a hard constraint on the radius of curvature (Dubins).

Another approach [30] consists in using the original fast-marching scheme designed for euclidean distance computations [54], but with the following addition: each time a point is added to the propagated front, a local backtracking is performed to estimate the curvature of the geodesic reaching this point, and the front propagation cost is locally adjusted as a result. The method uses a two-dimensional value map $u : \mathbb{R}^2 \to \mathbb{R}$, instead of the three-dimensional one $u : \mathbb{R}^2 \times \mathbb{S}^1 \to \mathbb{R}$ used in this paper, hence the physical projections of the paths extracted with this method *never* cross each other. This contradicts the observed behavior, see Fig. 1, and hence this approach *cannot* compute all curvature penalized minimal paths.

1.2 The Eikonal PDE Formalism

The objective of this paper is to numerically solve the following optimal control problem: find the shortest path from the domain boundary $\partial\Omega$ to any point in Ω. The value function $u : \overline{\Omega} \to [0, \infty]$ for this problem reads for all $\mathbf{q} \in \overline{\Omega}$

$$u(\mathbf{q}) := \inf_{\mathbf{p}\in\partial\Omega} d_{\mathcal{F}}(\mathbf{p}, \mathbf{q}). \tag{7}$$

A useful and natural generalization of this problem is to introduce a penalty $\sigma : \partial\Omega \to]-\infty, \infty]$ depending on the path origin $\mathbf{p}$, but for simplicity we stick to simplest instance (7) from a theoretical standpoint.

The function u associated with the Reeds–Shepp *reversible* metric is continuous; indeed, this model is sub-Riemannian, hence locally controllable by Chow's theorem [37]. In contrast, the function u can be discontinuous along $\partial\Omega$ for non-locally controllable models, such as the Reeds–Shepp *forward*, Euler-Elastica and Dubins models. In fact, u may even be discontinuous in the interior of Ω, in the Dubins case, as well as in the Reeds–Shepp case for some domain shapes, see Proposition 3.3. The level sets of u are illustrated in Fig. 3.

Despite its potential discontinuities, the function $u : \overline{\Omega} \to \mathbb{R}$ is a (discontinuous) viscosity solution to a generalized eikonal equation:

$$\forall \mathbf{p} \in \Omega,\ \mathcal{H}_{\mathbf{p}}(\mathrm{d}u(\mathbf{p})) = \frac{1}{2}\alpha(\mathbf{p})^2, \quad \forall \mathbf{p} \in \partial\Omega,\ u(\mathbf{p}) = 0. \tag{8}$$

See [2] and Sect. 3.2 for details, including the appropriate relaxation of the boundary conditions. The above PDE involves the Hamiltonian $\mathcal{H} : \mathbb{M} \times \mathbb{E}^* \to [0, \infty[$ of the model, which is defined as the Legendre–Fenchel conjugate of the Lagrangian $\mathcal{L} : \mathbb{M} \times \mathbb{E} \to [0, \infty]$. For any point $\mathbf{p} \in \mathbb{M}$ and any co-vector $\hat{\mathbf{p}} \in \mathbb{E}^*$

$$\mathcal{H}_{\mathbf{p}}(\hat{\mathbf{p}}) := \sup_{\dot{\mathbf{p}}\in\mathbb{E}} \langle \hat{\mathbf{p}}, \dot{\mathbf{p}} \rangle - \mathcal{L}_{\mathbf{p}}(\dot{\mathbf{p}}), \quad \text{where } \mathcal{L}_{\mathbf{p}}(\dot{\mathbf{p}}) := \frac{1}{2}\mathcal{F}_{\mathbf{p}}(\dot{\mathbf{p}})^2. \tag{9}$$

Another equivalent expression involves the control sets (4): for any point $\mathbf{p} \in \overline{\Omega}$, and any co-vector $\hat{\mathbf{p}} \in \mathbb{E}^*$

$$\mathcal{H}_{\mathbf{p}}(\hat{\mathbf{p}}) = \frac{1}{2} \sup\{\langle \hat{\mathbf{p}}, \dot{\mathbf{p}} \rangle_+^2;\ \dot{\mathbf{p}} \in \mathcal{B}(\mathbf{p})\}. \tag{10}$$

The explicit expressions of the Hamiltonians $\mathcal{H}^{\mathrm{RS}\pm}$, $\mathcal{H}^{\mathrm{RS}+}$, $\mathcal{H}^{\mathrm{EM}}$ and $\mathcal{H}^{\mathrm{D}}$ associated with the models of interest are provided in Sect. 2, where we also provide monotone and causal discretizations of the Hamilton–Jacobi–Bellman PDE (8). Once the solution u to (8) is computed, minimal paths from $\partial\Omega$ to any given $\mathbf{q} \in \Omega$ are extracted as solutions to the following ODE (solved backwards in time). For all $t \in [0, T]$

$$\dot{\gamma}(t) = \mathrm{d}\mathcal{H}_{\gamma(t)}\left(\mathrm{d}u(\gamma(t))\right), \tag{11}$$

with the terminal condition $\gamma(T) = \mathbf{q}$, where we denoted $T := u(\mathbf{q})$. The Hamiltonian $\mathcal{H}$ is differentiated w.r.t. the second variable $\hat{\mathbf{p}}$ in the ODE (11), see, e.g., Appendix B of [21].

1.3 Applications to Image Processing

Minimal path methods are a major tool in image processing [43]. One of our general objectives is to provide fast, accurate and proven numerical schemes, able to extract minimal paths w.r.t. new models, that can be used to enhance these methods. However, the present paper is primarily focused on the algorithmic aspects of minimal path computation, similarly to [33,34,36], and our experiments in Sect. 5 thus only involve synthetic data. Applications to real data will be published elsewhere in collaboration with experts in the field, as they previously were [15,16,21,49]. Nevertheless, and at the request of a reviewer, we briefly discuss three medical image processing tasks for which the algorithms introduced in this paper are relevant.

The *segmentation of tubular structures*, in two- and three-dimensional (medical) image data, is a common and

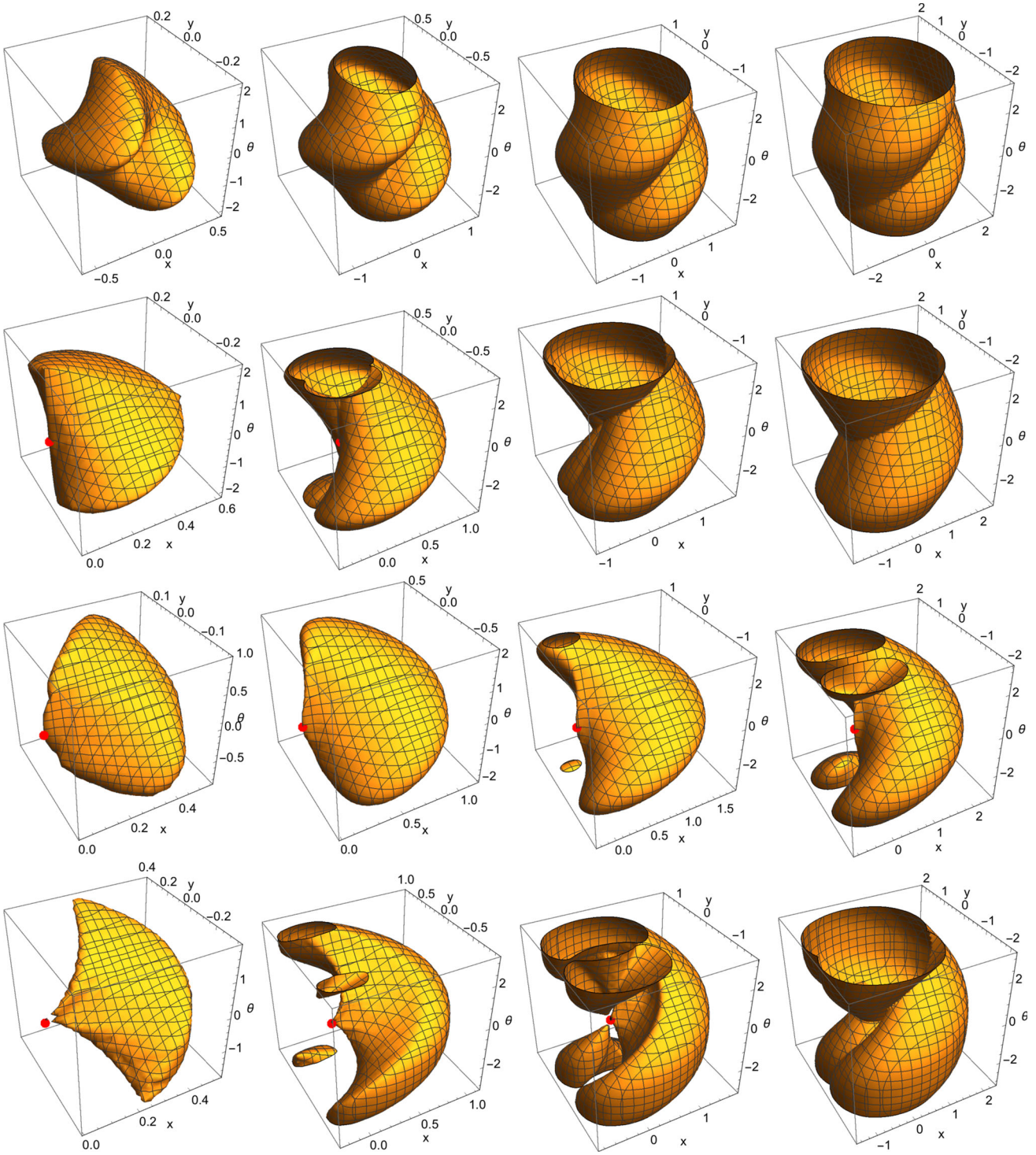

Fig. 3 Level sets, $\xi = 0.14$, at time 0.3, 0.6, 0.9, 1.2. Origin shown as red point (Color figure online)

challenging task. Kass et al [29] suggested to extract these features as paths minimizing an energy, referred to as the snake model, featuring in particular a second-order term, *akin to a curvature penalization*. Unfortunately, numerical implementations of this method often gets stuck in local minima of the non-convex snake energy, which makes it sensitive to the image noise and the path initialization. In order to address these robustness issues, Cohen et al [12] considered a simpler energy model, locally proportional to Euclidean path length, and for which *global minimization* is achievable using

the standard fast-marching algorithm [47,54]. This second method faces difficulties in two-dimensional images displaying overlays of vessels, such as retinal background images, or three-dimensional images featuring almost crossing tubular structures. For this reason, *dimension lifting techniques* have been introduced, based on computations within an extended domain featuring an abstract extra coordinate, accounting for, e.g., the extracted vessel local radius [31] or orientation [42]. The objective of the present paper, and of the works [6] and [16,21,49] (involving the author), is to combine the strengths of these different approaches: we extract tubular structures using curvature penalized paths, globally minimizing an energy, and obtained via computation in the orientation lifted domain $\mathbb{R}^d \times \mathbb{S}^{d-1}$. See the numerical experiments in Sect. 5.3.

Tractography and white matter fiber segmentation in diffusion-weighted MRI The extraction of brain connectivity maps also has motivated the development of a variety of minimal path models and algorithms. The individual white matter fibers are not visible in MRI scans, in contrast to the tubular structure segmentation tasks considered above, but a macroscopic fiber Orientation Distribution Function (ODF) is computed from the signal. The ODF can be summarized in a diffusion tensor, which interestingly is a meaningful quantity from the geometrical viewpoint, giving rise to a natural adjunct Riemannian metric [24]. A variety of numerical approaches have been developed to extract global brain connectivity measures from the local fiber ODF. Ordinary differential equations, sometimes enhanced with probabilisitic models [52], are commonly used for fiber tracking. Minimal path methods have also been used, sometimes with ad-hoc modifications. For instance, the classical fast-marching algorithm [47,54] is often augmented with a local backtracking used to dynamically adjust the front propagation speed depending on local direction [44] or curvature [18,30] of the shortest paths. A drawback of these heuristical enhancements is that the obtained "distance map" is not the viscosity solution to a proper eikonal equation, which limits its reliability, see also Remark 1.1 (second point). This motivates the introduction in [27] of a semi-Lagrangian fast-marching method based on a 26-points stencil, and able to compute genuine shortest paths w.r.t. (mildly) anisotropic Riemannian metrics.[2] Curvature penalized minimal paths, such as those considered in this paper, are also applicable to fiber tractography, see for instance the (synthetic) numerical examples in [21].

Object segmentation in two-dimensional images, for instance organ delineation in medical data, can be addressed by extracting the object boundary as a path minimizing an energy, similarly to tubular structure segmentation [12,29]. A specificity of this application is that objects contours are naturally oriented, e.g., counter-clockwise; hence they may be extracted as minimal paths w.r.t. a non-symmetric Finsler function designed to favor paths having the object at their right and the background at their left, see [56]. (See also [38] for more discussion on Finsler active contours.) In a similar spirit, [15] relies on the divergence theorem and an asymmetric Finsler metric, to globally minimize the Chan-Vese region segmentation energy [19]. Finally, curvature penalized shortest paths, such as those considered in this paper, are also applicable to object segmentation, see [14].

1.4 Contributions and Outline

In Sect. 2, we introduce new discretizations of the generalized eikonal PDEs (8) associated with the four models of interest. For that purpose, we use an original reformulation of the Euler–Mumford Hamiltonian, and a construction based on lattice geometry. Our numerical schemes are monotone and causal, enabling the use of the single pass fast-marching algorithm. Their stencils, carefully designed, are sparse, anisotropic, and have a reasonably small radius.

Section 3 is devoted to the convergence analysis. We prove in Sect. 3.1 that the discretized PDEs admit uniformly bounded solutions. We establish in Sect. 3.2 the convergence of the discrete solutions upper and lower continuous envelopes toward sub- and super-solutions of (8). We discuss in Sect. 3.3, the continuity properties of the value function u (7), which are related to the pointwise convergence of the discrete solutions toward u, depending on the model and on the domain geometry.

Section 4 is devoted to the proof of a key ingredient of our PDE discretization schemes, namely Proposition 2.2 below. It is based on tools from lattice geometry known as Voronoi's first reduction of quadratic forms, obtuse superbases, and Selling's algorithm.

Numerical experiments presented in Sect. 5 illustrate the potential of our approach in motion planning and image segmentation tasks. We also compare, for validation, our minimal geodesics with those obtained using a shooting method based on Hamilton's ODE of geodesics.

2 Discretization

In this section, we construct finite differences discretizations of the HJB PDEs (8) associated with the different models of interest in this paper. For that purpose, we derive the explicit expression of the relevant Hamiltonian and construct an approximation of a specific form. The Reeds–Shepp, Euler–Mumford, and Dubins models are, respectively, addressed in Sects. 2.1, 2.2 and 2.3.

[2] This specific discretization requires the metric tensors condition number to remain below $(\sqrt{3}+1)/2$, see [33] for an explanation of this bound and an unconditional method.

Our numerical schemes obey two fundamental properties, referred to as *monotony* and *causality*, which are recalled in the next definition, see [41,47], respectively. Monotony implies comparison principles, which are used in the convergence analysis Sect. 3. Causality allows to solve the discretized PDE in a single pass using dynamic programming, a generalization of Dijkstra's algorithm and the fast-marching method, which guarantees short computation times.

Definition 2.1 A (finite differences) scheme on a finite set X is a continuous map $\mathfrak{F} : X \times \mathbb{R} \times \mathbb{R}^X \to \mathbb{R}$. The scheme is said:

- Monotone, iff $\mathfrak{F}$ is non-decreasing w.r.t. the second and (each of the) third variables.
- Causal, iff $\mathfrak{F}$ only depends on the positive part of the third variable.

To the scheme is associated a function $\mathbb{R}^X \to \mathbb{R}^X$ still (abusively) denoted by $\mathfrak{F}$, and defined by

$$(\mathfrak{F}U)(\mathbf{x}) := \mathfrak{F}(\mathbf{x}, U(\mathbf{x}), (U(\mathbf{x}) - U(\mathbf{y}))_{\mathbf{y}\in X}), \tag{12}$$

for all $\mathbf{x} \in X$ and all $U \in \mathbb{R}^X$.

Let us fix a grid scale $h > 0$ of the form $2\pi/k$ for some positive integer k, and introduce the grid $\mathbb{M}_h \subseteq \mathbb{M} := \mathbb{R}^2 \times \mathbb{S}^1$, the finite discrete domain Ω_h, and the (formal) discrete boundary $\partial\Omega_h$ defined by

$$\begin{aligned} &\mathbb{M}_h := h\mathbb{Z}^2 \times (h\mathbb{Z}/2\pi\mathbb{Z}), \qquad &&\Omega_h := \Omega \cap \mathbb{M}_h, \\ &\partial\Omega_h := \mathbb{M}_h \setminus \Omega_h. \end{aligned} \tag{13}$$

Our discretizations of the HJB PDE (8) are presented as follows

$$\forall \mathbf{p} \in \Omega_h,\ HU(\mathbf{p}) = \frac{1}{2}\alpha(\mathbf{p})^2, \qquad \forall \mathbf{p} \in \partial\Omega_h,\ U(\mathbf{p}) = 0, \tag{14}$$

For their design, we first construct an approximation of the local hamiltonian of the model of interest, $\mathcal{H}_\mathbf{p} : \mathbb{E}^* \to [0, \infty[$ where $\mathbf{p} \in \overline{\Omega}$, under the following form

$$\mathcal{H}_\mathbf{p}(\hat{\mathbf{p}}) \approx \max_{i\in I} \left(\sum_{j\in J} \alpha_{ij} \langle \hat{\mathbf{p}}, \dot{\mathbf{e}}_{ij} \rangle_+^2 + \sum_{k\in K} \beta_{ik} \langle \hat{\mathbf{p}}, \dot{\mathbf{f}}_{ik} \rangle^2 \right), \tag{15}$$

where I, J and K are arbitrary finite sets. Here and in the rest of this paper, we denote by $a_+ := \max\{a, 0\}$ and $a_- := \max\{-a, 0\}$ the positive an negative parts of a scalar $a \in \mathbb{R}$. The chosen weights are always nonnegative: $\alpha_{ij}, \beta_{ik} \geq 0$, and the offsets are integral: $\mathbf{e}_{ij}, \mathbf{f}_{ik} \in \mathbb{Z}^3$. They depend on the base point $\mathbf{p}$, in our case on the angular coordinate $\theta \in \mathbb{S}^1$ of $\mathbf{p} = (\mathbf{x}, \theta) \in \mathbb{M}$ only. The PDE (8) is discretized using upwind finite differences, forward or symmetric

$$\begin{aligned} HU(\mathbf{p}) = h^{-2} \max_{i\in I} \Bigg(&\sum_{j\in J} \alpha_{ij} \max\{0,\ U(\mathbf{p}) - U(\mathbf{p} - h\dot{\mathbf{e}}_{ij})\}^2 \\ &+ \sum_{k\in K} \beta_{ik} \max\{0,\ U(\mathbf{p}) - U(\mathbf{p} - h\dot{\mathbf{f}}_{ik}), \\ &U(\mathbf{p}) - U(\mathbf{p} + h\dot{\mathbf{f}}_{ik})\}^2 \Bigg). \end{aligned}$$

The pattern of offsets $\{\dot{\mathbf{e}}_{ij}, \dot{\mathbf{f}}_{ik}, -\dot{\mathbf{f}}_{ik};\ i \in I, j \in J, k \in K\}$ is referred to as the *stencil* of the numerical scheme. Our PDE discretizations rely on point dependent, sparse and strongly anisotropic stencils, with reasonable radius, see Fig. 4. They are designed using the following result, whose proof presented in Sect. 4 relies on Voronoi's first reduction, a tool from discrete geometry characterizing the interaction of a positive quadratic form with an additive lattice [50]. Similar techniques are used for anisotropic diffusion PDEs in [26], for Monge-Ampere equations in [35], and for eikonal PDEs associated with Riemannian, sub-Riemannian and Rander metrics in [36].

More precisely, the next proposition shows how the (squared) positive part of a linear form $\hat{\mathbf{p}} \mapsto \langle \hat{\mathbf{p}}, \dot{\mathbf{n}} \rangle_+$ can be approximated using positive parts of linear forms $\hat{\mathbf{p}} \mapsto \langle \hat{\mathbf{p}}, \dot{\mathbf{e}} \rangle_+$ associated with few, small, *integral* vectors $\dot{\mathbf{e}} \in \mathbb{Z}^d$. This result allows in our numerical schemes to approximate the directional derivative $\langle \mathrm{d}u(\mathbf{p}), \dot{\mathbf{n}} \rangle_+$ at a point $\mathbf{p} \in \mathbb{M}$ using finite differences of the form $\frac{1}{h}(u(\mathbf{p}) - u(\mathbf{p} - h\dot{\mathbf{e}}))_+$, where $h > 0$ is the discretization grid scale.

Proposition 2.2 *Let $d \in \{2, 3\}$, let $\dot{\mathbf{n}} \in \mathbb{R}^d$, and let $\varepsilon \in]0, 1]$. Then, there exists nonnegative weights $\rho^\varepsilon_{\dot{\mathbf{e}}}(\dot{\mathbf{n}})$, $\dot{\mathbf{e}} \in \mathbb{Z}^d$, such that for all $\hat{\mathbf{p}} \in \mathbb{R}^d$*

$$\langle \hat{\mathbf{p}}, \dot{\mathbf{n}} \rangle_+^2 \leq \sum_{\dot{\mathbf{e}}\in\mathbb{Z}^d} \rho^\varepsilon_{\dot{\mathbf{e}}}(\dot{\mathbf{n}}) \langle \hat{\mathbf{p}}, \dot{\mathbf{e}} \rangle_+^2 \leq \langle \hat{\mathbf{p}}, \dot{\mathbf{n}} \rangle_+^2 + \varepsilon^2 \|\dot{\mathbf{n}}\|^2 \|\hat{\mathbf{p}}\|^2.$$

Furthermore, the support $\{\dot{\mathbf{e}} \in \mathbb{Z}^d;\ \rho^\varepsilon_{\dot{\mathbf{e}}}(\dot{\mathbf{n}}) > 0\}$ has at most 3 elements in dimension $d = 2$ (resp. 6 elements in dimension $d = 3$), and is contained in a ball of radius $C_{\mathrm{WS}}/\varepsilon$, where C_{WS} is an absolute constant. In addition $\sum_{\dot{\mathbf{e}}\in\mathbb{Z}^d} \rho^\varepsilon_{\dot{\mathbf{e}}}(\dot{\mathbf{n}}) \|\dot{\mathbf{e}}\|^2 = \|\dot{\mathbf{n}}\|^2(1 + (d-1)\varepsilon^2)$.

In practice, we usually choose the relaxation parameter $\varepsilon = 1/10$ and obtain a support which is 5 or 6 pixels wide, see Fig. 4. Our numerical method thus belongs to the category of *Wide-Stencil* schemes (hence the subscript to the constant C_{WS}).

2.1 The Reeds–Shepp Car Models

This section is focused on the discretization of the Reeds–Shepp *forward* model, postponing the discussion of the *reversible* model to Remark 2.7. The metric $\mathcal{F}^{\mathrm{RS}+}$ of the Reeds–Shepp forward model is obtained by inserting the curvature cost expression $\mathcal{C}^{\mathrm{RS}}(\kappa) := \sqrt{1+(\xi\kappa)^2}$ in the generic expression (3). Thus, for all $\mathbf{p} = (\mathbf{x}, \theta) \in \mathbb{M}$ and all $\dot{\mathbf{p}} = (\dot{\mathbf{x}}, \dot{\theta}) \in \mathbb{E}$

$$\mathcal{F}^{\mathrm{RS}+}_{\mathbf{p}}(\dot{\mathbf{p}}) = \sqrt{\|\dot{\mathbf{x}}\|^2 + |\xi\dot{\theta}|^2} \quad \text{if } \dot{\mathbf{x}} = \|\dot{\mathbf{x}}\|\mathbf{n}(\theta), \tag{16}$$

and $\mathcal{F}^{\mathrm{RS}+}_{\mathbf{p}}(\dot{\mathbf{p}}) = +\infty$ otherwise. The control set $\mathcal{B}^{\mathrm{RS}+}(\mathbf{p})$ is defined as the unit ball of the metric $\mathcal{F}^{\mathrm{RS}+}_{\mathbf{p}}$, for any $\mathbf{p} = (\mathbf{x}, \theta) \in \mathbb{M}$, see (4). Hence, it is an half ellipse, or a half disk if $\xi = 1$, as illustrated in Fig. 2.

$$\mathcal{B}^{\mathrm{RS}+}(\mathbf{p}) = \{(\dot{\mathbf{x}}, \dot{\theta}) \in \mathbb{E};\ \|\dot{\mathbf{x}}\|^2 + |\xi\dot{\theta}|^2 \leq 1,\ \dot{\mathbf{x}} = \|\dot{\mathbf{x}}\|\mathbf{n}(\theta)\}.$$

The Lagrangian of the Reeds–Shepp model is defined as the half square of the metric (16). Hence, denoting by $\mathrm{P}_{\mathbf{n}}(\dot{\mathbf{x}}) := \dot{\mathbf{x}} - \langle \mathbf{n}, \dot{\mathbf{x}}\rangle \mathbf{n}$ the component of a vector $\dot{\mathbf{x}}$ orthogonal to a direction $\mathbf{n}$, one has

$$\begin{aligned} 2\mathcal{L}^{\mathrm{RS}+}_{\mathbf{p}}(\dot{\mathbf{p}}) = (&\langle \mathbf{n}(\theta), \dot{\mathbf{x}}\rangle_+^2 + \infty \langle \mathbf{n}(\theta), \dot{\mathbf{x}}\rangle_-^2) \\ &+ \infty \| \mathrm{P}_{\mathbf{n}(\theta)}(\dot{\mathbf{x}})\|^2 + |\xi\dot{\theta}|^2, \end{aligned}$$

where, slightly abusively, we use infinite coefficients with the convention $0 \times \infty = 0$. The Hamiltonian, also presented in [21], reads for all $\mathbf{p} = (\mathbf{x}, \theta) \in \overline{\Omega}$, and all $\hat{\mathbf{p}} = (\hat{\mathbf{x}}, \hat{\theta}) \in \mathbb{E}^*$

$$2\mathcal{H}^{\mathrm{RS}+}_{\mathbf{p}}(\hat{\mathbf{p}}) = \langle \hat{\mathbf{x}}, \mathbf{n}(\theta)\rangle_+^2 + |\hat{\theta}/\xi|^2. \tag{17}$$

This expression follows from the piecewise quadratic and separable structure of the Lagrangian, and from two basic lemmas on the Legendre–Fenchel dual f^* of a function f, which are recalled below without proof.

Lemma 2.3 (Legendre–Fenchel dual of a separable sum) *Let $(\mathbf{e}_1, \ldots, \mathbf{e}_d)$ be an orthogonal basis of $\mathbb{R}^d$, and let $f_1, \ldots, f_d : \mathbb{R} \to]-\infty, \infty]$ be proper, convex and lower semi-continuous. Then,*

$$\begin{aligned} &\forall \mathbf{x} \in \mathbb{R}^d,\ f(\mathbf{x}) := \sum_{1 \leq i \leq d} f_i(\langle \mathbf{e}_i, \mathbf{x}\rangle) \\ &\quad \Rightarrow \forall \mathbf{x} \in \mathbb{R}^d,\ f^*(\mathbf{x}) = \sum_{1 \leq i \leq d} f_i^*(\langle \mathbf{e}_i, \mathbf{x}\rangle). \end{aligned}$$

Lemma 2.4 (Legendre–Fenchel dual of a quadratic function) *Let $a, b \in [0, \infty]$. Then,*

$$\begin{aligned} &\forall x \in \mathbb{R},\ f(x) = \frac{1}{2}(a^2 x_-^2 + b^2 x_+^2) \\ &\quad \Rightarrow \forall x \in \mathbb{R},\ f^*(x) = \frac{1}{2}(a^{-2} x_-^2 + b^{-2} x_+^2). \end{aligned}$$

We propose the following discretization scheme $H^{\mathrm{RS}+}_{\varepsilon,h}$ for the Hamiltonian $\mathcal{H}^{\mathrm{RS}+}$, which depends on a relaxation parameter $\varepsilon \in]0, 1]$ and on the grid scale h. Proposition 2.2 is instantiated in dimension two to provide the weights $\rho^{\varepsilon}_{\dot{\mathbf{e}}}(\mathbf{n}(\theta))$. The offsets appearing in this expression are illustrated in Fig. 4. For any discrete map $U : \mathbb{M}_h \to \mathbb{R}$ and any $\mathbf{p} = (\mathbf{x}, \theta) \in \Omega_h$

$$\begin{aligned} &2H^{\mathrm{RS}+}_{\varepsilon,h}U(\mathbf{p}) \\ &\quad := h^{-2} \sum_{\dot{\mathbf{e}} \in \mathbb{Z}^2} \rho^{\varepsilon}_{\dot{\mathbf{e}}}(\mathbf{n}(\theta)) \max\{0,\ U(\mathbf{x}, \theta) - U(\mathbf{x} - h\dot{\mathbf{e}}, \theta)\}^2 \\ &\qquad + (\xi h)^{-2} \max\{0,\ U(\mathbf{x}, \theta) - U(\mathbf{x}, \theta - h),\ U(\mathbf{x}, \theta) \\ &\qquad - U(\mathbf{x}, \theta + h)\}^2. \end{aligned} \tag{18}$$

Proposition 2.5 *The discretization scheme $H^{RS+}_{\varepsilon,h}$ is monotone and causal, for any $\varepsilon \in]0, 1]$ and any $h > 0$. It is supported on 6 points at most, at distance at most $C_{\mathrm{WS}}h/\varepsilon$ from $\mathbf{p}$. Furthermore, if U coincides with a linear function on these points, then*

$$\begin{aligned} &\mathcal{H}^{RS+}_{\mathbf{p}}(\mathrm{d}U(\mathbf{p})) \leq H^{RS+}_{\varepsilon,h}U(\mathbf{p}) \\ &\leq \mathcal{H}^{RS+}_{\mathbf{p}}(\mathrm{d}U(\mathbf{p})) + \frac{\varepsilon^2}{2}\|\mathrm{d}U(\mathbf{p})\|^2. \end{aligned}$$

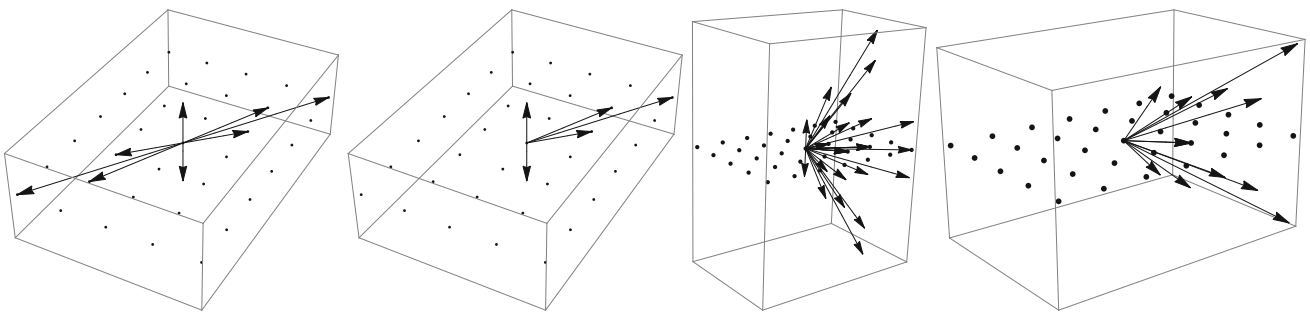

Fig. 4 Discretization stencils used for the Reeds–Shepp reversible, Reeds–Shepp forward, Euler–Mumford, and Dubins models. Note the sparseness and anisotropy of the stencils. Model parameters: $\theta = \pi/3$, $\xi = 0.2$. Discretization parameters: $\varepsilon = 0.1$, and for Euler–Mumford $K = 5$

Proof The monotony and causality properties are clearly satisfied, see also Proposition 3.6 for a general class of schemes which obey these properties. The support cardinality and radius estimates follow from Proposition 2.2. If U is locally linear around $\mathbf{p} = (\mathbf{x}, \theta) \in \mathbb{M}_h$, then denoting $\mathrm{d}U(\mathbf{p}) = (\hat{\mathbf{x}}, \hat{\theta})$ and observing that $U(\mathbf{x}, \theta) - U(\mathbf{x} - h\dot{\mathbf{e}}, \theta) = \langle \hat{\mathbf{x}}, \dot{\mathbf{e}} \rangle$ and $U(\mathbf{x}, \theta) - U(\mathbf{x}, \theta - h) = \hat{\theta} h$, one obtains

$$H^{\mathrm{RS}+}_{\varepsilon,h} U(\mathbf{p}) = \sum_{\dot{\mathbf{e}} \in \mathbb{Z}^2} \rho^{\varepsilon}_{\dot{\mathbf{e}}}(\mathbf{n}(\theta)) \langle \hat{\mathbf{x}}, \dot{\mathbf{e}} \rangle^2_+ + \xi^{-2} \max\{0, \hat{\theta}, -\hat{\theta}\}^2,$$

and the announced estimate follows by (17) and Proposition 2.2. □

Proposition 2.5 easily extends to three-dimensional Reeds–Shepp forward model, posed on $\mathbb{R}^3 \times \mathbb{S}^2$. We refer to [21] for more discussion on this extension and numerical experiments,[3] and we focus our attention on two-dimensional path models in this paper. Nevertheless, we describe our three-dimensional discretization strategy in the following lines, since it is only briefly evoked in [21]. For that purpose, the two-dimensional unit sphere is parametrized as $\mathbf{n}(\theta, \varphi) := (\cos\theta, \sin\theta\cos\varphi, \sin\theta\sin\varphi)$, where $(\theta, \varphi) \in \mathbb{A}_2 := [0, \pi] \times [0, 2\pi]$ are similar to the Euler angles. The Reeds–Shepp forward metric reads in this context:

$$\widetilde{\mathcal{F}}^{\mathrm{RS}+}_{\mathbf{p}}(\dot{\mathbf{p}}) := \sqrt{\|\dot{\mathbf{x}}\|^2 + |\xi\dot{\theta}|^2 + |\dot{\varphi}\xi\sin\theta|^2} \text{ if } \dot{\mathbf{x}} = \|\dot{\mathbf{x}}\|\mathbf{n}(\theta, \varphi)$$

and $\widetilde{\mathcal{F}}^{\mathrm{RS}+}_{\mathbf{p}}(\dot{\mathbf{p}}) = +\infty$ otherwise, for all $\mathbf{p} = (\mathbf{x}, \theta, \varphi) \in \mathbb{R}^3 \times \mathbb{A}_2$ and all $\dot{\mathbf{p}} = (\dot{\mathbf{x}}, \dot{\theta}, \dot{\varphi}) \in \mathbb{R}^3 \times \mathbb{R}^2$. Using, as above, the separable and piecewise quadratic structure of the Lagrangian, we obtain

$$2\widetilde{\mathcal{H}}^{\mathrm{RS}+}_{\mathbf{p}}(\hat{\mathbf{p}}) = \langle \hat{\mathbf{x}}, \mathbf{n}(\theta, \varphi) \rangle^2_+ + |\hat{\theta}/\xi|^2 + |\hat{\varphi}/(\xi\sin\theta)|^2$$

for all $\hat{\mathbf{p}} = (\hat{\mathbf{x}}, \hat{\theta}, \hat{\varphi}) \in (\mathbb{R}^3)^* \times (\mathbb{R}^2)^*$. The rectangle $\mathbb{A}_2$ is equipped with the adequate boundary conditions $(\theta, 0) \sim (\theta, 2\pi)$, $(0, \varphi) \sim (0, \psi)$, $(\pi, \varphi) \sim (\pi, \psi)$, for all $\theta \in [0, \pi]$, $\varphi, \psi \in [0, 2\pi]$, and discretized using a cartesian grid of scale $h = \pi/k$ for some positive integer k. Proposition 2.2 is instantiated in dimension three to provide the weights $\rho^{\varepsilon}_{\dot{\mathbf{e}}}(\mathbf{n}(\theta, \varphi))$.

$$\begin{aligned} 2\widetilde{H}^{\mathrm{RS}+}_{\varepsilon,h} U(\mathbf{p}) &:= h^{-2} \sum_{\dot{\mathbf{e}} \in \mathbb{Z}^3} \rho^{\varepsilon}_{\dot{\mathbf{e}}}(\mathbf{n}(\theta, \varphi)) \max\{0, U(\mathbf{p}) - U(\mathbf{x} - h\dot{\mathbf{e}}, \theta, \varphi)\}^2 \\ &\quad + (\xi h)^{-2} \max\{0,\ U(\mathbf{p}) - U(\mathbf{x}, \theta - h, \varphi),\ U(\mathbf{p}) \\ &\quad - U(\mathbf{x}, \theta + h, \varphi)\}^2 \\ &\quad + (\xi h \sin\theta)^{-2} \max\{0,\ U(\mathbf{p}) - U(\mathbf{x}, \theta, \varphi - h),\ U(\mathbf{p}) \\ &\quad - U(\mathbf{x}, \theta, \varphi + h)\}^2. \end{aligned}$$

Proposition 2.6 *The discretization scheme $\widetilde{H}^{RS+}_{\varepsilon,h}$ is monotone and causal, for any $\varepsilon \in]0, 1]$, $h > 0$. It is supported on 11 points at most, at distance at most $C_{\mathrm{WS}} h/\varepsilon$ from $\mathbf{p}$. Furthermore, if U coincides with a linear function on these points, then*

$$\widetilde{\mathcal{H}}^{RS+}_{\mathbf{p}}(\mathrm{d}U(\mathbf{p})) \le \widetilde{H}^{RS+}_{\varepsilon,h} U(\mathbf{p}) \le \widetilde{\mathcal{H}}^{RS+}_{\mathbf{p}}(\mathrm{d}U(\mathbf{p})) + \frac{\varepsilon^2}{2}\|\mathrm{d}U(\mathbf{p})\|^2.$$

We do not state the proofs Proposition of 2.6 and of the following remark, since they are entirely similar to that of Proposition 2.5.

Remark 2.7 (The reversible Reeds–Shepp model) The metric of the Reeds–Shepp *reversible* model has the same expression as (16), except for the modified constraint: $\dot{\mathbf{x}} = \langle \mathbf{n}(\theta), \dot{\mathbf{x}} \rangle \mathbf{n}(\theta)$. As a result, the Lagrangian and Hamiltonian read, with the same conventions as above

$$\begin{aligned} 2\mathcal{L}^{\mathrm{RS}\pm}_{\mathbf{p}}(\dot{\mathbf{p}}) &= \langle \mathbf{n}(\theta), \dot{\mathbf{x}} \rangle^2 + \infty \| \mathrm{P}_{\mathbf{n}(\theta)}(\dot{\mathbf{x}}) \|^2 + |\xi\dot{\theta}|^2, \\ 2\mathcal{H}^{\mathrm{RS}\pm}_{\mathbf{p}}(\hat{\mathbf{p}}) &= \langle \hat{\mathbf{x}}, \mathbf{n}(\theta) \rangle^2 + |\hat{\theta}/\xi|^2. \end{aligned}$$

The discretization scheme (18) can be adapted by appropriately modifying its first line:

$$\begin{aligned} 2H^{\mathrm{RS}\pm}_{\varepsilon,h} U(\mathbf{p}) &:= h^{-2} \sum_{\dot{\mathbf{e}} \in \mathbb{Z}^2} \rho^{\varepsilon}_{\dot{\mathbf{e}}}(\mathbf{n}(\theta)) \max\{0, U(\mathbf{x}, \theta) \\ &\quad - U(\mathbf{x} - h\dot{\mathbf{e}}, \theta), U(\mathbf{x}, \theta) - U(\mathbf{x} + h\dot{\mathbf{e}}, \theta)\}^2 + \cdots. \end{aligned}$$

This scheme supported on 9 points, and for a linear U on these points one has the identity

$$H^{\mathrm{RS}\pm}_{\varepsilon,h} U(\mathbf{p}) = \mathcal{H}^{\mathrm{RS}\pm}_{\mathbf{p}}(\mathrm{d}U(\mathbf{p})) + \frac{\varepsilon^2}{2}\|\mathrm{d}U(\mathbf{p})\|^2.$$

A similar remark applies to the three-dimensional Reeds–Shepp reversible model.

2.2 The Euler–Mumford Elastica Model

The metric $\mathcal{F}^{\mathrm{EM}}$ of the Euler–Mumford elastica model is obtained by inserting the curvature cost $\mathcal{C}^{\mathrm{EM}}(\kappa) := 1 + (\xi\kappa)^2$ in the generic expression (3). Thus for all $\mathbf{p} = (\mathbf{x}, \theta) \in \mathbb{M}$ and all $\dot{\mathbf{p}} = (\dot{\mathbf{x}}, \dot{\theta}) \in \mathbb{E}$

$$\mathcal{F}^{\mathrm{EM}}_{\mathbf{p}}(\dot{\mathbf{p}}) = \|\dot{\mathbf{x}}\| + \frac{|\xi\dot{\theta}|^2}{\|\dot{\mathbf{x}}\|} \quad \text{if } \dot{\mathbf{x}} = \|\dot{\mathbf{x}}\|\mathbf{n}(\theta),$$

[3] Using a semi-lagrangian discretization for three-dimensional the Reeds–Shepp reversible model, and the present discretization for the three-dimensional forward model.

and $\mathcal{F}_{\mathbf{p}}^{\mathrm{EM}}(\dot{\mathbf{p}}) = +\infty$ otherwise. Observing that

$$\|\dot{\mathbf{x}}\| + \frac{|\xi\dot{\theta}|^2}{\|\dot{\mathbf{x}}\|} \leq 1 \Leftrightarrow \|\dot{\mathbf{x}}\|^2 + |\xi\dot{\theta}|^2 \leq \|\dot{\mathbf{x}}\|$$
$$\Leftrightarrow (\|\dot{\mathbf{x}}\| - 1/2)^2 + |\xi\dot{\theta}|^2 \leq 1/4$$

we obtain that the control sets $\mathcal{B}^{\mathrm{EM}}$ are ellipses, or disks if $\xi = 1$. Note, however, that the origin 0 of the tangent space $\mathbb{E}$ is not in their center but on their boundary, see Fig. 2.

$$\mathcal{B}^{\mathrm{EM}}(\mathbf{p}) = \{(\dot{\mathbf{x}}, \dot{\theta}) \in \mathbb{E};\ (\|\dot{\mathbf{x}}\| - 1/2)^2 + |\xi\dot{\theta}|^2 \leq 1/4,\ \dot{\mathbf{x}} = \|\dot{\mathbf{x}}\|\mathbf{n}(\theta)\},$$
$$= \left\{ \frac{1}{2}\left((a+1)\mathbf{n}(\theta), b/\xi\right);\ a, b \in \mathbb{R},\ a^2 + b^2 \leq 1 \right\}.$$

Lemma 2.8 *The Euler–Mumford elastica Hamiltonian reads, for all* $\mathbf{p} = (\mathbf{x}, \theta) \in \mathbb{M}$ *and all* $\hat{\mathbf{p}} = (\hat{\mathbf{x}}, \hat{\theta}) \in \mathbb{E}^*$

$$2\mathcal{H}_{\mathbf{p}}^{EM}(\hat{\mathbf{p}}) := \frac{1}{4}\left(\langle \hat{\mathbf{x}}, \mathbf{n}(\theta)\rangle + \sqrt{\langle \hat{\mathbf{x}}, \mathbf{n}(\theta)\rangle^2 + |\hat{\theta}/\xi|^2} \right)^2. \tag{19}$$

Proof The announced result follows from (10) and from the computation

$$2 \sup_{\dot{\mathbf{p}} \in \mathcal{B}^{\mathrm{EM}}(\mathbf{p})} \langle \hat{\mathbf{p}}, \dot{\mathbf{p}}\rangle = \langle \hat{\mathbf{x}}, \mathbf{n}(\theta)\rangle + \sup_{a^2+b^2 \leq 1} a\langle \hat{\mathbf{x}}, \mathbf{n}(\theta)\rangle + b\hat{\theta}/\xi$$
$$= \langle \hat{\mathbf{x}}, \mathbf{n}(\theta)\rangle + \sqrt{\langle \hat{\mathbf{x}}, \mathbf{n}(\theta)\rangle + |\hat{\theta}/\xi|^2}.$$

□

The expression (19) suggests to regard the Euler/Mumford model as a degenerate case of Rander geometry [45]. This approach is considered numerically in [14]. Unfortunately, existing numerical schemes for eikonal equations involving Rander metrics are either limited to two dimensions [34], or lack causality [36] and thus cannot be solved using the fast-marching algorithm, which significantly impacts the numerical cost and the flexibility of their implementations. In this paper, we advocate for a different approach, based on a second expression of the Hamiltonian $\mathcal{H}^{\mathrm{EM}}$, in integral form, which to our knowledge is original.

Proposition 2.9 *For any point* $\mathbf{p} = (\mathbf{x}, \theta) \in \mathbb{M}$ *and any covector* $\hat{\mathbf{p}} \in \mathbb{E}^*$*, one has*

$$2\mathcal{H}_{\mathbf{p}}^{EM}(\hat{\mathbf{p}}) = \frac{3}{4}\int_{-\pi/2}^{\pi/2} \langle \hat{\mathbf{p}},\ (\mathbf{n}(\theta)\cos\varphi,\ \xi^{-1}\sin\varphi)\rangle_+^2\ \cos(\varphi)\,\mathrm{d}\varphi.$$

Proof The first step of the proof, left as an exercise to the reader, is to show that

$$\int_{-\pi/2}^{\pi/2} (\cos(\varphi - \psi))_+^2 \cos\varphi\,\mathrm{d}\varphi = \frac{1}{3}(1 + \cos\psi)^2, \tag{20}$$

for any $\psi \in \mathbb{R}$. The second step is the claim that for any $\dot{\mathbf{e}}_0, \dot{\mathbf{e}}_1 \in \mathbb{E}$ one has

$$\int_{-\pi/2}^{\pi/2} \langle \hat{\mathbf{p}}, \cos(\varphi)\dot{\mathbf{e}}_0 + \sin(\varphi)\dot{\mathbf{e}}_1\rangle_+^2 \cos\varphi\,\mathrm{d}\varphi$$
$$= \frac{1}{3}\left(\sqrt{\langle \hat{\mathbf{p}}, \dot{\mathbf{e}}_0\rangle^2 + \langle \hat{\mathbf{p}}, \dot{\mathbf{e}}_1\rangle^2} + \langle \hat{\mathbf{p}}, \dot{\mathbf{e}}_0\rangle \right)^2. \tag{21}$$

Indeed, if $\langle \hat{\mathbf{p}}, \dot{\mathbf{e}}_0\rangle = \langle \hat{\mathbf{p}}, \dot{\mathbf{e}}_1\rangle = 0$, then there is nothing to prove. Otherwise, up to rescaling $\hat{\mathbf{p}}$, we may assume that $\langle \hat{\mathbf{p}}, \dot{\mathbf{e}}_0\rangle^2 + \langle \hat{\mathbf{p}}, \dot{\mathbf{e}}_1\rangle^2 = 1$, thus $\langle \hat{\mathbf{p}}, \dot{\mathbf{e}}_0\rangle = \cos\psi$ and $\langle \hat{\mathbf{p}}, \dot{\mathbf{e}}_1\rangle = \sin\psi$ for some $\psi \in \mathbb{R}$. Therefore, $\langle \hat{\mathbf{p}}, \cos(\varphi)\dot{\mathbf{e}}_0 + \sin(\varphi)\dot{\mathbf{e}}_1\rangle = \cos\varphi\cos\psi + \sin\varphi\sin\psi = \cos(\varphi - \psi)$ for any $\varphi \in \mathbb{R}$, hence (21) follows from (20). Choosing $\mathbf{e}_0 := (\mathbf{n}(\theta), 0)$ and $\mathbf{e}_1 := (0_{\mathbb{R}^2}, \xi^{-1})$, we conclude the proof. □

In order to discretize the Euler–Mumford Hamiltonian, we consider a second-order consistent quadrature rule on the interval $[-\pi/2, \pi/2]$ with cosine weight. Quadrature rules on the interval $[-1, 1]$ for the uniform cost, such as the Clenshaw-Curtis or Fejer rules [25], are for instance easily adapted to our needs thanks to the identity

$$\int_{-1}^{1} f(t)\,\mathrm{d}t = \int_{-\pi/2}^{\pi/2} f(\sin\varphi)\cos\varphi\,\mathrm{d}\varphi.$$

More precisely, let K be a positive integer, and let $(\alpha_k, \varphi_k) \in (\mathbb{R}_+ \times [-\pi/2, \pi/2])^K$ be such that for any twice continuously differentiable $f : [-\pi/2, \pi/2] \to \mathbb{R}$

$$\left| \sum_{1 \leq k \leq K} \alpha_k f(\varphi_k) - \int_{-\pi/2}^{\pi/2} f(\varphi)\cos(\varphi)\,\mathrm{d}\varphi \right|$$
$$\leq \frac{C}{K^2} \sup\left\{ |f''(t)|;\ t \in [-\pi/2, \pi/2] \right\}, \tag{22}$$

where C is independent of f and K. Note that choosing $f \equiv 1$ on $[-\pi/2, \pi/2]$, one obtains

$$\sum_{1 \leq k \leq K} \alpha_k = \int_{-\pi/2}^{\pi/2} \cos\varphi\,\mathrm{d}\varphi = 2. \tag{23}$$

We propose the following discretization of the Euler–Mumford Hamiltonian

$$2H_{\varepsilon,K,h}^{\mathrm{EM}} U(\mathbf{p}) := \frac{3}{4}h^{-2} \sum_{0 \leq k \leq K} \alpha_k \sum_{\dot{\mathbf{e}} \in \mathbb{Z}^3} \rho_{\dot{\mathbf{e}}}^{\varepsilon}(\mathbf{n}(\theta)\cos\varphi_k,\ \xi^{-1}\sin\varphi_k)$$
$$\max\{0,\ U(\mathbf{p}) - U(\mathbf{p} - h\dot{\mathbf{e}})\}^2.$$

It is based on the three-dimensional instantiation of Proposition 2.2, applied to the vectors $(\mathbf{n}(\theta)\cos\varphi_k,\ \xi^{-1}\sin\varphi_k)$, $0 \leq k \leq K$ with the relaxation parameter $\varepsilon \in]0, 1]$.

Proposition 2.10 *The discretization scheme $H^{EM}_{\varepsilon,K,h}$ is monotone and causal, for any $\varepsilon \in]0,1]$, $K \geq 1$, $h > 0$. It is supported on at most $6K+1$ points, at distance at most $C_{\mathrm{WS}} h/\varepsilon$ from $\mathbf{p}$. Furthermore, if U coincides with a linear function on these points, then*

$$\begin{aligned}\mathcal{H}^{EM}_{\mathbf{p}}(\mathrm{d}U(\mathbf{p})) - CK^{-2}\|\mathrm{d}U(\mathbf{p})\|^2 \leq H^{EM}_{\varepsilon,K,h}U(\mathbf{p})\\ \leq \mathcal{H}^{EM}_{\mathbf{p}}(\mathrm{d}U(\mathbf{p})) + C(\varepsilon^2 + K^{-2})\|\mathrm{d}U(\mathbf{p})\|^2,\end{aligned}$$

with $C = C_0 \max\{1, \xi^{-2}\}$ for some absolute constant C_0.

Proof Monotony, causality, and the stencil cardinality and radius estimates can be proved similarly to Proposition 2.5. Let $\mathbf{p} = (\mathbf{x}, \theta) \in \Omega$ be fixed, and let $\hat{\mathbf{p}} = \mathrm{d}U(\mathbf{p})$. Let $\dot{\mathbf{v}}(\varphi) := (\mathbf{n}(\theta)\cos\varphi,\ \xi^{-1}\sin\varphi)$ for all $\varphi \in [-\pi/2, \pi/2]$. Using Proposition 2.2 and observing that $\|\dot{\mathbf{v}}(\varphi)\| \leq \max\{1, \xi^{-1}\}$, one obtains

$$\begin{aligned}0 \leq \frac{8}{3}H^{\mathrm{EM}}_{\varepsilon,h}U(\mathbf{p}) - \sum_{1\leq k\leq K}\alpha_k\langle\hat{\mathbf{p}}, \dot{\mathbf{v}}(\varphi_k)\rangle_+^2\\ \leq \sum_{1\leq k\leq K}\alpha_k\varepsilon^2\max\{1,\xi^{-2}\}\|\hat{\mathbf{p}}\|^2,\end{aligned}$$

where we used the nonnegativity of the weights $(\alpha_k)_{k=0}^K$. Therefore using (23)

$$\begin{aligned}-C_1\|\hat{\mathbf{p}}\|^2K^{-2} \leq \frac{8}{3}H^{\mathrm{EM}}_{\varepsilon,h}U(\mathbf{p}) - \int_{-\pi/2}^{\pi/2}\langle\hat{\mathbf{p}}, \dot{\mathbf{v}}(\varphi)\rangle_+^2\sin\varphi\,\mathrm{d}\varphi\\ \leq C_1\|\hat{\mathbf{p}}\|^2K^{-2} + C_2\varepsilon^2\|\hat{\mathbf{p}}\|^2, \qquad (24)\end{aligned}$$

where $C_2 = 2\max\{1,\xi^{-2}\}$, and where we applied (22) to the function $\varphi \mapsto \langle\hat{\mathbf{p}}, \dot{\mathbf{v}}(\varphi)\rangle_+^2$, whose second derivative makes sense as an L^∞ function and is bounded by $C_1\|\hat{\mathbf{p}}\|^2$. Here, $C_1 = C_1(\xi)$ denotes the absolute constant of (22) times an upper bound for the partial second derivative $\partial^2/\partial\varphi^2$ of the trigonometric polynomial

$$\begin{aligned}\langle\hat{\mathbf{q}}, \dot{\mathbf{v}}(\varphi)\rangle^2 &= \langle\hat{\mathbf{q}}, (\mathbf{n}(\theta)\cos\varphi,\ \xi^{-1}\sin\varphi)\rangle^2\\ &= a(\hat{\mathbf{q}},\theta,\xi)\cos(2\varphi) + b(\hat{\mathbf{q}},\theta,\xi)\sin(2\varphi), \qquad (25)\end{aligned}$$

uniformly w.r.t. all $\theta \in \mathbb{S}^1$ and all $\hat{\mathbf{q}} \in \mathbb{E}^*$ such that $\|\hat{\mathbf{q}}\| = 1$. Note that the coefficients a and b, hence also C_1, are $\mathcal{O}(\xi^{-2})$. The positive part appearing in the expression $\langle\hat{\mathbf{p}}, \dot{\mathbf{v}}(\varphi)\rangle_+^2$ of (24) and not in (25) is not an issue, thanks to a minor technical argument presented in Lemma 2.11 below. The announced result follows from (24) and Proposition 2.9. □

Lemma 2.11 *Let $f \in C^2(\mathbb{R},\mathbb{R})$, and let $g(x) := f(x)_+^2$ for all $x \in \mathbb{R}$. Then, $g'' \in L^\infty_{\mathrm{loc}}(\mathbb{R})$, $g''(x) = \frac{\mathrm{d}^2}{\mathrm{d}x^2}(f(x)^2)$ if $f(x) > 0$, and $g''(x) = 0$ for almost every x such that $f(x) = 0$.*

Proof Clearly, g is locally Lipschitz, with derivative $g'(x) = 2f'(x)f(x)_+$. This expression shows that g' is continuous and also locally Lipschitz, and hence g is almost everywhere twice differentiable, with the announced expression. This concludes the proof. □

2.3 The Dubins Car Model

The metric of $\mathcal{F}^{\mathrm{D}}$ of the Dubins car model is obtained by inserting the cost function $\mathcal{C}^{\mathrm{D}}(\kappa) := 1$ if $|\xi\kappa| \leq 1$, $\mathcal{C}^{\mathrm{D}}(\kappa) = +\infty$ otherwise, in the generic expression (3). Hence, for all $\mathbf{p} = (\mathbf{x},\theta) \in \mathbb{M}$ and all $\dot{\mathbf{p}} = (\dot{\mathbf{x}}, \dot{\theta}) \in \mathbb{E}$

$$\mathcal{F}_{\mathbf{p}}(\dot{\mathbf{p}}) = \|\dot{\mathbf{x}}\| \quad \text{if } \dot{\mathbf{x}} = \|\dot{\mathbf{x}}\|\mathbf{n}(\theta) \text{ and } |\xi\dot{\theta}| \leq \|\dot{\mathbf{x}}\|, \qquad (26)$$

and $\mathcal{F}_{\mathbf{p}}(\dot{\mathbf{p}}) = +\infty$ otherwise. The control set $\mathcal{B}^{\mathrm{D}}(\mathbf{p})$ is an isosceles triangle, or a half square if $\xi = 1$, whose apex is the origin of $\mathbb{E}$.

$$\begin{aligned}\mathcal{B}^{\mathrm{D}}(\mathbf{p}) &= \{(\dot{\mathbf{x}},\dot{\theta}) \in \mathbb{E};\ \xi|\dot{\theta}| \leq \|\dot{\mathbf{x}}\| \leq 1,\ \dot{\mathbf{x}} = \|\dot{\mathbf{x}}\|\mathbf{n}(\theta)\}\\ &= \{(a\mathbf{n}(\theta), b\xi^{-1});\ 0 \leq |b| \leq a \leq 1\}.\end{aligned}$$

The Dubins Hamiltonian is the square of a piecewise linear function.

Lemma 2.12 *For all $\mathbf{p} = (\mathbf{x},\theta) \in \mathbb{M}$ and all $\hat{\mathbf{p}} = (\hat{\mathbf{x}},\hat{\theta}) \in \mathbb{E}^*$, one has*

$$\begin{aligned}2\mathcal{H}^D_{\mathbf{p}}(\hat{\mathbf{p}}) &= \max\{0,\ \langle\hat{\mathbf{p}}, (\mathbf{n}(\theta), \xi^{-1})\rangle,\ \langle\hat{\mathbf{p}}, (\mathbf{n}(\theta), -\xi^{-1})\rangle\}^2\\ &= (\langle\hat{\mathbf{x}}, \mathbf{n}(\theta)\rangle + \xi^{-1}|\hat{\theta}|)_+^2\end{aligned}$$

Proof The result follows from the expression (10) of the Hamiltonian, and from the observation that the linear function $\langle\hat{\mathbf{p}}, \cdot\rangle$ always attains its maximum at an extreme point of the convex set $\mathcal{B}^{\mathrm{D}}(\mathbf{p})$, hence at one the three vertices 0, $(\mathbf{n}(\theta), \xi^{-1})$ and $(\mathbf{n}(\theta), -\xi^{-1})$ of this triangle. □

We propose the following discretization scheme $H^{\mathrm{D}}_{\varepsilon,h}$, with gridscale $h > 0$ and relaxation parameter $\varepsilon \in]0,1]$. It relies on the three-dimensional instantiation of Proposition 2.2 applied to the two vectors $(\mathbf{n}(\theta), \pm\xi^{-1})$. For any $U : \mathbb{M}_h \to \mathbb{R}$ and any $\mathbf{p} = (\mathbf{x},\theta) \in \Omega_h$, define $H^{\mathrm{D}}_{\varepsilon,h}U(\mathbf{p}) :=$

$$\begin{aligned}h^{-2}\max\Big\{\sum_{\dot{\mathbf{e}}\in\mathbb{Z}^3}\rho^\varepsilon_{\dot{\mathbf{e}}}(\mathbf{n}(\theta),\xi^{-1})(U(\mathbf{p}) - U(\mathbf{p}-h\dot{\mathbf{e}}))_+^2,\\ \sum_{\dot{\mathbf{e}}\in\mathbb{Z}^3}\rho^\varepsilon_{\dot{\mathbf{e}}}(\mathbf{n}(\theta),-\xi^{-1})(U(\mathbf{p}) - U(\mathbf{p}-h\dot{\mathbf{e}}))_+^2\Big\}.\end{aligned}$$

Proposition 2.13 *The discretization scheme $H^D_{\varepsilon,h}U(\mathbf{p})$ is monotone and causal. It is supported on 13 points at most, within distance $C_{\mathrm{WS}}h/\varepsilon$ from $\mathbf{p}$. Furthermore, if U coincides*

with a linear function on these points, then

$$\mathcal{H}^D_{\mathbf{p}}(\mathrm{d}U(\mathbf{p})) \leq H^D_{\varepsilon,h}(\mathbf{p}) \leq \mathcal{H}^D_{\mathbf{p}}(\mathrm{d}U(\mathbf{p})) + \frac{\varepsilon^2}{2}\|\mathrm{d}U(\mathbf{p})\|^2.$$

The proof, entirely similar to Proposition 2.5, is left to the reader.

3 Convergence Analysis

This section is devoted to the convergence analysis of the discretization schemes introduced in Sect. 2, and applied to the optimal control problem (7). We prove in Theorems 3.1 and 3.2 that the resulting discrete systems of equations are solvable using the fast-marching algorithm, and that the upper and lower continuous envelopes of the discrete solutions converge to sub- and super-solutions to the HJB PDE, as the grid scale h and relaxation parameter ε tend to 0 suitably. We also establish in Proposition 3.3 some continuity properties of the value function to our optimal control problem (7), which are related to the pointwise convergence of the discrete solutions.

For that purpose, following the notations of [2], we introduce a close relative $\hat{u} : \overline{\Omega} \to \mathbb{R}$ to the value function u defined by (7). For any $\mathbf{q} \in \overline{\Omega}$, denoting by $\mathcal{F}$ the metric of the model

$$\hat{u}(\mathbf{q}) := \inf_{\mathbf{p}\in\mathbb{R}^2\setminus\overline{\Omega}} d_{\mathcal{F}}(\mathbf{p},\mathbf{q}). \tag{27}$$

We denote by $B(\mathbf{p},r) \subseteq \mathbb{M}$ the Euclidean unit ball of center $\mathbf{p} \in \mathbb{M}$ and radius $r > 0$. The discretization grid Ω, $\partial\Omega_h$, is defined in (13).

Theorem 3.1 *Let $\Omega \subseteq \mathbb{M}$ be an open and bounded domain, and let $\alpha : \mathbb{M} \to]0,\infty[$ have Lipschitz regularity. Then, for any $h > 0$ and $\varepsilon \in]0,1]$ the system*

$$\forall \mathbf{p} \in \Omega_h,\ H^{RS+}_{\varepsilon,h}U(\mathbf{p}) = \frac{1}{2}\alpha(\mathbf{p})^2, \quad \forall \mathbf{p} \in \partial\Omega_h,\ U(\mathbf{p}) = 0, \tag{28}$$

admits a unique solution denoted $U_{\varepsilon,h} : \mathbb{M}_h \to \mathbb{R}$. This solution can be computed using the fast-marching algorithm with complexity $\mathcal{O}(N_h \ln N_h)$, where $N_h := \#(\Omega_h)$.

Let $U_n := U_{\varepsilon_n,h_n}$, where $\varepsilon_n \to 0$ and $h_n/\varepsilon_n \to 0$ as $n \to \infty$. Define for all $\mathbf{p} \in \overline{\Omega}$

$$\underline{u}(\mathbf{p}) := \lim_{r\to 0} \liminf_{n\to\infty} \inf_{\mathbb{M}_h\cap B(\mathbf{p},r)} U_n,$$
$$\overline{u}(\mathbf{p}) := \lim_{r\to 0} \limsup_{n\to\infty} \sup_{\mathbb{M}_h\cap B(\mathbf{p},r)} U_n.$$

Then, $u \leq \underline{u} \leq \overline{u} \leq \hat{u}$ on $\overline{\Omega}$.

The first part of this result, on the discretized systems, is established in Sect. 3.1. The second part, on the comparison with u and $\hat{u}$, which are, respectively, the smallest super-solution and the largest sub-solution to the HJB PDE (8), is addressed in Sect. 3.2. These results are of course not limited to the Reeds–Shepp forward model.

Theorem 3.2 *Theorem 3.1 applies to the Reeds–Shepp reversible, the Euler–Mumford elastica, and the Dubins models as well. Obviously, the discretization schemes are $H^{RS\pm}_{\varepsilon,h}$, $H^{EM}_{\varepsilon,K,h}$ and $H^{D}_{\varepsilon,h}$, and the metrics are $\mathcal{F}^{RS\pm}$, $\mathcal{F}^{EM}$ and $\mathcal{F}^{D}$ in problem (7), respectively. In the Euler–Mumford case, the additional discretization parameter K must be taken into account as follows: the fast-marching complexity is $\mathcal{O}(K N_h \ln N_h)$, and convergence holds for $U_n = U_{\varepsilon_n,K_n,h_n}$ provided $\varepsilon_n \to 0$, $h_n/\varepsilon_n \to 0$ and $K_n \to \infty$ as $n \to \infty$.*

The convergence result presented in Theorem 3.1 is incomplete until one proves that $u = \hat{u}$ on a large subset of the domain $\overline{\Omega}$. Our knowledge on this topic is gathered in the following proposition, proved in Sect. 3.3. As a side product, this result establishes some continuity properties of the value function to the optimal control problem (7), which are interesting from a qualitative point of view. The interior of a set A is denoted by $\mathrm{int}(A)$.

Proposition 3.3 *Under the assumptions of Theorem 3.1, and in addition $\mathrm{int}(\overline{\Omega}) = \Omega$. The value functions $u, \hat{u} : \overline{\Omega} \to \mathbb{R}$ are equal in the following cases:*

- *(Reeds–Shepp reversible model) $u = \hat{u}$ on $\overline{\Omega}$.*
- *(Reeds–Shepp forward model) $u = \hat{u}$ on Ω, if this domain has the form $\Omega = \Omega_0 \times \mathbb{S}^1$.*
- *(Euler–Mumford model) $u = \hat{u}$ on Ω.*
- *(Dubins model) $u = \hat{u}$ on a dense subset of Ω.*

Furthermore, in each case, u and $\hat{u}$ are continuous at each point $\mathbf{p} \in \overline{\Omega}$ where $u(\mathbf{p}) = \hat{u}(\mathbf{p})$.

The most interesting aspect of Proposition 3.3 is what it does *not* prove. In particular, $u^{\mathrm{RS+}}$ and u^{EM} need not be continuous at the boundary of $\overline{\Omega}$, and u^{D} may be discontinuous in the interior of Ω, as well as $u^{\mathrm{RS+}}$ if Ω has not the shape specified in Proposition 3.3. The assumption $\mathrm{int}(\overline{\Omega}) = \Omega$, can also be formulated $\overline{\mathrm{int}\,\mathcal{T}} = \mathcal{T}$ as in [2], where $\mathcal{T} := \mathbb{M}\setminus\Omega$ is the target set. It forbids the presence of isolated points in the target, which are inconvenient from a theoretical perspective, although they are common in applications.

In order to simplify the proofs, we introduce the dual $\mathcal{F}^*$ of any metric $\mathcal{F}$, defined for any point $\mathbf{p} \in \mathbb{M}$ and co-vector $\hat{\mathbf{p}} \in \mathbb{E}^*$ by

$$\mathcal{F}^*_{\mathbf{p}}(\hat{\mathbf{p}}) := \sup_{\dot{\mathbf{p}}\neq 0} \frac{\langle \hat{\mathbf{p}}, \dot{\mathbf{p}}\rangle}{\mathcal{F}_{\mathbf{p}}(\dot{\mathbf{p}})} = \sup_{\dot{\mathbf{p}}\in\mathcal{B}(\mathbf{p})} \langle \hat{\mathbf{p}}, \dot{\mathbf{p}}\rangle = \sqrt{2\mathcal{H}_{\mathbf{p}}(\hat{\mathbf{p}})}. \tag{29}$$

where the control set $\mathcal{B}$ and Hamiltonian $\mathcal{H}$ are defined by (4) and (9), see also (10). The dual norm $\mathcal{F}_{\mathbf{p}}^*$ is positively 1-homogeneous and obeys the triangular inequality:

$$\mathcal{F}_{\mathbf{p}}^*(\lambda\hat{\mathbf{p}}) = \lambda\mathcal{F}_{\mathbf{p}}^*(\hat{\mathbf{p}}) \qquad \mathcal{F}_{\mathbf{p}}^*(\hat{\mathbf{p}}_1 + \hat{\mathbf{p}}_2) \leq \mathcal{F}_{\mathbf{p}}^*(\hat{\mathbf{p}}_1) + \mathcal{F}_{\mathbf{p}}^*(\hat{\mathbf{p}}_2) \tag{30}$$

for any $\lambda \geq 0$, $\mathbf{p} \in \mathbb{M}$, $\hat{\mathbf{p}}, \hat{\mathbf{p}}_1, \hat{\mathbf{p}}_2 \in \mathbb{E}^*$.

3.1 Existence, Uniqueness and Boundedness of a Discrete Solution

We establish the existence and uniqueness of a solution to the discretized problem (28) for the models of interest. We also prove upper bounds on this solution which are independent of the gridscale h, assuming that the relaxation parameter satisfies $0 < \varepsilon \leq h$. (This property remains valid if $0 < \varepsilon \leq Ch$, where C is an absolute constant.)

Definition 3.4 Let $\mathfrak{F}$ be a PDE discretization scheme on a finite set X, in the sense of Definition 2.1. A discrete map $U \in \mathbb{R}^X$ is called a sub- (resp. strict sub-, resp. super-, resp. strict super-) solution of the scheme $\mathfrak{F}$ iff $\mathfrak{F}U \leq 0$ (resp. $\mathfrak{F}U < 0$, resp. $\mathfrak{F}U \geq 0$, resp. $\mathfrak{F}U > 0$) pointwise on X. If $\mathfrak{F}U = 0$, then U is a solution to the scheme.

When the scheme $\mathfrak{F}$ is obvious from context, we simply speak of sub- and super-solution. The existence, uniqueness, and computability of the solutions to PDE schemes are discussed in the next result, using the notions of *monotony* and *causality* introduced in Definition 2.1. Theorem 3.5 is not an original contribution, but gathers classical results from [41,47,54], see also [36] for a proof.

Theorem 3.5 (Solving monotone schemes) *Let $\mathfrak{F}$ be a monotone scheme on a finite set X s.t.*

(i) *There exists a sub-solution U^- and a super-solution U^+ to the scheme $\mathfrak{F}$.*
(ii) *Any super-solution to $\mathfrak{F}$ is the pointwise limit of a sequence of strict super-solutions.*

Then, there exists a unique solution $U \in \mathbb{R}^X$ to $\mathfrak{F}U = 0$, and it satisfies $U^- \leq U \leq U^+$. If in addition the scheme is causal, then this solution can be obtained via the dynamic programming algorithm, also called Dijkstra or fast-marching, with complexity $\mathcal{O}(M \ln N)$ where

$$N = \#(X), \quad M = \#(\{(\mathbf{x}, \mathbf{y}) \in X \times X;\ \mathfrak{F}U(\mathbf{y}) \text{ depends on } U(\mathbf{x})\}). \tag{31}$$

The logarithmic factor $\ln N$ in the complexity comes from the cost of maintaining a priority queue. We counted as elementary, complexity-wise, a scheme-dependent local update which in our case amounts to solving a univariate quadratic equation. We refer to [47] for more details on the fast-marching algorithm.

General properties of our PDE schemes In this paragraph, we prove that the PDE discretization schemes introduced in Sect. 2 are monotone, causal, admit a sub-solution, and satisfy Property (ii) of Theorem 3.5. For that purpose, we express them as specializations of a generic design, described in the next proposition.

Proposition 3.6 *Let X be a finite set, and let $F : \mathbb{R}^X \to \mathbb{R}^X$ be defined by*

$$(FU(\mathbf{x}))^2 := \max_{i \in I} \sum_{\mathbf{y} \in X \cup \partial X} b(i, \mathbf{x}, \mathbf{y})(U(\mathbf{x}) - U(\mathbf{y}))_+^2, \tag{32}$$

for all $U : X \to \mathbb{R}$ and all $\mathbf{x} \in X$. We denoted by I and ∂X some arbitrary finite sets, and by $b : I \times X \times (X \cup \partial X) \to [0, \infty[$ some nonnegative weights. By convention, U is extended by 0 on ∂X.

Then, $F(\lambda U) = \lambda F(U)$ and $F(U+V) \leq F(U) + F(V)$, pointwise on X, for any $\lambda \geq 0$ and any $U, V : \mathbb{R}^X \to \mathbb{R}$. Let also

$$HU(\mathbf{x}) := \frac{1}{2}(FU(\mathbf{x}))^2 \qquad \mathfrak{F}U(\mathbf{x}) := -a(\mathbf{x}) + HU(\mathbf{x}), \tag{33}$$

where $a : X \to]0, \infty[$ is arbitrary. Then, $\mathfrak{F}$ is a monotone and causal scheme, admits $U \equiv 0$ a as sub-solution, and $(1+\varepsilon)U$ is a strict super-solution for any super-solution U and any $\varepsilon > 0$.

Proof The 1-homogeneity of F is obvious. The triangular inequality follows from the expression

$$FU(\mathbf{x}) = \max_{i \in I} \left\| \left(\sqrt{b(i, \mathbf{x}, \mathbf{y})}(U(\mathbf{x}) - U(\mathbf{y}))_+ \right)_{y \in X \cup \partial X} \right\|,$$

and from the basic inequality $(a+b)_+ \leq a_+ + b_+$ applied to $a = U(\mathbf{x}) - U(\mathbf{y})$, $b = V(\mathbf{x}) - V(\mathbf{y})$.

The scheme $\mathfrak{F}$ is monotone since F is non-decreasing w.r.t. the differences $(U(\mathbf{x}) - U(\mathbf{y}))_{y \in X}$, and it is causal since $\mathfrak{F}$ only depends on their positive part. The null map $U \equiv 0$ satisfies $\mathfrak{F}U(\mathbf{x}) = -a(\mathbf{x}) < 0$, hence is a (strict) sub-solution. Finally, if U is a super-solution and if $\varepsilon > 0$, then $\mathfrak{F}((1+\varepsilon)U) = (1+\varepsilon)^2 \mathfrak{F}U + ((1+\varepsilon)^2 - 1)a \geq 2\varepsilon a > 0$ pointwise, by homogeneity of F, hence $(1+\varepsilon)U$ is a strict super-solution. □

Each of the schemes introduced in Sect. 2 can be written in the form H of Proposition 3.6. Note that a slight reformulation is required for the Reeds–Shepp models $H_{\varepsilon,h}^{\mathrm{RS}+}U(\mathbf{p})$, $H_{\varepsilon,h}^{\mathrm{RS}\pm}U(\mathbf{p})$, which involve symmetric finite differences,

hence expressions of the form

$$\sum_{1\le i\le N} \max\{0,\ U(\mathbf{p})-U(\mathbf{q}_i),\ U(\mathbf{x})-U(\mathbf{r}_i)\}^2 = \sum_{1\le i\le N} \max\left\{(U(\mathbf{p})-U(\mathbf{q}_i))_+^2,\ (U(\mathbf{p})-U(\mathbf{r}_i))_+^2\right\}.$$

This expression can be put in the form (32) using the distributivity of the "+" operator over the "max" operator, namely $a+\max\{b,c\}=\max\{a+b,a+c\}$. For consistency of (33, right) with (28), one must choose $a(\mathbf{x})=\frac{1}{2}\alpha(\mathbf{x})^2$.

Construction of a continuous super-solution In this paragraph, we construct a super-solution to the generalized eikonal PDE (8), see Sect. 3.2 for more details on this concept. It is sampled on the discrete domain Ω_h in the next paragraph, which yields a discrete super-solution bounded independently of the gridscale $h>0$. In the rest of this subsection, we let for all $\mathbf{p}=(\mathbf{x},\theta)\in\mathbb{M}$

$$u(\mathbf{p}) := \alpha_0 + \langle \mathbf{n}(\theta_0), \mathbf{x}\rangle + \frac{\xi}{2} d_{\mathbb{S}^1}(\theta,\theta_0)^2, \tag{34}$$

where $\alpha_0 = C_{\mathrm{WS}} + \max\{\|\mathbf{p}\|;\ \mathbf{p}\in\Omega\}$. (In other sections of this paper, the symbol u still stands for the value function defined by (7).) The angle $\theta_0\in\mathbb{S}^1$ in (34) is arbitrary but fixed, and $d_{\mathbb{S}^1}$ denotes the distance function on $\mathbb{S}^1:=\mathbb{R}/(2\pi\mathbb{Z})$. For all $\mathbf{p}=(\mathbf{x},\theta)\in\mathbb{M}$ such that $d_{\mathbb{S}^1}(\theta,\theta_0)\neq\pi$, one has

$$\mathrm{d}u(\mathbf{p}) = (\mathbf{n}(\theta_0), \xi\varphi)\in\mathbb{E}^*, \tag{35}$$

where $\varphi\in]-\pi,\pi[$ is the unique element congruent with $\theta-\theta_0$ modulo 2π. The function u is *not* differentiable where $d_{\mathbb{S}^1}(\theta,\theta_0)=\pi$, but by convention we still define $\mathrm{d}u(\mathbf{p})$ as (35) with $\varphi:=\pi$. As shown in the following lemma, this expression defines a super-gradient of u.

Lemma 3.7 *Let $u:\mathbb{M}\to\mathbb{R}$ be defined by (34). Then, for all $\mathbf{p}=(\mathbf{x},\theta)\in\mathbb{M}$ and all $\dot{\mathbf{p}}=(\dot{\mathbf{x}},\dot{\theta})\in\mathbb{E}$ one has*

$$u(\mathbf{p}+\dot{\mathbf{p}}) \le u(\mathbf{p}) + \langle \mathrm{d}u(\mathbf{p}), \dot{\mathbf{p}}\rangle + \frac{\xi}{2}\dot{\theta}^2.$$

Proof Let $\varphi\in]-\pi,\pi]$ be congruent with $\theta-\theta_0$ modulo 2π. Then, $d_{\mathbb{S}^1}(\theta+\dot\theta,\theta_0)^2\le|\varphi+\dot\theta|^2=\varphi^2+2\varphi\dot\theta+\dot\theta^2=d_{\mathbb{S}^1}(\theta,\theta_0)^2+2\langle\varphi,\dot\theta\rangle+\dot\theta^2$, which implies the announced result. □

The next proposition lower bounds the dual metric applied to the differential of (34).

Proposition 3.8 *Let $\mathcal{F}$ be $\mathcal{F}^{RS+}$, $\mathcal{F}^{RS\pm}$, $\mathcal{F}^{EM}$, or $\mathcal{F}^{D}$. Then, the dual metric (29) obeys $\mathcal{F}^*_{\mathbf{p}}(\mathrm{d}u(\mathbf{p}))\ge c_0$ for any $\mathbf{p}\in\mathbb{M}$, where $c_0>0$ is an absolute constant.*

Proof Let $\mathbf{p}=(\mathbf{x},\theta)\in\Omega$ and let $\varphi\in]-\pi,\pi]$ be congruent with $\theta-\theta_0$ modulo 2π. Then,

$$\begin{aligned}
\mathcal{F}^{\mathrm{RS}+*}_{\mathbf{p}}(\mathrm{d}u(\mathbf{p}))^2 &= \langle\mathbf{n}(\theta),\mathbf{n}(\theta_0)\rangle_+^2 + |\theta-\theta_0|^2 = (\cos\varphi)_+^2+\varphi^2,\\
\mathcal{F}^{\mathrm{RS}\pm*}_{\mathbf{p}}(\mathrm{d}u(\mathbf{p}))^2 &= \langle\mathbf{n}(\theta),\mathbf{n}(\theta_0)\rangle^2 + |\theta-\theta_0|^2 = (\cos\varphi)^2+\varphi^2,\\
2\mathcal{F}^{\mathrm{EM}*}_{\mathbf{p}}(\mathrm{d}u(\mathbf{p})) &= \langle\mathbf{n}(\theta),\mathbf{n}(\theta_0)\rangle + \sqrt{\langle\mathbf{n}(\theta),\mathbf{n}(\theta_0)\rangle^2+|\theta-\theta_0|^2}\\
&= \cos\varphi+\sqrt{\cos^2\varphi+\varphi^2},\\
\mathcal{F}^{\mathrm{D}*}_{\mathbf{p}}(\mathrm{d}u(\mathbf{p})) &= (\langle\mathbf{n}(\theta),\mathbf{n}(\theta_0)\rangle+|\theta-\theta_0|)_+ = (\cos\varphi+|\varphi|)_+.
\end{aligned}$$

The right-hand sides are continuous and non-vanishing functions of $\varphi\in[-\pi,\pi]$. More precisely, one easily finds the following lower bounds: for the two Reeds–Shepp models and the Dubins model $c_0=1$, attained for $\varphi=0$; for the Euler–Mumford elastica model $c_0=\pi/4$, attained for $\varphi=\pi/2$. □

Proposition 3.8 implies that λu is a super-solution of the HJB PDE (8), in the sense of Definition 3.14 below, where $\lambda=\|\alpha\|_\infty/c_0$. Indeed, this follows from the positive 1-homogeneity of $\mathcal{F}^*$, and the nonnegativity of u on $\partial\Omega$. We do *not* directly use this fact in this subsection, since we aim at constructing a *discrete* super-solution, but it explains the particular role played by u.

Discretization of the super-solution We construct a discrete super-solution to the problem (28) by sampling the continuous one constructed in Proposition 3.8. This implies the existence of a bounded solution to our PDE discretization, see Corollary 3.11. For that purpose, a preliminary estimate on the discrete Hamiltonian regularity is required.

Lemma 3.9 *Let $F:=\sqrt{2H}$ where H is $H^{RS+}_{\varepsilon,h}$, $H^{RS\pm}_{\varepsilon,h}$, $H^{EM}_{\varepsilon,K,h}$ or $H^{D}_{\varepsilon,h}$, and where $\varepsilon\le 1$. Let $\mathbf{p}_0\in\Omega_h$, and let $V,W:\mathbb{M}_h\to\mathbb{R}$ obey for all $\dot{\mathbf{p}}\in\mathbb{M}_h$*

$$V(\mathbf{p}_0+\dot{\mathbf{p}}) \ge V(\mathbf{p}_0) - \|\dot{\mathbf{p}}\|^2, \quad W(\mathbf{p}_0+\dot{\mathbf{p}}) \ge W(\mathbf{p}_0) - \|\dot{\mathbf{p}}\|.$$

Then, for some $C=C_0(1+\xi^{-1})$, where C_0 is an absolute constant, one has

$$FV(\mathbf{p}_0) \le Ch/\varepsilon, \quad FW(\mathbf{p}_0) \le C.$$

Proof For any $\dot{\mathbf{n}}\in\mathbb{R}^d$ one obtains using Proposition 2.2

$$\begin{aligned}
&h^{-2}\sum_{\dot{\mathbf{e}}\in\mathbb{Z}^d}\rho^\varepsilon_{\dot{\mathbf{e}}}(\dot{\mathbf{n}})(W(\mathbf{p}_0)-W(\mathbf{p}_0-h\dot{\mathbf{e}}))_+^2\\
&\quad\le h^{-2}\sum_{\dot{\mathbf{e}}\in\mathbb{Z}^d}\rho^\varepsilon_{\dot{\mathbf{e}}}(\dot{\mathbf{n}})\|h\dot{\mathbf{e}}\|^2 = \|\dot{\mathbf{n}}\|^2(1+(d-1)\varepsilon^2)
\end{aligned} \tag{36}$$

In the case of V, observing that $V(\mathbf{p}_0)-V(\mathbf{p}_0-h\dot{\mathbf{e}})\le\|h\dot{\mathbf{e}}\|^2\le(C_{\mathrm{WS}}h/\varepsilon)\|h\dot{\mathbf{e}}\|$ and reasoning similarly, we obtain the upper bound (36, right) multiplied by $(C_{\mathrm{WS}}h/\varepsilon)^2$.

The announced result is equivalent to $HV(\mathbf{p}_0)\le\frac{1}{2}(Ch/\varepsilon)^2$ (resp. $HW(\mathbf{p}_0)\le\frac{1}{2}C^2$). It follows from the above estimates

since the discretized Hamiltonians of interest are sums of expressions like (36, left), with $\|\dot{\mathbf{n}}\| = \mathcal{O}(1+\xi^{-1})$. In the case of $H^{\mathrm{EM}}_{\varepsilon,K,h}$, one must additionally observe that $\sum_{k=1}^{K} \alpha_k = 2$ is bounded independently of K, see (23). □

In the following two results, the notation $C \lesssim 1+\xi^{\alpha}$, where $\alpha \in \mathbb{R}$, means that C depends only on the parameter ξ and satisfies $C \leq C'(1+\xi^{\alpha})$ for all $\xi \in]0, \infty[$, where C' is an absolute constant.

Proposition 3.10 *Let $F := \sqrt{2H}$ where H is $H^{RS+}_{\varepsilon,h}$, $H^{RS\pm}_{\varepsilon,h}$ or $H^{D}_{\varepsilon,h}$, and where $0 < h \leq \varepsilon \leq 1$. Define $U : \mathbb{Z}^h \to \mathbb{R}$ by $U(\mathbf{p}) = u(\mathbf{p})$ for all $\mathbf{p} \in \Omega_h$, and $U(\mathbf{p}) = 0$ for all $\mathbf{p} \in \partial\Omega_h$, where u is defined in (34). Then,*

$$FU(\mathbf{p}) \geq c_0 - C_0 h/\varepsilon \tag{37}$$

for all $\mathbf{p} \in \Omega_h$, where $C_0 \lesssim 1+\xi$ and c_0 is from Proposition 3.8. In the Euler–Mumford case, the constant c_0 in (37) must be replaced with $\sqrt{c_0^2 - 2C_1K^{-2}}$, where $C_1 \lesssim 1+\xi^{-2}$ is the constant from Proposition 2.10.

Proof In this proof, we let $\mathbf{p}_0 = (\mathbf{x}_0, \theta_0) \in \Omega_h$ be fixed, $\mathbf{p} = (\mathbf{x}, \theta) \in \Omega_h$ be an arbitrary point, and denote by $\dot{\theta} \in]-\pi, \pi]$ the unique angle congruent to $\theta - \theta_0$. Let $\overline{U} : \mathbb{M}_h \to \mathbb{R}$ be defined by $\overline{U}(\mathbf{p}) := u(\mathbf{p}_0) + \langle \mathrm{d}u(\mathbf{p}_0), (\mathbf{x} - \mathbf{x}_0, \dot{\theta})\rangle$. By consistency of the discretization, see Propositions 2.5, 2.10, 2.13, and by Proposition 3.8 we obtain, denoting by $\mathcal{H}$ the Hamiltonian of the model

$$H\overline{U}(\mathbf{p}_0) \geq \mathcal{H}_{\mathbf{p}_0}(\mathrm{d}u(\mathbf{p}_0)) \geq \frac{1}{2}c_0^2, \tag{38}$$

except in the Euler–Mumford case, where $H\overline{U}(\mathbf{p}_0) \geq \frac{1}{2}c_0^2 - C_1K^{-2}$, with $C_1 \lesssim 1+\xi^{-2}$. Thus, $F\overline{U}(\mathbf{p}_0) \geq c_0$, or in the Euler–Mumford case $F\overline{U}(\mathbf{p}_0) \geq \sqrt{c_0 - 2C_1K^{-2}}$.

For any $\mathbf{p} \in \Omega_h$, one has $\overline{U}(\mathbf{p}) + \frac{\xi}{2}\dot{\theta}^2 \geq U(\mathbf{p})$, by Lemma 3.7, with the above notation for $\dot{\theta} \in]-\pi, \pi]$. On the other hand, if $\mathbf{p} \in \partial\Omega_h$ is within distance C_{WS} of Ω_h, then $\overline{U}(\mathbf{p}) \geq 0 = U(\mathbf{p})$, by choice of α_0 in the definition of u, see (34). Hence, denoting $V := \overline{U} - U$ we obtain $V(\mathbf{p}_0 + \dot{\mathbf{p}}) = \overline{U}(\mathbf{p}_0 + \dot{\mathbf{p}}) - U(\mathbf{p}_0 + \dot{\mathbf{p}}) \geq -\frac{\xi}{2}\|\dot{\mathbf{p}}\|^2$ for any $\dot{\mathbf{p}} \in h\mathbb{Z}^3$ such that $\|\dot{\mathbf{p}}\| \leq C_{\mathrm{WS}}$. Therefore, $FV(\mathbf{p}_0) \leq \xi C_2(1+\xi^{-1})h/\varepsilon = C_2(1+\xi)h/\varepsilon$, by Lemma 3.9 and the 1-homogeneity of F, where C_2 is independent of ξ. We used the fact that the expression of $FV(\mathbf{p}_0)$ only involves points within distance $C_{\mathrm{WS}}h/\varepsilon \leq C_{\mathrm{WS}}$ of $\mathbf{p}_0$, see Propositions 2.5, 2.10, 2.13. Using the triangular inequality $F\overline{U} = F(U+V) \leq FU + FV$, pointwise on Ω_h, see Proposition 3.6, we thus obtain

$$FU(\mathbf{p}_0) \geq F\overline{U}(\mathbf{p}_0) - FV(\mathbf{p}_0) \geq c_0 - C_2(1+\xi)h/\varepsilon.$$

In the Euler–Mumford case, the constant c_0 in the above expression must be replaced with $\sqrt{c_0 - 2C_1K^{-2}}$, see (38). The result follows. □

Corollary 3.11 *Assume that $0 < h \leq \varepsilon \leq 1$ and $\varepsilon \leq K_0 h$, where $K_0 \lesssim 1+\xi$. Let H be the discretized Hamiltonian $H^{RS+}_{\varepsilon,h}$, $H^{RS\pm}_{\varepsilon,h}$ or $H^{D}_{\varepsilon,h}$. Then, the system of equations $HU(\mathbf{p}) = \alpha(\mathbf{p})^2/2$ for all $\mathbf{p} \in \Omega_h$, and $U(\mathbf{p}) = 0$ for all $\mathbf{p} \in \partial\Omega_h$, admits an unique solution $U : \mathbb{M}_h \to \mathbb{R}$, which is bounded independently of h and ε.*

The same holds for the Hamiltonian $H^{EM}_{\varepsilon,K,h}$, provided $K \geq K_1 \gtrsim 1+\xi^{-1}$.

Proof Assume that the parameters ε, h and K obey the above constraints, with the constants $K_0 = 2C_0$ and $K_1 = 4\sqrt{C_1}$, where C_0 and C_1 are from Proposition 3.10. Then, the considered system of equations admits the super-solution λU, where U is defined in Proposition 3.10 and $\lambda = 2\|\alpha\|_{L^\infty}/c_0$. Applying Theorem 3.5, whose assumptions were established in Proposition 3.6 for the models of interest, except for the existence of a super-solution which we just proved, we conclude the proof. □

3.2 Discontinuous Viscosity Solutions of Eikonal PDEs

In this subsection, we establish Theorem 3.1 using the theory of discontinuous solutions to static first-order Hamilton–Jacobi–Bellman PDEs. We rely on the framework of section V of [2], intended for time optimal control problems without controllability, either local or global. Let $\mathcal{F}$ be $\mathcal{F}^{\mathrm{RS}+}$, $\mathcal{F}^{\mathrm{RS}\pm}$, $\mathcal{F}^{\mathrm{EM}}$ or $\mathcal{F}^{\mathrm{D}}$, and consider the PDE.

$$\begin{aligned} &\forall \mathbf{p} \in \Omega,\ \mathcal{F}^*_{\mathbf{p}}(\mathrm{d}u(\mathbf{p})) = \alpha(\mathbf{p}), \\ &\forall \mathbf{p} \in \partial\Omega,\ u(\mathbf{p}) = 0 \text{ or } \mathcal{F}^*_{\mathbf{p}}(\mathrm{d}u(\mathbf{p})) = \alpha(\mathbf{p}), \end{aligned} \tag{39}$$

where $\mathcal{F}^*$ refers to the dual metric, defined on the co-tangent space $\mathbb{M} \times \mathbb{E}^*$, see (29). In comparison with our initial formulation (8), two remarks are in order: (I) we used the relation $\mathcal{H} = \frac{1}{2}(\mathcal{F}^*)^2$ relating the Hamiltonian $\mathcal{H}$ with the dual metric $\mathcal{F}^*$ (29) to reformulate the HJB PDE in Ω, and (II) we emphasized that boundary conditions must be interpreted in a relaxed sense, following the notations of [2], due to the possible discontinuity of the solution. The study of solutions to this system relies on one-sided notions of continuity.

Definition 3.12 Let (X, d) be metric space, and let $u : X \to \mathbb{R}$. The function u is said lower semi-continuous (resp. upper semi-continuous) iff for any converging sequence $\mathbf{p}_n \to \mathbf{p} \in X$

$$\liminf_{n\to\infty} u(\mathbf{p}_n) \geq u(\mathbf{p}) \quad (\text{resp. } \limsup_{n\to\infty} u(\mathbf{p}_n) \leq u(\mathbf{p}).)$$

The acronyms used for these properties (resp. and also Boundedness) are USC and LSC (resp. BUSC and BLSC). Recall that the cartesian grid of scale h is denoted $\mathbb{M}_h \subseteq \mathbb{M}$, see (40), and that $B(\mathbf{p}, r) \subseteq \mathbb{M}$ is the Euclidean ball of center $\mathbf{p} \in \mathbb{M}$ and radius $r > 0$.

Lemma 3.13 *For each $n \geq 0$ let $h_n > 0$ and $U_n : \mathbb{M}_{h_n} \to \mathbb{R}$. Assume that $h_n \to 0$ as $n \to \infty$, and that U_n is uniformly bounded independently of n. Then, $\overline{u}, \underline{u} : \mathbb{M} \to \mathbb{R}$ defined as follows are, respectively, BUSC and BLSC*

$$\underline{u}(\mathbf{p}) := \lim_{r\to 0} \liminf_{n\to\infty} \inf_{\substack{\mathbf{q}\in\mathbb{M}_{h_n}\\ \|\mathbf{q}-\mathbf{p}\|<r}} U_n(\mathbf{q}),$$
$$\overline{u}(\mathbf{p}) := \lim_{r\to 0} \limsup_{n\to\infty} \sup_{\substack{\mathbf{q}\in\mathbb{M}_{h_n}\\ \|\mathbf{q}-\mathbf{p}\|<r}} U_n(\mathbf{q}). \tag{40}$$

Proof We focus on the case of $\underline{u}$, since the case of $\overline{u}$ is similar. First note that $\underline{u}(\mathbf{p})$ is well defined and uniformly bounded w.r.t. $\mathbf{p} \in \mathbb{M}$. Indeed (i) for any fixed $r > 0$, and for sufficiently large n, the set $\mathbb{M}_{h_n} \cap B(\mathbf{p}, r)$ is non-empty since $h_n \to 0$ as $n \to \infty$, (ii) U_n is uniformly bounded, and (iii) the leftmost limit as $r \to 0$ is monotone, namely increasing as r decreases to 0, hence well defined.

In order to establish the Lower Semi-Continuity of $\underline{u}$, let us consider an arbitrary sequence $(\mathbf{p}_n)_{n\geq 0}$ converging to $\mathbf{p} \in \mathbb{M}$. Let also $r_n \to 0$ and $\varepsilon_n \to 0$ be vanishing sequences of positive reals. By construction, for any $n \geq 0$ there exists $\varphi(n) \geq n$ and $\mathbf{q}_n \in B(\mathbf{p}_n, r_n)$ such that $U_{\varphi(n)}(\mathbf{q}_n) \leq \underline{u}(\mathbf{p}_n) + \varepsilon_n$. Then, as announced, since $\mathbf{q}_n \to \mathbf{p}$ and $\varphi(n) \to \infty$ as $n \to \infty$,

$$\liminf_{n\to\infty} \underline{u}(\mathbf{p}_n) \geq \liminf_{n\to\infty} U_{\varphi(n)}(\mathbf{q}_n) \geq \underline{u}(\mathbf{p}). \qquad \square$$

Following [8], we introduce the concept of sub- and super-solutions to the system (39).

Definition 3.14 • A sub-solution of (39) is a BUSC $\overline{u} : \overline{\Omega} \to \mathbb{R}$ such that for any $\mathbf{p} \in \overline{\Omega}$ and any $\varphi \in C^1(\overline{\Omega}, \mathbb{R})$ for which $\overline{u} - \varphi$ attains a local maximum at $\mathbf{p}$, one has:

$$\mathbf{p} \in \Omega \Rightarrow \mathcal{F}^*_{\mathbf{p}}(\mathrm{d}\varphi(\mathbf{p})) \leq \alpha(\mathbf{p}),$$
$$\mathbf{p} \in \partial\Omega \Rightarrow \min\{\overline{u}(\mathbf{p}),\ \mathcal{F}^*_{\mathbf{p}}(\mathrm{d}\varphi(\mathbf{p})) - \alpha(\mathbf{p})\} \leq 0.$$

• A super-solution of (39) is a BLSC $\underline{u} : \overline{\Omega} \to \mathbb{R}$ such that for any $\mathbf{p} \in \overline{\Omega}$ and any $\varphi \in C^1(\overline{\Omega}, \mathbb{R})$ for which $\underline{u} - \varphi$ attains a local minimum at $\mathbf{p}$, one has:

$$\mathbf{p} \in \Omega \Rightarrow \mathcal{F}^*_{\mathbf{p}}(\mathrm{d}\varphi(\mathbf{p})) \geq \alpha(\mathbf{p}),$$
$$\mathbf{p} \in \partial\Omega \Rightarrow \max\{\underline{u}(\mathbf{p}),\ \mathcal{F}^*_{\mathbf{p}}(\mathrm{d}\varphi(\mathbf{p})) - \alpha(\mathbf{p})\} \geq 0.$$

It is known that replacing "local maximum" with "strict global maximum" (resp. "local minimum" with "strict global minimum") in Definition 3.14 yields an equivalent definition, see [8].

Following a classical strategy [11], we estimate in the next lemma the discretization error of our numerical scheme when applied to continuously differentiable functions, and conclude in the subsequent proposition that suitable limits of solutions to our discrete numerical schemes are sub- and super-solutions to the HJB PDE (39).

Lemma 3.15 *Let $F_{\varepsilon,h} := \sqrt{2H_{\varepsilon,h}}$ where $H_{\varepsilon,h}$ is $H^{RS+}_{\varepsilon,h}$, $H^{RS\pm}_{\varepsilon,h}$ or $H^{D}_{\varepsilon,h}$ and $0 < h \leq \varepsilon \leq 1$. Let $\varphi \in C^1(\mathbb{M}, \mathbb{R})$, and let ω be the modulus of continuity of* $\mathrm{d}\varphi$. *Then,*

$$|F_{\varepsilon,h}\varphi(\mathbf{p}) - \mathcal{F}^*_{\mathbf{p}}(\mathrm{d}\varphi(\mathbf{p}))| \leq C(\omega(C_{\mathrm{WS}}h/\varepsilon) + \varepsilon\|\mathrm{d}\varphi(\mathbf{p})\|). \tag{41}$$

In the Euler–Mumford case, $|F_{\varepsilon,K,h}\varphi(\mathbf{p}) - \mathcal{F}^*_{\mathbf{p}}(\mathrm{d}\varphi(\mathbf{p}))| \leq C(\omega(C_{\mathrm{WS}}h/\varepsilon) + (\varepsilon + K_n^{-1})\|\mathrm{d}\varphi(\mathbf{p})\|)$.

Proof In this proof, if $\mathbf{p} = (\mathbf{x}, \theta), \mathbf{q} = (\mathbf{x}', \theta') \in \mathbb{M} = \mathbb{R}^2 \times \mathbb{S}^1$, then $\mathbf{q} - \mathbf{p}$ (abusively) stands for $(\mathbf{x}' - \mathbf{x}, \varphi) \in \mathbb{E} := \mathbb{R}^2 \times \mathbb{R}$ where $\varphi \in]-\pi, \pi]$ is congruent with $\theta' - \theta$. Fix the point $\mathbf{p} \in \mathbb{M}$, and define the tangent map $\Phi : \mathbf{q} \in \mathbb{M} \mapsto \varphi(\mathbf{p}) + \langle \mathrm{d}\varphi(\mathbf{p}), \mathbf{q} - \mathbf{p}\rangle$. Then, $|\varphi(\mathbf{q}) - \Phi(\mathbf{q})| \leq \|\mathbf{p} - \mathbf{q}\|\omega(\|\mathbf{p} - \mathbf{q}\|)$ for any $\mathbf{q} \in \mathbb{M}$. This implies $F(\varphi - \Phi)(\mathbf{p}) \leq C\omega(C_{\mathrm{WS}}h/\varepsilon)$ where $F := F_{\varepsilon,h}$ and $C \lesssim 1+\xi^{-1}$, by Lemma 3.9, the 1-homogeneity of F, and since any point $\mathbf{q}$ appearing in the expression of $FU(\mathbf{p})$ satisfies $\|\mathbf{p} - \mathbf{q}\| \leq C_{\mathrm{WS}}h/\varepsilon$. Proceeding likewise for $F(\Phi - \varphi)(\mathbf{p})$ and using the triangular inequality, proved for F in Proposition 3.6, we obtain

$$\begin{aligned}|F\varphi(\mathbf{p}) - F\Phi(\mathbf{p})| &\leq \max\{F(\Phi - \varphi)(\mathbf{p}), F(\varphi - \Phi)(\mathbf{p})\}\\ &\leq C\,\omega(C_{\mathrm{WS}}h/\varepsilon).\end{aligned}$$

The second contribution to (41) comes from the estimate

$$\begin{aligned}|F\Phi(\mathbf{p}) - \mathcal{F}^*_{\mathbf{p}}(\mathrm{d}\varphi(\mathbf{p}))| &= \sqrt{2}|\sqrt{H\Phi(\mathbf{p})} - \sqrt{\mathcal{H}_{\mathbf{p}}(\mathrm{d}\varphi(\mathbf{p}))}|\\ &\leq \sqrt{2}\sqrt{|H\Phi(\mathbf{p}) - \mathcal{H}_{\mathbf{p}}(\mathrm{d}\varphi(\mathbf{p}))|},\end{aligned}$$

where we used the classical inequality $|\sqrt{a} - \sqrt{b}| \leq \sqrt{|a - b|}$ for any $a, b \geq 0$. Inserting the discretization error of the Hamiltonian, see Propositions 2.5, 2.10 and 2.13, we conclude the proof. $\square$

Proposition 3.16 *Let $\underline{u}, \overline{u} : \mathbb{M} \to \mathbb{R}$ be defined as in Theorem 3.1 (resp. Theorem 3.2). Then, $\underline{u}$ is a super-solution, and $\overline{u}$ is a sub-solution, in the sense of Definition 3.14.*

Proof We focus on the case of $\overline{u}$, since the case of $\underline{u}$ is similar. By Lemma 3.13, $\overline{u}$ is BUSC as required. Let $\mathbf{p} \in \overline{\Omega}$ and $\varphi \in C^1(\overline{\Omega}, \mathbb{R})$ be such that $\overline{u}$ attains a *strict global* maximum at $\mathbf{p}$.

For each $n \geq 0$, define $X_n := \{\mathbf{q} \in \mathbb{M}_{h_n};\ d(\mathbf{q}, \Omega) \leq C_{\mathrm{WS}} h_n\}$, where d denotes the Euclidean distance, and let $\mathbf{p}_n \in X_n$ be a point where $U_n - \varphi$ attains its global maximum. Then, $U_n(\mathbf{p}_n) - \varphi(\mathbf{p}_n) \to \overline{u}(\mathbf{p}) - \varphi(\mathbf{p})$ as $n \to \infty$, up to extracting a subsequence [because of the lim inf operator in (40)]. This implies $\mathbf{p}_n \to \mathbf{p}$ as $n \to \infty$, by strictness of the maximum of $\overline{u} - \varphi$ at $\mathbf{p}$. In addition, $U_n(\mathbf{p}_n) = (U_n(\mathbf{p}_n) - \varphi(\mathbf{p}_n)) + \varphi(\mathbf{p}_n) \to (\overline{u}(\mathbf{p}) - \varphi(\mathbf{p})) + \varphi(\mathbf{p}) = \overline{u}(\mathbf{p})$ as $n \to \infty$, by choice of the sequence $(\mathbf{p}_n)_{n \geq 0}$ and by continuity of φ. In order to conclude the proof, we distinguish wether the test point $\mathbf{p} \in \overline{\Omega}$ lies in the interior or on the boundary of the domain.

Case where $\mathbf{p} \in \Omega$. By construction of $\mathbf{p}_n$, one has $U_n(\mathbf{p}_n) - U_n(\mathbf{q}) \geq \varphi(\mathbf{p}_n) - \varphi(\mathbf{q})$ for all $\mathbf{q} \in X_n$. Hence,

$$\begin{aligned}\alpha(\mathbf{p}_n) = F U_n(\mathbf{p}_n) &\geq F\varphi(\mathbf{q}_n) \geq \mathcal{F}^*_{\mathbf{p}_n}(\mathrm{d}\varphi(\mathbf{p}_n)) \\ &\quad - C(\omega(C_{\mathrm{WS}} h_n/\varepsilon_n) + \varepsilon_n \|\mathrm{d}\varphi(\mathbf{p}_n)\|),\end{aligned}$$

where the first inequality is by monotony of the discretized operator $F := F_{\varepsilon,h}$, and the second one is by Lemma 3.15. Thus $\alpha(\mathbf{p}) = \lim \alpha(\mathbf{p}_n) \geq \lim \mathcal{F}^*_{\mathbf{p}_n}(\mathrm{d}\varphi(\mathbf{p}_n)) = \mathcal{F}^*_{\mathbf{p}}(\mathrm{d}\varphi(\mathbf{p}))$ as $n \to \infty$.

Case where $\mathbf{p} \in \partial\Omega$. We distinguish two sub-cases: if $\mathbf{p}_n \in \Omega$ for infinitely many integers $n \geq 0$, then $\mathcal{F}^*_{\mathbf{p}}(\mathrm{d}\varphi(\mathbf{p})) \leq \alpha(\mathbf{p})$ as before, thus the (relaxed) boundary condition is satisfied as desired. Otherwise, up to extracting a subsequence, one has $0 = U_n(\mathbf{p}_n) \to \overline{u}(\mathbf{p})$ as $n \to \infty$, thus $\overline{u}(\mathbf{p}) = 0$ and the boundary condition is satisfied. □

The following result concludes the proof of Theorems 3.1 and 3.2.

Proposition 3.17 (Adapted from [2]) *The value function u defined by (7) is the smallest super-solution to the HJB PDE (39), and $\hat{u}$ defined by (27) is the largest sub-solution.*

The fact that u is the smallest super-solution follows from Theorem 3.7 in chapter V [2] and the fact that $\hat{u}$ is the largest super-solution from Theorem 4.29 in the same chapter. To be complete, we describe below the slight reformulation of the optimal control problem (7) required to match the notations of [2], and check that the assumptions used in [2] are satisfied. For that purpose, we introduce a compact and convex set $\mathbb{A} \subseteq \mathbb{R} \times \mathbb{R}$ and regard its elements $a = (\dot{x}, \dot{\theta}) \in \mathbb{A}$ as a (scalar) physical velocity, and an angular velocity. The following instantiations of $\mathbb{A}$ are considered

$$\begin{aligned}\mathbb{A}^{\mathrm{RS}+} &:= \{(\dot{x}, \dot{\theta}) \in \mathbb{R}^2;\ \dot{x}^2 + \dot{\theta}^2 \leq 1,\ \dot{x} \geq 0\},\\ \mathbb{A}^{\mathrm{RS}\pm} &:= \{(\dot{x}, \dot{\theta}) \in \mathbb{R}^2;\ \dot{x}^2 + \dot{\theta}^2 \leq 1\},\\ \mathbb{A}^{\mathrm{EM}} &:= \{(\dot{x}, \dot{\theta}) \in \mathbb{R}^2;\ (\dot{x} - 1/2)^2 + \dot{\theta}^2 \leq (1/2)^2\},\\ \mathbb{A}^{\mathrm{D}} &:= \{(\dot{x}, \dot{\theta}) \in \mathbb{R}^2;\ 0 \leq |\dot{\theta}| \leq \dot{x}\}.\end{aligned} \tag{42}$$

Define $f : \mathbb{M} \times \mathbb{A} \to \mathbb{E}$ and $l : \mathbb{M} \times \mathbb{A} \to \mathbb{R}$ as

$$f((\mathbf{x}, \theta), (\dot{x}, \dot{\theta})) := -(\dot{x}\mathbf{n}(\theta), \dot{\theta})/\alpha(\mathbf{x}, \theta), \quad l((\mathbf{x}, \theta), a) := 1, \tag{43}$$

where $\alpha : \mathbb{M} \to]0, \infty[$ is the local cost function. Let also $\mathcal{T} := \mathbb{M} \setminus \Omega$ be the target region. Consider, following [2], the optimal control problem

$$\begin{aligned}v(\mathbf{p}) &:= \inf_{(a,T) \in \mathcal{A}} \int_0^T l(\mathbf{q}_{\mathbf{p},a}(t), a(t))\, e^{-t}\, \mathrm{d}t,\\ &\text{subject to } \begin{cases}\dot{\mathbf{q}}_{\mathbf{p},a}(t) = f(\mathbf{q}_{\mathbf{p},a}(t), a(t)),\ \forall t \in [0, T],\\ \mathbf{q}_{\mathbf{p},a}(0) = \mathbf{p} \text{ and } \mathbf{q}_{\mathbf{p},a}(T) \in \mathcal{T},\end{cases}\end{aligned} \tag{44}$$

where $\mathcal{A}$ consists of all pairs of (free) terminal times $T \geq 0$ and measurable function $a : [0, T] \to \mathbb{A}$. We claim that, with the choices (42), one has

$$v(\mathbf{p}) = \int_0^{u(\mathbf{p})} e^{-t} dt = 1 - \exp(-u(\mathbf{p})), \tag{45}$$

for any $\mathbf{p} \in \overline{\Omega}$. Indeed, consider a Lipschitz path $\gamma : [0, 1] \to \overline{\Omega}$ from $\partial\Omega$ to $\mathbf{p} \in \Omega$ and such that $u(\mathbf{p}) = \mathrm{length}_{\mathcal{F}}(\gamma) < \infty$. Introduce a time reparametrization $\eta : [0, T] \to \overline{\Omega}$ of γ, from $\partial\Omega$ to $\mathbf{p}$, at unit speed w.r.t. the reversed metric in the sense that $\mathcal{F}_{\eta(t)}(-\dot{\eta}(t)) = 1$ for all $t \in [0, T]$. Then, clearly $T = \mathrm{length}_{\mathcal{F}}(\gamma) = u(\mathbf{p})$, and one can uniquely define controls $a : [0, T] \to \mathbb{A}$ by $f(\eta(t), a(t)) = -\dot{\eta}(t)$ for all $t \in [0, T]$. Introducing an additional time-reversal reparametrization, $t \in [0, T] \mapsto T - t$, required since (44) considers contrary to us paths from $\mathbf{p}$ to $\partial\Omega$, we obtain $v(\mathbf{p}) \leq \int_0^T e^{-t}\mathrm{d}t = 1 - \exp(-u(\mathbf{p}))$. Conversely, admissible paths for (44) can be reparametrized into admissible paths for (7), and the identity (45) follows. Similarly, one can define $\hat{v}$ by replacing $\mathcal{T}$ with its interior in (44), and obtain that $\hat{v} = 1 - \exp(-\hat{u})$ in $\overline{\Omega}$.

The following PDEs are thus equivalent, the rightmost being the one considered in [2]

$$\begin{aligned}&\mathcal{H}_{\mathbf{p}}(\mathrm{d}u(\mathbf{p})) = \frac{1}{2}\alpha(\mathbf{p})^2, \quad \mathcal{F}^*_{\mathbf{p}}(\mathrm{d}u(\mathbf{p})) = \alpha(\mathbf{p}),\\ &v(\mathbf{p}) + \mathcal{F}_{\mathbf{p}}(\mathrm{d}v(\mathbf{p})) - \alpha(\mathbf{p}) = 0,\end{aligned}$$

where $\mathbf{p} \in \Omega$ is arbitrary. The main reason why [2] considers $v = 1 - \exp(-u)$ instead of u is that v remains bounded even for problems lacking global controllability, whereas u may take infinite values. This technicality is, however, irrelevant for the problems considered in this paper, since global controllability does hold as shown in Sect. 3.1.

Finally, we check the specific assumptions of Theorems 3.7 and 4.29 in chapter V of [2]. These are (I) the compactness of the set $\mathbb{A}$ of controls (42), (II) the Lipschitz continuity of f

and l, see (43), which follows from the Lipschitz continuity of the cost α, and its boundedness below on the compact domain $\overline{\Omega}$, and (III) the closedness of $\mathcal{T}$, following from the openness of Ω.

3.3 Continuity Properties of the Value Function

This subsection is devoted to the proof of Proposition 3.3, which describes sets where the two variants $u, \hat{u}$ of the value function coincide. The announced properties of the Reeds–Shepp reversible and the Dubins models follow from rather general arguments. Point (I) indeed follows from the locally controllability of the Reeds–Shepp reversible model, which is due to its sub-riemannian structure and to Chow's theorem, see [37] and the discussion in [21]. Hence, $u = \hat{u}$ and the value function u is in fact not only continuous, but 1/2-Holder continuous in this case. Point (IV) on the Dubins model follows from another general argument of [2], involving Baire's theorem, see Lemma 3.25. In contrast, the proof of points (II) and (III) on the Reeds–Shepp forward and Euler–Mumford models requires a geometrical pertubation argument, which involves lifting diffeomorphisms from $\mathbb{R}^2$ to $\mathbb{M} := \mathbb{R}^2 \times \mathbb{S}^1$, as presented below.

The argument $\arg(\dot{\mathbf{x}})$ of a nonzero vector $\dot{\mathbf{x}} \in \mathbb{R}^2$ is defined as the unique angle $\theta \in \mathbb{S}^1$ such that $\dot{\mathbf{x}} = \|\dot{\mathbf{x}}\|\mathbf{n}(\theta)$. The matrix vector product is denoted by "$\cdot$".

Lemma 3.18 *Let ψ be a C^n diffeomorphism of $\mathbb{R}^2$, where $n \geq 2$. Define $\Psi(\mathbf{x}, \theta) = (\mathbf{y}, \varphi)$ by*

$$\mathbf{y} := \psi(\mathbf{x}), \quad \varphi := \arg(\mathrm{d}\psi(\mathbf{x}) \cdot \mathbf{n}(\theta)), \tag{46}$$

for all $(\mathbf{x}, \theta) \in \mathbb{R}^2 \times \mathbb{S}^1$. Then, Ψ is a C^{n-1} diffeomorphism of $\mathbb{R}^2 \times \mathbb{S}^1$. Furthermore, let $(\dot{\mathbf{x}}, \dot{\theta}) \in \mathbb{R}^2 \times \mathbb{R}$ and let $(\dot{\mathbf{y}}, \dot{\varphi}) := \mathrm{d}\Psi(\mathbf{x}, \theta) \cdot (\dot{\mathbf{x}}, \dot{\theta})$. Then,

$$\underline{K}\|\dot{\mathbf{x}}\| \leq \|\dot{\mathbf{y}}\| \leq \overline{K}\|\dot{\mathbf{x}}\|, \quad |\dot{\varphi}| \leq (\overline{K}|\dot{\theta}| + K_2\|\dot{\mathbf{x}}\|)/\underline{K}, \tag{47}$$

where $\underline{K} = \|(\mathrm{d}\psi(\mathbf{x}))^{-1}\|^{-1}$, $\overline{K} := \|\mathrm{d}\psi(\mathbf{x})\|$, and $K_2 := \|\mathrm{d}^2\psi(\mathbf{x})\|$.

Proof The bijectivity of $\theta \in \mathbb{S}^1 \mapsto \varphi := \arg(\mathrm{d}\psi(\mathbf{x}) \cdot \mathbf{n}(\theta))$, for any fixed $\mathbf{x}$, follows from the invertibility of $\mathrm{d}\psi(\mathbf{x})$. The estimate (47, left) follows from the definition of the operator norm $\|A\| := \sup_{\dot{\mathbf{x}} \neq 0} \|A\dot{\mathbf{x}}\|/\|\dot{\mathbf{x}}\|$ of a matrix A. The upper bound on $|\dot{\varphi}|$ is obtained by composing the following two Taylor expansions: the first one

$$\arg(\mathbf{x} + \dot{\mathbf{x}}) = \arg(\mathbf{x}) + \|\mathbf{x}\|^{-2}\langle \mathbf{x}^{\perp}, \dot{\mathbf{x}} \rangle + o(\|\dot{\mathbf{x}}\|),$$

is obtained by basic geometric reasoning, and the second one

$$\mathrm{d}\psi(\mathbf{x} + \dot{\mathbf{x}}) \cdot \mathbf{n}(\theta + \dot{\theta}) = \mathrm{d}\psi(\mathbf{x}) \cdot \mathbf{n}(\theta) + (\mathrm{d}^2\psi(\mathbf{x}) \cdot \dot{\mathbf{x}}) \cdot \mathbf{n}(\theta) + \dot{\theta}\mathrm{d}\psi(\mathbf{x}) \cdot \mathbf{n}(\theta)^{\perp} + o(\|\dot{\mathbf{x}}\| + |\dot{\theta}|),$$

by bilinearity of the matrix-vector product. □

The next lemma upper bounds the composition of the metric, of the models RS+, RS± and EM, with the tangent map to a diffeomorphism of the form (46). No similar estimate can be established for the Dubins metric, due to the hard constraint $|\xi\dot{\theta}| \leq \|\dot{\mathbf{x}}\|$ appearing in (26).

Lemma 3.19 *Under the assumptions of Lemma 3.18, denoting $\mathbf{p} := (\mathbf{x}, \theta)$, $\dot{\mathbf{p}} := (\dot{\mathbf{x}}, \dot{\theta})$, $\mathbf{q} := (\mathbf{y}, \varphi)$ and $\dot{\mathbf{q}} := (\dot{\mathbf{y}}, \dot{\varphi})$, one has*

$$\mathcal{F}^{RS+}_{\mathbf{q}}(\dot{\mathbf{q}}) \leq K_{RS}\mathcal{F}^{RS+}_{\mathbf{p}}(\dot{\mathbf{p}}), \quad \mathcal{F}^{RS\pm}_{\mathbf{q}}(\dot{\mathbf{q}}) \leq K_{RS}\mathcal{F}^{RS\pm}_{\mathbf{p}}(\dot{\mathbf{p}}),$$
$$\mathcal{F}^{EM}_{\mathbf{q}}(\dot{\mathbf{q}}) \leq K_{EM}\mathcal{F}^{EM}_{\mathbf{p}}(\dot{\mathbf{p}}),$$

with $K^2_{RS} := \max\{\overline{K}^2 + \xi^2\varepsilon(1+\varepsilon),\ (1+\varepsilon)\underline{K}\}$ and $K_{EM} := \max\{\overline{K} + \xi^2\varepsilon(1+\varepsilon)/\underline{K},\ (1+\varepsilon)\overline{K}^2/\underline{K}\}$, where $\varepsilon := K_2/\underline{K}$ and $\overline{K} := \overline{K}/\underline{K}$.

Proof By construction of the diffeomorphism Ψ, the colinearity constraint involved in the Definition (3) of the metrics is preserved: $\dot{\mathbf{x}} = \|\dot{\mathbf{x}}\|\mathbf{n}(\theta) \Rightarrow \dot{\mathbf{y}} = \|\dot{\mathbf{y}}\|\mathbf{n}(\varphi)$, and likewise for the unsigned colinearity constraint $\dot{\mathbf{x}} = \langle \dot{\mathbf{x}}, \mathbf{n}(\theta)\rangle\mathbf{n}(\theta) \Rightarrow \dot{\mathbf{y}} = \langle \dot{\mathbf{y}}, \mathbf{n}(\varphi)\rangle\mathbf{n}(\varphi)$. Using the inequality $(a+\varepsilon b)^2 \leq (1+\varepsilon)(a^2+\varepsilon b^2)$, valid for any $a, b \in \mathbb{R}, \varepsilon > 0$, we obtain as announced

$$\begin{aligned}
\|\dot{\mathbf{y}}\|^2 + \xi^2\dot{\varphi}^2 &\leq (\overline{K}\|\dot{\mathbf{x}}\|)^2 + \xi^2(\overline{K}\dot{\theta} + \varepsilon\|\dot{\mathbf{x}}\|)^2 \\
&\leq \left(\overline{K}^2 + \xi^2\varepsilon(1+\varepsilon)\right)\|\dot{\mathbf{x}}\|^2 + (1+\varepsilon)\overline{K}^2\xi^2\dot{\theta}^2 \\
\|\dot{\mathbf{y}}\| + \xi^2\frac{\dot{\varphi}^2}{\|\dot{\mathbf{y}}\|} &\leq \overline{K}\|\dot{\mathbf{x}}\| + \xi^2\frac{(\overline{K}\dot{\theta}^2 + \varepsilon\|\dot{\mathbf{x}}\|)^2}{\underline{K}\|\dot{\mathbf{x}}\|} \\
&\leq (\overline{K} + \xi^2\varepsilon(1+\varepsilon)/\underline{K})\|\dot{\mathbf{x}}\| \\
&\quad + (1+\varepsilon)\frac{\overline{K}^2}{\underline{K}}\xi^2\frac{\dot{\theta}^2}{\|\dot{\mathbf{x}}\|}.
\end{aligned}$$

□

The previous lemma is next specialized to diffeomorphisms defined by the flow of a vector field.

Corollary 3.20 *Let $v : \mathbb{R}^2 \to \mathbb{R}^2$ be a vector field with continuous and uniformly bounded first and second derivatives. Let $(\psi_t)_{t\geq 0}$ be the family of C^2 diffeomorphisms of $\mathbb{R}^2$ defined by*

$$\psi_0(\mathbf{x}) = \mathbf{x}, \quad \frac{\mathrm{d}}{\mathrm{d}t}\psi_t(\mathbf{x}) = v(\psi(\mathbf{x})), \tag{48}$$

for any $\mathbf{x} \in \mathbb{R}^2$. Then, for any path $\gamma \in \mathrm{Lip}([0,1], \mathbb{R}^2 \times \mathbb{S}^1)$ one has $\mathrm{length}_{\mathcal{F}}(\Psi_t \circ \gamma) \leq (1 + Ct)\,\mathrm{length}_{\mathcal{F}}(\gamma)$ where $C = C(v, \xi)$, where Ψ_t is defined from ψ_t by (46), and where the metric $\mathcal{F}$ is $\mathcal{F}^{RS+}$, $\mathcal{F}^{RS\pm}$ or $\mathcal{F}^{EM}$.

Proof Define for any $t \geq 0$ the constants

$$\underline{K}(t) := \inf_{\mathbf{x}\in\mathbb{R}^2} \|(\mathrm{d}\psi_t(\mathbf{x}))^{-1}\|^{-1},$$
$$\overline{K}(t) := \sup_{\mathbf{x}\in\mathbb{R}^2} \|\mathrm{d}\psi_t(\mathbf{x})\|, \quad K_2(t) := \sup_{\mathbf{x}\in\mathbb{R}^2} \|\mathrm{d}^2\psi_t(\mathbf{x})\|.$$

The Taylor expansion $\psi_t(\mathbf{x}) = \mathbf{x} + t\nu(\mathbf{x}) + o(t)$ can be differentiated twice w.r.t. $\mathbf{x} \in \mathbb{R}^2$ since the two sides are C^2 smooth. This yields $\mathrm{d}\psi_t(\mathbf{x}) = \mathrm{Id} + t\mathrm{d}\nu(\mathbf{x}) + o(t)$ and $\mathrm{d}^2\psi_t(\mathbf{x}) = t\mathrm{d}^2\nu(\mathbf{x}) + o(t)$. Hence, $\underline{K}(t) = 1 + \mathcal{O}(t)$, $\overline{K}(t) = 1 + \mathcal{O}(t)$ and $K_2(t) = \mathcal{O}(t)$. Therefore, the corresponding constants of Lemma 3.19 obey $K_{\mathrm{RS}}(t) = 1 + \mathcal{O}(t)$ and $K_{\mathrm{EM}}(t) = 1 + \mathcal{O}(t)$. Inserting these estimates into the path length expression (5), and using the Lipschitz regularity of the cost function α, we obtain the announced result. □

The following lemma further specializes the diffeomorphisms considered, which are designed so as to offset one endpoint of a given path, and leave the other endpoint unaffected.

Lemma 3.21 *Let $\gamma : [0, 1] \to \mathbb{R}^2 \times \mathbb{S}^1$ be a Lipschitz path. Denote $\gamma(0) = (\mathbf{x}_0, \theta_0)$, $\gamma(1) := (\mathbf{x}_1, \theta_1)$, and assume that $\mathbf{x}_0 \neq \mathbf{x}_1$. Let $\mathcal{F}$ be $\mathcal{F}^{RS+}$, $\mathcal{F}^{RS\pm}$ or $\mathcal{F}^{EM}$ and let us assume that $\mathrm{length}_{\mathcal{F}}(\gamma) < \infty$. Then, there exists a family of diffeomorphisms $\psi_{\dot{\mathbf{p}}}$, $\dot{\mathbf{p}} \in \mathbb{R}^2 \times \mathbb{R}$ such that: for any sufficiently small $\dot{\mathbf{p}}$*

$$\mathrm{length}_{\mathcal{F}}(\psi_{\dot{\mathbf{p}}} \circ \gamma) \leq (1 + \mathcal{O}(\|\dot{\mathbf{p}}\|))\, \mathrm{length}_{\mathcal{F}}(\gamma),$$
$$\psi_{\dot{\mathbf{p}}}(\gamma(0)) = \gamma(0) + \dot{\mathbf{p}}, \quad \psi_{\dot{\mathbf{p}}}(\gamma(1)) = \gamma(1).$$

Proof Denote $r := \|\mathbf{x}_0 - \mathbf{x}_1\| > 0$. Let $\nu_1, \nu_2, \nu_3 : \mathbb{R}^2 \to \mathbb{R}^2$ be smooth vector fields supported on $B(\mathbf{x}_0, r/2)$, and defined by $\nu_1(\mathbf{x}) = (1, 0)$, $\nu_2(\mathbf{x}) = (0, 1)$, and $\nu_3(\mathbf{x}) = \mathbf{x}_0 + (\mathbf{x} - \mathbf{x}_0)^{\perp}$, respectively, for all $\mathbf{x} \in B(\mathbf{x}_0, r/4)$, where $B(\mathbf{x}, r) \subseteq \mathbb{R}^2$ denotes the Euclidean unit ball centered at $\mathbf{x} \in \mathbb{R}^2$ and of radius $r > 0$. Let ψ_t^{ν} denote the diffeomorphism generated by the flow at time t of a vector field ν, as defined in (48).

By construction, one has $\psi_{t_1}^{\nu_1}(\mathbf{x}, \theta) = (\mathbf{x} + (t_1, 0), \theta)$, $\psi_{t_2}^{\nu_2}(\mathbf{x}, \theta) = (\mathbf{x} + (0, t_2), \theta)$, and $\psi_{t_3}^{\nu_3}(\mathbf{x}, \theta) = (\mathbf{x}_0 + R_{t_3}(\mathbf{x} - \mathbf{x}_0), \theta + t_3)$ for any sufficiently small $t_1, t_2, t_3 \in \mathbb{R}$, for any $\mathbf{x} \in \mathbb{R}^2$ sufficiently close to $\mathbf{x}_0$, and for any $\theta \in \mathbb{R}$. Also $\psi_{t_1}^{\nu_1} = \psi_{t_2}^{\nu_2} = \psi_{t_3}^{\nu_3} = \mathrm{Id}$ on a neighborhood of $\mathbf{x}_1$, for any $t_1, t_2, t_3 \in \mathbb{R}$. Defining $\psi_{\dot{\mathbf{p}}} := \psi_{t_1}^{\nu_1} \circ \psi_{t_2}^{\nu_2} \circ \psi_{t_3}^{\nu_3}$, where $\dot{\mathbf{p}} = (t_1, t_2, t_3) \in \mathbb{R}^2 \times \mathbb{R}$, and using Corollary 3.20 one obtains the announced result. □

Points (II) and (III) of Proposition 3.3 are established in the next proposition and corollary. For that purpose, we need to distinguish a particular class of degenerate paths: we say that $\gamma : [0, 1] \to \mathbb{R}^2 \times \mathbb{S}^1$ is a *purely angular motion* iff it has the form $\gamma(t) = (\mathbf{x}, \theta(t))$, for all $t \in [0, 1]$, where $\mathbf{x} \in \mathbb{R}^2$ is a constant and $\theta : [0, 1] \to \mathbb{S}^1$ is an arbitrary function.

Proposition 3.22 *Let $\mathbf{p} \in \Omega$ be such that the minimal path $\gamma : [0, 1] \to \overline{\Omega}$ for $u(\mathbf{p})$ is not a purely angular motion. Assume also that $\mathrm{int}(\overline{\Omega}) = \Omega$, and the model is Reeds–Shepp forward or Euler–Mumford. Then, $u(\mathbf{p}) = \hat{u}(\mathbf{p})$.*

Proof As noted in Introduction, a minimal path γ exists by Appendix A of [14] (it may be non-unique). Since γ is not a purely angular motion, there exists $t_* \in]0, 1]$ such that denoting $\mathbf{p}_0 = (\mathbf{x}_0, \theta_0) = \gamma(0)$ and $\mathbf{p}_1 = (\mathbf{x}_1, \theta_1) = \gamma(t_*)$ one has $\mathbf{x}_0 \neq \mathbf{x}_1$. Denote $\gamma_0 := \gamma_{|[0,t_*]}$ and $\gamma_1 := \gamma_{|[t_*,1]}$. For any sufficiently small $\dot{\mathbf{p}} \in \mathbb{R}^2 \times \mathbb{R}$, we may construct an admissible path from $\mathbf{p}_0 + \dot{\mathbf{p}}$ to $\mathbf{p} = \gamma(1)$, by concatenation of $\psi_{\dot{\mathbf{p}}} \circ \gamma_0$ with γ_1, where $\psi_{\dot{\mathbf{p}}}$ is as defined in Lemma 3.21. If $\mathbf{p}_0 + \dot{\mathbf{p}} \in \mathbb{M} \setminus \overline{\Omega}$, this implies

$$\begin{aligned}\hat{u}(\mathbf{p}) &\leq \mathrm{length}_{\mathcal{F}}(\psi_{\dot{\mathbf{p}}} \circ \gamma_0) + \mathrm{length}_{\mathcal{F}}(\gamma_1)\\ &\leq (1 + \mathcal{O}(\|\dot{\mathbf{p}}\|))\, \mathrm{length}_{\mathcal{F}}(\gamma) = (1 + \mathcal{O}(\|\dot{\mathbf{p}}\|))u(\mathbf{p}).\end{aligned}$$

The assumption $\mathrm{int}(\overline{\Omega}) = \Omega$ implies that one can find arbitrarily small $\dot{\mathbf{p}} \in \mathbb{E}$ such that $\mathbf{p}_0 + \dot{\mathbf{p}} \in \mathbb{M} \setminus \overline{\Omega}$, hence $\hat{u}(\mathbf{p}) \leq u(\mathbf{p})$. Finally, $\hat{u}(\mathbf{p}) = u(\mathbf{p})$ since by construction $\hat{u}(\mathbf{p}) \geq u(\mathbf{p})$. □

Corollary 3.23 *Under the assumptions of Proposition 3.3. The Reeds–Shepp forward model satisfies $u = \hat{u}$ on Ω if this domain has the shape $\Omega = U \times \mathbb{S}^1$. The Euler–Mumford model satisfies $u = \hat{u}$ on Ω.*

Proof We only need to show that purely angular motions cannot be minimizing for the optimal control problem (7) under these assumptions, and apply Lemma 3.21. In the case where $\Omega = U \times \mathbb{S}^1$, the domain shape forbids that a purely angular motion has one endpoint in $\partial\Omega$ and the other in Ω, hence it is not even an admissible candidate path. In the Euler–Mumford case, any non-constant purely angular motion has infinite length, hence it cannot be minimizing. □

The continuity of the value function(s) u and $\hat{u}$ at the points where $u = \hat{u}$, announced in Proposition 3.3, follows the next elementary lemma. Recall that u and $\hat{u}$ are, respectively, BLSC and BUSC, since they are sub- and super-solutions of (39), see Proposition 3.17.

Lemma 3.24 *Let (X, d) be a metric space, and let $u, \hat{u} : X \to \mathbb{R}$ be, respectively, LSC and USC, and obey $u \leq \hat{u}$ on X. If $\mathbf{p} \in X$ is such that $u(\mathbf{p}) = \hat{u}(\mathbf{p})$, then u and $\hat{u}$ are continuous at $\mathbf{p}$.*

Proof Let $(\mathbf{p}_n)_{n\geq 0}$ be an arbitrary sequence converging to $\mathbf{p} \in X$. Using successively that u is LSC, that $u \leq \hat{u}$, and that $\hat{u}$ is USC, one obtains

$$u(\mathbf{p}) \leq \liminf_{n\to\infty} u(\mathbf{p}_n) \leq \limsup_{n\to\infty} \hat{u}(\mathbf{p}_n) \leq \hat{u}(\mathbf{p}).$$

If $u(\mathbf{p}) = \hat{u}(\mathbf{p})$, then the sequences $u(\mathbf{p}_n)$ and $\hat{u}(\mathbf{p}_n)$ must be converging to this common limit, which implies the announced continuity of u and $\hat{u}$ at $\mathbf{p}$. □

Finally, we discuss the case of the Dubins model. By Corollary 4.30 in section V [2] (which uses in particular the assumption $\mathrm{int}(\overline{\Omega}) = \Omega$), one has $\hat{u}_* = u \leq \hat{u}$, where v_* (resp. v^*) denotes the lower (resp. upper) semi-continuous envelope of a function v. Hence, $u = \hat{u}$ at each point of continuity of $\hat{u}$. The next elementary lemma shows that these points are dense, which concludes the proof of Proposition 3.3. Recall that a residual set is an intersection of open dense sets, i.e., the complement of a meager set, and that by Baire's theorem any residual subset of a complete metric space is dense.

Lemma 3.25 *Let (X, d) be a metric space, and let $u : X \to \mathbb{R}$ be BLSC or BUSC. Then, the points of continuity of u form a residual set.*

Proof We focus on the BLSC case and note that the BUSC case follows by considering $-u$. Let u^* be the upper semi-continuous envelope of u, and for each $n \geq 1$ let $C_n := \{\mathbf{x} \in X;\ u^*(\mathbf{x}) - u(\mathbf{x}) < 1/n\}$. For any $\mathbf{x} \in X$, one has the equivalences:

$$u \text{ is continuous at } \mathbf{x} \Leftrightarrow u^*(\mathbf{x}) = u(\mathbf{x}) \Leftrightarrow \mathbf{x} \in \cap_{n\geq 1} C_n.$$

In the following, we fix $n \geq 1$ and establish that C_n is open and dense, and hence $\cap_{n\geq 1} C_n$ is a residual set which concludes the proof. The openness of C_n follows from the upper semi-continuity of $u^* - u$. Assume for contradiction that C_n is not dense, and hence that there exists an open ball $B(\mathbf{x}_0, r)$ on which $u^* - u \geq 1/n$ identically. Let also $M := \sup\{u(\mathbf{x}) - u(\mathbf{y});\ \mathbf{x}, \mathbf{y} \in X\}$, which is finite by assumption.

Let $K > 2nM$ be an integer. We construct inductively a sequence $(\mathbf{x}_k)_{0\leq k\leq K}$ by choosing $\mathbf{x}_{k+1}$ such that $d(\mathbf{x}_k, \mathbf{x}_{k+1}) < r/K$ and $u(\mathbf{x}_{k+1}) > u(\mathbf{x}_k) + 1/(2n)$. This is possible since $d(\mathbf{x}_k, \mathbf{x}_0) < kr/K \leq r$, hence $\mathbf{x}_k \notin C_n$, thus $u(\mathbf{x}_k) + 1/(2n) < u^*(\mathbf{x}_k) = \limsup_{y\to\mathbf{x}_k} u(\mathbf{y})$. Eventually, we obtain $u(\mathbf{x}_K) - u(\mathbf{x}_0) = \sum_{i=0}^{K-1} u(\mathbf{x}_{i+1}) - u(\mathbf{x}_i) > K/(2n) \geq M$, which contradicts the definition of M. Hence, C_n must be dense, and the proof is complete. □

4 Basis Reduction Techniques

This section is devoted to the proof of Proposition 2.2, using techniques from lattice geometry. For that purpose, we study an optimization problem referred to as Voronoi's first reduction in quadratic forms [50], using special coordinate systems known as obtuse superbases of lattices [17]. Similar techniques are used for the discretization on cartesian grids of anisotropic diffusion in [10,26], of Monge-Ampere equations in [4], and of anisotropic eikonal equations in [36].

We first need to introduce some notation. Let $d \geq 1$ be the ambient dimension, $d \in \{2, 3\}$ for the applications intended in this paper. The canonical d-dimensional Euclidean space, and d-dimensional integer lattice are denoted

$$\mathbb{E}_d := \mathbb{R}^d, \qquad \mathbb{L}_d := \mathbb{Z}^d.$$

The dual space and dual lattice are denoted $\mathbb{E}_d^*$ and $\mathbb{L}_d^*$. Thanks to the Euclidean structure, there is a canonical identification $\mathbb{E}_d \cong \mathbb{E}_d^*$ and $\mathbb{L}_d \cong \mathbb{L}_d^*$, but the distinction is kept for clarity. Let $\mathrm{S}(\mathbb{E}_d) \subseteq \mathrm{L}(\mathbb{E}_d, \mathbb{E}_d^*)$ denote the set of symmetric linear maps, and let $\mathrm{S}^{++}(\mathbb{E}_d) \subseteq \mathrm{S}^{+}(\mathbb{E}_d) \subseteq \mathrm{S}(\mathbb{E}_d)$ be the subsets of positive definite and semi-definite ones. To each $M \in \mathrm{S}^{++}(\mathbb{E}_d)$ is associated a scalar product $\langle \cdot, \cdot \rangle_M$ and a norm $\| \cdot \|_M$, defined for all $\dot{\mathbf{e}}, \dot{\mathbf{f}} \in \mathbb{E}_d$ by

$$\langle \dot{\mathbf{e}}, \dot{\mathbf{f}} \rangle_M := \langle M\dot{\mathbf{e}}, \dot{\mathbf{f}} \rangle, \quad \|\dot{\mathbf{e}}\|_M := \sqrt{\langle \dot{\mathbf{e}}, \dot{\mathbf{e}} \rangle_M}.$$

Let us point out that it is equivalent, up to a linear change of coordinates, to study the geometry of an arbitrary lattice of $\mathbb{E}_d$ w.r.t. the canonical Euclidean norm, or to study the geometry of the canonical lattice $\mathbb{L}_d$ w.r.t. the norm $\| \cdot \|_M$ induced by an arbitrary $M \in \mathrm{S}^{++}(\mathbb{E}_d)$.

Voronoi's first reduction [50] consists of a convex set $\mathcal{P} \subseteq \mathrm{S}^{++}(\mathbb{E}_d^*)$, and for each $M \in \mathrm{S}^{++}(\mathbb{E}_d)$ of a linear programming problem $\mathcal{L}(M)$:

$$\begin{aligned} \mathcal{P} &:= \{D \in \mathrm{S}^{++}(\mathbb{E}_d^*);\ \forall \hat{\mathbf{v}} \in \mathbb{L}_d^* \setminus \{0\},\ \|\hat{\mathbf{v}}\|_D \geq 1\}, \\ \mathcal{L}(M) &:= \inf_{D\in\mathcal{P}} \mathrm{Tr}(MD). \end{aligned} \tag{49}$$

Denote by $\langle\!\langle M, D \rangle\!\rangle := \mathrm{Tr}(MD)$ the duality bracket between $\mathrm{S}(\mathbb{E})$ and $\mathrm{S}(\mathbb{E}^*)$, and observe that $\|\hat{\mathbf{v}}\|_D^2 = \langle\!\langle D, \hat{\mathbf{v}} \otimes \hat{\mathbf{v}} \rangle\!\rangle$, where $\hat{\mathbf{v}} \otimes \hat{\mathbf{v}} \in \mathrm{S}^{+}(\mathbb{E}_d)$ denotes the outer product of a co-vector $\hat{\mathbf{v}} \in \mathbb{E}_d^*$ with itself. Note also that the semi-definite constraint $D \succ 0$ in (49, left) is redundant. One can therefore rephrase Voronoi's optimization problem $\mathcal{L}(M)$ to make its linear structure more apparent:

$$\text{minimize } \langle\!\langle M, D \rangle\!\rangle \text{ subject to } \langle\!\langle D, \hat{\mathbf{v}} \otimes \hat{\mathbf{v}} \rangle\!\rangle \geq 1 \text{ for all } \hat{\mathbf{v}} \in \mathbb{L}_d^* \setminus \{0\}. \tag{50}$$

The linear program (50) was shown by Voronoi to be feasible in arbitrary dimension $d \geq 1$, in the sense that $\mathcal{L}(M)$ has a non-empty and compact set of minimizers for any $M \in \mathrm{S}^{++}(\mathbb{E}_d)$. The Karush–Kuhn–Tucker optimality conditions for this problem read as follows: there exists nonnegative weights $\lambda_k \geq 0$ and integral co-vectors $\hat{\mathbf{v}}_k \in \mathbb{L}_d^*$, where $1 \leq k \leq d' := \dim \mathrm{S}(\mathbb{E}_d) = d(d+1)/2$, such that

$$M = \sum_{1\leq k\leq d'} \lambda_k \hat{\mathbf{v}}_k \otimes \hat{\mathbf{v}}_k. \tag{51}$$

This formula is reminiscent of the eigenvector-eigenvalue decomposition, but the co-vectors $\hat{\mathbf{v}}_k$ have integer coordinates, and the number of terms is larger: $d(d+1)/2$ instead of d. It is used to design monotone finite differences PDE schemes in [10,26,36], implicitly in the first two references. In Sect. 4.1 we describe Selling's algorithm which is a constructive, simple and efficient method for solving (50) in dimension $d \leq 3$, used as is in our numerical experiments. We estimate in Sect. 4.2 the largest norm of the co-vectors appearing in (51). We finally conclude in Sect. 4.3 the proof of Proposition 2.2.

4.1 Obtuse Superbases and Selling's Algorithm

We introduce in this section the concept of obtuse superbase of lattice, a preferred coordinate system which provides, in particular, a complete solution to Voronoi's first reduction (49), see Proposition 4.6. An obtuse superbase exists for all lattices of dimension two and three and can be constructed using Selling's algorithm, see Proposition 4.7. The results of this subsection are mostly reformulations of [9,17], but they are prerequisites for the original results of the next subsections. Proofs are provided for completeness.

Definition 4.1 A superbase of $\mathbb{L}_d$ is a $(d+1)$ tuple $(\dot{\mathbf{e}}_0, \dots, \dot{\mathbf{e}}_d) \in \mathbb{L}_d^{d+1}$ such that $\dot{\mathbf{e}}_0 + \cdots + \dot{\mathbf{e}}_d = 0$ and $|\det(\dot{\mathbf{e}}_0, \dots, \dot{\mathbf{e}}_d)| = 1$. A superbase is said M-obtuse, where $M \in \mathrm{S}^{++}(\mathbb{E}_d)$, iff $\langle \dot{\mathbf{e}}_i, \dot{\mathbf{e}}_j \rangle_M \leq 0$ for all $0 \leq i < j \leq d$.

We attach to each superbase a family of $d(d+1)$ co-vectors.

Definition 4.2 Let $(\dot{\mathbf{e}}_0, \dots, \dot{\mathbf{e}}_d)$ be a superbase of $\mathbb{L}_d$. For all distinct $i, j \in [\![0, d]\!]$, we define a co-vector $\hat{\mathbf{v}}_{ij} \in \mathbb{L}_d^*$ by the linear equalities

$$\langle \hat{\mathbf{v}}_{ij}, \dot{\mathbf{e}}_k \rangle = \delta_{ik} - \delta_{jk}, \quad \text{for all } 0 \leq k \leq d, \tag{52}$$

Note that $\hat{\mathbf{v}}_{ij} = -\hat{\mathbf{v}}_{ji}$ and that the definition (52) of the d-dimensional co-vector $\hat{\mathbf{v}}_{ij}$ using $d+1$ linear constraints makes sense thanks to the (single) redundancy relation

$$\begin{aligned} &\langle \hat{\mathbf{v}}_{ij}, \dot{\mathbf{e}}_0 + \cdots + \dot{\mathbf{e}}_d \rangle = \langle \hat{\mathbf{v}}_{ij}, 0 \rangle = 0, \\ &\text{and } (\delta_{i0} - \delta_{j0}) + \cdots + (\delta_{id} - \delta_{jd}) = \delta_{ii} - \delta_{jj} = 0. \end{aligned}$$

In dimension $d \in \{2, 3\}$, the construction of Definition 4.2 has a simple geometrical interpretation

$$\begin{aligned} &\text{Case } d = 2 : \hat{\mathbf{v}}_{ij} = \pm \dot{\mathbf{e}}_k^{\perp}, \\ &\text{Case } d = 3 : \hat{\mathbf{v}}_{ij} = \pm \dot{\mathbf{e}}_k \times \dot{\mathbf{e}}_l, \end{aligned} \tag{53}$$

where (i, j, k) is a permutation of $\{0, 1, 2\}$, (resp. (i, j, k, l) of $\{0, 1, 2, 3\}$), and the $\pm$ sign refers to its signature.

Proposition 4.3 *With the notations of Definition 4.2,* $(\hat{\mathbf{v}}_{01}, \hat{\mathbf{v}}_{12}, \cdots, \hat{\mathbf{v}}_{d0})$ *is a superbase of* $\mathbb{L}_d^*$.

Proof By construction $\langle \hat{\mathbf{v}}_{01} + \cdots + \hat{\mathbf{v}}_{d0}, \dot{\mathbf{e}}_k \rangle = 0$ for any $0 \leq k \leq d$, hence $\hat{\mathbf{v}}_{01} + \cdots + \hat{\mathbf{v}}_{d0} = 0$ as required. Furthermore, using the change of basis formula for determinants one obtains

$$\begin{aligned} \det(\hat{\mathbf{v}}_{12}, \dots, \hat{\mathbf{v}}_{d0}) \det(\dot{\mathbf{e}}_1, \dots, \dot{\mathbf{e}}_d) &= \det\left[\hat{\mathbf{v}}_{i,i+1}(\dot{\mathbf{e}}_j)\right]_{i,j=1}^d \\ &= \det\left[\delta_{i,j} - \delta_{i+1,j}\right]_{i,j=1}^d \\ &= 1. \end{aligned}$$

□

The next lemma describes the decomposition of a symmetric matrix M using the directions $\hat{\mathbf{v}}_{ij} \in \mathbb{L}_d^*$ attached to a superbase. As one can suspect, it is related to the KKT relations (51), see Proposition 4.6.

Lemma 4.4 *Let* $M \in \mathrm{S}(\mathbb{E}_d)$, *and let* $(\dot{\mathbf{e}}_0, \dots, \dot{\mathbf{e}}_d)$ *be a superbase of* $\mathbb{Z}^d$. *Then,*

$$M = \sum_{i<j} \lambda_{ij}\, \hat{\mathbf{v}}_{ij} \otimes \hat{\mathbf{v}}_{ij}, \quad \textit{where } \lambda_{ij} := -\langle \dot{\mathbf{e}}_i, M \dot{\mathbf{e}}_j \rangle \tag{54}$$

Proof For any $i, j, k, l \in [\![0, d]\!]$ such that $i \neq j$ and $k \neq l$, one has $\langle \hat{\mathbf{v}}_{ij}, \dot{\mathbf{e}}_k \rangle \langle \hat{\mathbf{v}}_{ij}, \dot{\mathbf{e}}_l \rangle = -1$ if $\{i, j\} = \{k, l\}$, and 0 otherwise. Hence, denoting by M' the r.h.s. of (54) one has $\langle \dot{\mathbf{e}}_k, M' \dot{\mathbf{e}}_l \rangle = -\lambda_{kl} = \langle \dot{\mathbf{e}}_k, M \dot{\mathbf{e}}_l \rangle$ for all $k \neq l$. Equality also holds if $k = l$, using the identity $\dot{\mathbf{e}}_k = -\sum_{i \neq k} \dot{\mathbf{e}}_i$. Since $(\dot{\mathbf{e}}_1, \dots, \dot{\mathbf{e}}_d)$ is a basis of $\mathbb{E}_d$, this implies $M = M'$ as announced. □

The following lemma attaches to any superbase b of $\mathbb{L}_d$ a *vertex* D_b of the polytope $\mathcal{P}$, defined in (49). Vertices of $\mathcal{P}$ are referred to as *perfect forms*, and play a central role in lattice geometry [50]. Interestingly, Voronoi proved that the polytope $\mathcal{P}$ has only finitely many distinct equivalence classes of vertices under the action of linear changes of coordinates preserving the lattice $\mathbb{L}_d$, see [50]. The perfect forms $\{D_b;\ b \text{ superbase of } \mathbb{L}_d\}$ are such a class, and in fact are the only one[4] in dimension $d \leq 3$.

Lemma 4.5 *Let* $b = (\dot{\mathbf{e}}_0, \dots, \dot{\mathbf{e}}_d)$ *be a superbase of* $\mathbb{L}_d$, *and let*

$$D_b := \frac{1}{2^d} \sum_{I \subseteq [\![0,d]\!]} \dot{\mathbf{e}}_I \otimes \dot{\mathbf{e}}_I, \quad \textit{where } \dot{\mathbf{e}}_I := \sum_{i \in I} \dot{\mathbf{e}}_i.$$

Then, $\|\hat{\mathbf{v}}_{ij}\|_{D_b} = 1$ *for all* $0 \leq i < j \leq d$ *and* $\|\hat{\mathbf{v}}\|_{D_b} \geq 1$ *for any* $\hat{\mathbf{v}} \in \mathbb{L}_d^* \setminus \{0\}$. *In particular,* D_b *is a vertex of the polytope* $\mathcal{P} \subseteq \mathrm{S}(\mathbb{E}_d)$, *at the intersection of the facets defined by* $\{D \in \mathcal{P};\ \langle\!\langle D, \hat{\mathbf{v}}_{ij} \otimes \hat{\mathbf{v}}_{ij} \rangle\!\rangle = 1\}$, $i, j \in [\![0, d]\!]$.

[4] Indeed, as shown below in Proposition 4.6, the minimum (49) of the linear program $\mathcal{L}(M)$ on K is always attained at a matrix D_b attached to a superbase b.

Proof Let $\delta_i^I = 1$ if $i \in I$ and $\delta_i^I = 0$ otherwise, for any $i \in [\![0,d]\!]$ and $I \subseteq [\![0,d]\!]$. Clearly, $(\delta_i^I)^2 = \delta_i^I$, and for any pairwise distinct $i_0, \dots, i_k \in [\![0,d]\!]$ one has

$$\sum_{I \subseteq [\![0,d]\!]} \delta_{i_0}^I \cdots \delta_{i_k}^I = \#\{I \subseteq [\![0,d]\!];\ \{i_0, \cdots, i_k\} \subseteq I\} = 2^{d-k}.$$

Hence, for any pairwise distinct $i, j, k, l \in [\![0,d]\!]$, noting that $\langle \hat{\mathbf{v}}_{ij}, \dot{\mathbf{e}}_I \rangle = \delta_i^I - \delta_j^I$ for any $I \subseteq [\![0,d]\!]$,

$$\begin{aligned} 2^d \langle \hat{\mathbf{v}}_{ij}, \hat{\mathbf{v}}_{ik} \rangle_{D_b} &= \sum_{I \subseteq [\![0,d]\!]} (\delta_i^I - \delta_j^I)(\delta_i^I - \delta_k^I) \\ &= \sum_{I \subseteq [\![0,d]\!]} (\delta_i^I - \delta_i^I \delta_j^I - \delta_i^I \delta_k^I + \delta_j^I \delta_k^I) \\ &= 2^d - 2^{d-1} - 2^{d-1} + 2^{d-1}. \end{aligned}$$

This establishes $\langle \hat{\mathbf{v}}_{ij}, \hat{\mathbf{v}}_{ik} \rangle_{D_b} = 1/2$. Likewise $\langle \hat{\mathbf{v}}_{ij}, \hat{\mathbf{v}}_{kl} \rangle_{D_b} = 0$, and $\|\hat{\mathbf{v}}_{ij}\|_{D_b}^2 = \langle \hat{\mathbf{v}}_{ij}, \hat{\mathbf{v}}_{ij} \rangle_{D_b} = 1$ as announced. Since $(\hat{\mathbf{v}}_{12}, \cdots, \hat{\mathbf{v}}_{d0})$ is a basis of $\mathbb{L}_d^*$, see Proposition 4.3, we obtain by bilinearity that $\|\hat{\mathbf{v}}\|_{D_b}^2 \in \mathbb{Z}$ for all $\hat{\mathbf{v}} \in \mathbb{L}_d^*$. Since D_b is positive definite, one has $\|\hat{\mathbf{v}}\|_{D_b} > 0$ for all $\hat{\mathbf{v}} \in \mathbb{E}_d^* \setminus \{0\}$, hence $\|\hat{\mathbf{v}}\|_{D_b} \geq 1$ for all $\hat{\mathbf{v}} \in \mathbb{L}_d^* \setminus \{0\}$ as announced.

By definition $D_b \in \mathcal{P}$, and D_b obeys the $d(d+1)/2 = \dim \mathrm{S}(\mathbb{E}_d)$ linear equalities $\langle\!\langle D_b, \hat{\mathbf{v}}_{ij} \otimes \hat{\mathbf{v}}_{ij} \rangle\!\rangle = 1$, for all $0 \leq i < j \leq d$, which are linearly independent by Lemma 4.4. Thus D_b is a vertex of $\mathcal{P}$. □

The two previous lemmas, combined, yield a complete solution to the optimization problem (49), when an M-obtuse superbase is known.

Proposition 4.6 *Let $M \in \mathrm{S}^{++}(\mathbb{E}_d)$, and let us assume that there exists an M-obtuse superbase b of $\mathbb{L}_d$. Then, D_b is a minimizer of $\mathcal{L}(M)$, and applying Lemma 4.4 to the basis b yields the explicit value $\mathcal{L}(M) = \sum_{i<j} \lambda_{ij}$, as well as an optimality certificate: the Karush–Kuhn–Tucker conditions are (54, left).*

Proof Clearly, $D_b \in \mathcal{P}$, and for any $D \in \mathcal{P}$ one has $\langle M, D - D_b \rangle = \sum_{i<j} \lambda_{ij} (\langle\!\langle D, \hat{\mathbf{v}}_{ij} \otimes \hat{\mathbf{v}}_{ij} \rangle\!\rangle - \langle\!\langle D_b, \hat{\mathbf{v}}_{ij} \otimes \hat{\mathbf{v}}_{ij} \rangle\!\rangle) = \sum_{i<j} \lambda_{ij} (\|\hat{\mathbf{v}}_{ij}\|_D^2 - 1) \geq 0$. The result follows. □

The previous proposition leaves open the question of the existence of an M-obtuse superbase b, given $M \in \mathrm{S}^{++}(\mathbb{E}_d)$. In dimension $d \in \{2,3\}$, such a b always exists, and can be constructed via Selling's algorithm [51] which is implemented "as is" in our numerical experiments Sect. 5. Note that this algorithm could in principle be accelerated by a preliminary basis reduction step [40], but the advantage is only visible for extremely large condition numbers, which are irrelevant for applications to anisotropic PDEs.

Proposition 4.7 (Selling's algorithm) *Let $M \in \mathrm{S}^{++}(\mathbb{E}_d)$, where $d \in \{2,3\}$, and let $b = (\dot{\mathbf{e}}_0, \dots, \dot{\mathbf{e}}_d)$ be a superbase of $\mathbb{L}^d$. Define a second superbase b' of $\mathbb{L}_d$ by*

$$\begin{aligned} &\textit{Case } d = 2 : b' := (-\dot{\mathbf{e}}_0, \dot{\mathbf{e}}_1, \dot{\mathbf{e}}_0 - \dot{\mathbf{e}}_1), \\ &\textit{Case } d = 3 : b' := (-\dot{\mathbf{e}}_0, \dot{\mathbf{e}}_1, \dot{\mathbf{e}}_0 + \dot{\mathbf{e}}_2, \dot{\mathbf{e}}_0 + \dot{\mathbf{e}}_3). \end{aligned}$$

Then, $\mathrm{Tr}(M D_b) - \mathrm{Tr}(M D_{b'}) = 2^{2-d} \langle \dot{\mathbf{e}}_0, \dot{\mathbf{e}}_1 \rangle_M$. Selling's algorithm consists in iteratively, and until b is an M-obtuse superbase: (a) reordering the superbase b so that $\langle \dot{\mathbf{e}}_0, \dot{\mathbf{e}}_1 \rangle_M > 0$, and (b) applying the transformation $b \leftarrow b'$.

This algorithm terminates, and in particular there exists an M-obtuse superbase of $\mathbb{L}_d$.

Proof Applying Definition 4.1 we find that b' is indeed a superbase of $\mathbb{L}_d$. The expression of $\mathrm{Tr}(M D_b) - \mathrm{Tr}(M D_{b'})$ follows from a direct computation. Denoting by b_n be the superbase obtained at the n-th step of Selling's algorithm, one observes that $\mathrm{Tr}(M D_{b_n})$ strictly decreases as n increases by construction. In view of

$$2^d \mathrm{Tr}(M D_b) = \sum_{I \subseteq \{0,\dots,d\}} \|\dot{\mathbf{e}}_I\|_M^2 \geq \sum_{0 \leq i \leq d} \|\dot{\mathbf{e}}_i\|_M^2$$

we observe that there are only finitely many superbases $b = (\dot{\mathbf{e}}_0, \dots, \dot{\mathbf{e}}_d) \in \mathbb{L}_d^d$ such that $\mathrm{Tr}(M D_b)$ is below any given bound, hence Selling's algorithm must terminate, and the result follows. □

A closer inspection shows that Selling's algorithm is equivalent to the Simplex algorithm applied to the linear program (50). Selling's algorithm is also described in Appendix B of [9]. In dimension $d = 2$, Selling's algorithm is equivalent to exploring the an arithmetic structure named the Stern-Brocot tree, see [10] for details on this approach and an application to second-order HJB PDEs for stochastic control.

4.2 Radius of the Decomposition

We bound in this section the Euclidean norm of the integral co-vectors involved in the matrix decomposition (51). Our estimate is sharper than the one presented in [36], which has significant consequences on the convergence analysis Sect. 3, see the discussion after Theorem 4.11. The results of this subsection and of the next are new to the author's knowledge. One reason for this is that most studies on lattice geometry consider a single norm, and not the interaction of two norms as here, namely the Euclidean norm $\|\cdot\|$ and an anisotropic norm $\|\cdot\|_M$.

Our first step is to upper bound the norm of the elements of an M-obtuse superbase. Throughout this subsection, we denote by $\hat{\mathbf{v}}_{ij} \in \mathbb{L}_d^*$ the co-vectors associated by Definition 4.2 to a superbase $(\dot{\mathbf{e}}_0, \dots, \dot{\mathbf{e}}_d)$.

Proposition 4.8 *Let $M \in \mathbb{S}_d^{++}$ and let $b = (\dot{\mathbf{e}}_0, \dots, \dot{\mathbf{e}}_d)$ be an M-obtuse superbase (if one exists). Then, $\|\dot{\mathbf{e}}_i\| \leq C\,\mathrm{Cond}(M)$, for each $0 \leq i \leq d$, where $C_d := \sqrt{2^{d-1}d}$ and $\mathrm{Cond}(M) := \sqrt{\|M\|\|M^{-1}\|}$.*

Proof Denote by $\lambda_{\min}^2$ and $\lambda_{\max}^2$ the smallest and largest eigenvalues of M. Observe that $2^d D_b \succeq \dot{\mathbf{e}}_i \otimes \dot{\mathbf{e}}_i + (-\dot{\mathbf{e}}_i) \otimes (-\dot{\mathbf{e}}_i) = 2\mathbf{e}_i \otimes \dot{\mathbf{e}}_i$, where $A \succeq B$ means that $A - B \in \mathrm{S}^+(\mathbb{E}_d)$. Observe also that $\mathrm{Id}, D_b \in \mathcal{P}$, and that D_b is optimal for (50). Thus, as announced

$$\lambda_{\min}^2 \|\dot{\mathbf{e}}_i\|^2 \leq \|\dot{\mathbf{e}}_i\|_M^2 \leq 2^{d-1}\,\mathrm{Tr}(M D_b) \leq 2^{d-1}\,\mathrm{Tr}(M\,\mathrm{Id}) \leq 2^{d-1} d \lambda_{\max}^2. \qquad \square$$

In order to proceed, we recall some identities relating the scalar products associated with M and $D := M^{-1}$, where $M \in \mathrm{S}^{++}(\mathbb{E}_d)$. For any $\dot{\mathbf{e}}_0, \dot{\mathbf{e}}_1, \dot{\mathbf{e}}_2 \in \mathbb{E}_d$

$$\text{If } d = 2 \quad (\det M)\langle \dot{\mathbf{e}}_0^{\perp}, \dot{\mathbf{e}}_1^{\perp} \rangle_D = \langle \dot{\mathbf{e}}_0, \dot{\mathbf{e}}_1 \rangle_M, \tag{55}$$

$$\text{If } d = 3 \quad (\det M)\langle \dot{\mathbf{e}}_0 \times \dot{\mathbf{e}}_1,\ \dot{\mathbf{e}}_0 \times \dot{\mathbf{e}}_2 \rangle_D = \|\dot{\mathbf{e}}_0\|_M^2 \langle \dot{\mathbf{e}}_1, \dot{\mathbf{e}}_2 \rangle_M - \langle \dot{\mathbf{e}}_0, \dot{\mathbf{e}}_1 \rangle_M \langle \dot{\mathbf{e}}_0, \dot{\mathbf{e}}_2 \rangle_M, \tag{56}$$

where $\times$ denotes the cross product of three-dimensional vectors. These identities are easily checked when $M = \mathrm{Id}$, and otherwise follow from a change of variables by $M^{\frac{1}{2}}$.

In the next two propositions, we investigate the geometrical properties relating a superbase $(\dot{\mathbf{e}}_0, \dots, \dot{\mathbf{e}}_d)$ of $\mathbb{L}_d$ with the dual superbase $(\hat{\mathbf{v}}_{01}, \hat{\mathbf{v}}_{12}, \dots, \hat{\mathbf{v}}_{d0})$ introduced in Proposition 4.3. Proposition 4.10 is in particular an original technical argument.

Proposition 4.9 *Let $(\dot{\mathbf{e}}_0, \dot{\mathbf{e}}_1, \dot{\mathbf{e}}_2)$ be an M-obtuse superbase of $\mathbb{L}_2$, where $M \in \mathrm{S}^{++}(\mathbb{E}_2)$. Then, $(\hat{\mathbf{v}}_{01}, \hat{\mathbf{v}}_{12}, \hat{\mathbf{v}}_{20})$ is a D-obtuse superbase of $\mathbb{L}_2^*$, where $D := M^{-1}$.*

Proof By (53), one has $(\hat{\mathbf{v}}_{01}, \hat{\mathbf{v}}_{12}, \hat{\mathbf{v}}_{20}) = (\dot{\mathbf{e}}_2^{\perp}, \dot{\mathbf{e}}_0^{\perp}, \dot{\mathbf{e}}_1^{\perp})$, and the result follows from (55). $\square$

Proposition 4.10 *Let $b = (\dot{\mathbf{e}}_0, \dot{\mathbf{e}}_1, \dot{\mathbf{e}}_2, \dot{\mathbf{e}}_3)$ be an M-obtuse superbase of $\mathbb{L}_3$, where $M \in \mathrm{S}^{++}(\mathbb{E}_3)$. Then, at least one of $\hat{b}_0 := (\hat{\mathbf{v}}_{01}, \hat{\mathbf{v}}_{12}, \hat{\mathbf{v}}_{23}, \hat{\mathbf{v}}_{30})$, $\hat{b}_1 := (\hat{\mathbf{v}}_{01}, \hat{\mathbf{v}}_{13}, \hat{\mathbf{v}}_{32}, \hat{\mathbf{v}}_{20})$, and $\hat{b}_2 := (\hat{\mathbf{v}}_{02}, \hat{\mathbf{v}}_{21}, \hat{\mathbf{v}}_{13}, \hat{\mathbf{v}}_{30})$ is a D-obtuse superbase of $\mathbb{L}_3^*$, where $D := M^{-1}$.*

Proof All three of $\hat{b}_0$, $\hat{b}_1$ and $\hat{b}_2$ are superbases of $\mathbb{L}_3^*$, by applying Proposition 4.3 to permutations of b. One has $\langle \hat{\mathbf{v}}_{ij}, \hat{\mathbf{v}}_{jk} \rangle_D = \langle \dot{\mathbf{e}}_k \times \dot{\mathbf{e}}_l, \dot{\mathbf{e}}_i \times \dot{\mathbf{e}}_l \rangle_D \leq 0$ by (53) and (56), and by the M-obtuseness of b, whenever $\{i, j, k, l\} = \{0, 1, 2, 3\}$. The remaining scalar products of interest are

$$\alpha_0 := \langle \hat{\mathbf{v}}_{13}, \hat{\mathbf{v}}_{20} \rangle_D, \quad \alpha_1 := \langle \hat{\mathbf{v}}_{12}, \hat{\mathbf{v}}_{03} \rangle_D, \quad \alpha_2 := \langle \hat{\mathbf{v}}_{01}, \hat{\mathbf{v}}_{23} \rangle_D.$$

Recalling that $\hat{\mathbf{v}}_{ij} = -\hat{\mathbf{v}}_{ji}$ for any $i \neq j$ one observes the following: if $\alpha_1 \geq 0 \geq \alpha_2$, then $\hat{b}_0$ is D-obtuse, if $\alpha_2 \geq 0 \geq \alpha_0$, then $\hat{b}_1$ is D-obtuse, and if $\alpha_0 \geq 0 \geq \alpha_1$, then $\hat{b}_2$ is D-obtuse. On the other hand, expressing $(\alpha_i)_{i=0}^2$ in terms of cross products yields

$$\alpha_0 := \langle \dot{\mathbf{e}}_2 \times \dot{\mathbf{e}}_0,\ \dot{\mathbf{e}}_1 \times \dot{\mathbf{e}}_3 \rangle_D, \quad \alpha_1 := \langle \dot{\mathbf{e}}_0 \times \dot{\mathbf{e}}_3,\ \dot{\mathbf{e}}_1 \times \dot{\mathbf{e}}_2 \rangle_D,$$
$$\alpha_2 := \langle \dot{\mathbf{e}}_2 \times \dot{\mathbf{e}}_3,\ \dot{\mathbf{e}}_0 \times \dot{\mathbf{e}}_1 \rangle_D,$$

and inserting the identity $\dot{\mathbf{e}}_0 := -(\dot{\mathbf{e}}_1 + \dot{\mathbf{e}}_2 + \dot{\mathbf{e}}_3)$ in the above expressions one obtains that $\alpha_0 + \alpha_1 + \alpha_2 = 0$. Therefore these three scalars cannot have the same sign strictly. Thus in the sequence $\alpha_0, \alpha_1, \alpha_2, \alpha_0$ there is at least one nonnegative scalar α_i followed with a non-positive scalar α_{i+1}, where indices are understood modulo 3. By the previous argument, $\hat{b}_{i-1}$ is D-obtuse, and the announced result follows. $\square$

In the rest of this section, we denote by C_d the constant of Proposition 4.8.

Theorem 4.11 *Let $(\dot{\mathbf{e}}_0, \dots, \dot{\mathbf{e}}_d)$ be an M-obtuse superbase of $\mathbb{Z}^d$, where $M \in \mathrm{S}^{++}(\mathbb{E}_d)$ and $d \in \{2, 3\}$. Then, $\|\hat{\mathbf{v}}_{ij}\| \leq 2C_d\,\mathrm{Cond}(M)$ for all $i \neq j$.*

Proof Case $d = 2$. By Propositions 4.8 and 4.9, one has $\|\hat{\mathbf{v}}_{ij}\| \leq C_d\,\mathrm{Cond}(D) = C_d\,\mathrm{Cond}(M)$ as announced (the factor 2 is here useless). Case $d = 3$. By Propositions 4.8 and 4.10, assuming w.l.o.g. that $\hat{b}_0$ is D-obtuse, the co-vectors $\hat{\mathbf{v}}_{01}, \hat{\mathbf{v}}_{12}, \hat{\mathbf{v}}_{23}, \hat{\mathbf{v}}_{30}$ have their norm bounded by $C_d\,\mathrm{Cond}(D) = C_d\,\mathrm{Cond}(M)$. The remaining two co-vectors $\hat{\mathbf{v}}_{02}$ and $\hat{\mathbf{v}}_{13}$ can be expressed as:

$$\hat{\mathbf{v}}_{13} = \dot{\mathbf{e}}_2 \times \dot{\mathbf{e}}_0 = \dot{\mathbf{e}}_2 \times (-\dot{\mathbf{e}}_1 - \dot{\mathbf{e}}_2 - \dot{\mathbf{e}}_3) = -\dot{\mathbf{e}}_2 \times \dot{\mathbf{e}}_1 - \dot{\mathbf{e}}_2 \times \dot{\mathbf{e}}_3 = \hat{\mathbf{v}}_{30} + \hat{\mathbf{v}}_{01},$$

and likewise $\hat{\mathbf{v}}_{02} = \hat{\mathbf{v}}_{01} + \hat{\mathbf{v}}_{12}$. Thus $\|\hat{\mathbf{v}}_{13}\| \leq \|\hat{\mathbf{v}}_{30}\| + \|\hat{\mathbf{v}}_{01}\| \leq 2C_d\,\mathrm{Cond}(M)$, and likewise $\|\hat{\mathbf{v}}_{02}\| \leq 2C_d\,\mathrm{Cond}(M)$. The announced result follows. $\square$

Our next result describes a nonnegative, lattice-adapted decomposition of symmetric tensors. It coincides with the one considered in Proposition 1.1 of [36], but the stencil radius estimate is sharper: linear in the condition number of M, instead of quadratic $\|\hat{\mathbf{v}}\| \leq C\,\mathrm{Cond}(M)^2$ in dimension $d = 3$. This improvement has theoretical consequences, since the assumption $h_n/\varepsilon_n \to 0$ in Theorem 3.1 would otherwise need to be replaced with the stronger (and unrealistic in applications) assumption $h_n/\varepsilon_n^2 \to 0$.

Corollary 4.12 *Let $M \in \mathrm{S}^{++}(\mathbb{E}_d)$, where $d \in \{2, 3\}$. Then, there exists nonnegative weights $\rho_{\hat{\mathbf{v}}}(M)$, supported on at most $d(d+1)/2$ elements $\hat{\mathbf{v}} \in \mathbb{L}_d^*$, such that*

$$\sum_{\hat{\mathbf{v}} \in \mathbb{L}_d^*} \rho_{\hat{\mathbf{v}}}(M) \hat{\mathbf{v}} \otimes \hat{\mathbf{v}} = M. \tag{57}$$

Furthermore, $\|\hat{\mathbf{v}}\| \leq 2C_d\,\mathrm{Cond}(M)$ whenever $\rho_{\hat{\mathbf{v}}}(M) > 0$, and $\sum_{\hat{\mathbf{v}} \in \mathbb{L}_d^*} \rho_{\hat{\mathbf{v}}}^{\varepsilon}(\hat{\mathbf{n}}) \|\hat{\mathbf{v}}\|^2 = \mathrm{Tr}(M)$.

Proof By Proposition 4.7 there exists an M-obtuse superbase, by Lemma 4.4 it yields a decomposition of the announced form (58), and by Theorem 4.11 the norms of the support co-vectors are bounded as announced. The last identity follows by taking the trace of (57). □

It is possible to construct tensor decompositions of the form (57) by other means than Voronoi's first reduction, but the resulting stencil radius is typically larger, and provably larger [35] in dimension $d = 2$. PDE schemes of small stencil size are appreciated in numerical applications for reasons of robustness, accuracy, implementation of boundary conditions, and parallelization potential.

Corollary 4.13 *Let $d \in \{2, 3\}$, let $0 < \varepsilon \leq 1$, and let $\hat{\mathbf{n}} \in \mathbb{E}_d^*$ such that $\|\hat{\mathbf{n}}\| = 1$. Then, there exists nonnegative weights $\rho_{\hat{\mathbf{v}}}^{\varepsilon}(\hat{\mathbf{n}})$, supported on at most $d(d+1)/2$ elements $\hat{\mathbf{v}} \in \mathbb{L}_d^*$, such that*

$$\forall \dot{\mathbf{p}} \in \mathbb{E}_d, \quad \sum_{\hat{\mathbf{v}} \in \mathbb{L}_d^*} \rho_{\hat{\mathbf{v}}}^{\varepsilon}(\hat{\mathbf{n}}) \langle \hat{\mathbf{v}}, \dot{\mathbf{p}} \rangle^2 = \langle \hat{\mathbf{n}}, \dot{\mathbf{p}} \rangle^2 + \varepsilon^2 (\|\dot{\mathbf{p}}\|^2 - \langle \hat{\mathbf{n}}, \dot{\mathbf{p}} \rangle^2). \tag{58}$$

Furthermore, $\|\hat{\mathbf{v}}\| \leq 2C_d \varepsilon^{-1}$ whenever $\rho_{\hat{\mathbf{v}}}^{\varepsilon}(\hat{\mathbf{n}}) > 0$, and $\sum \rho_{\hat{\mathbf{v}}}^{\varepsilon}(\hat{\mathbf{n}}) \|\hat{\mathbf{v}}\|^2 = 1 + \varepsilon^2 (d-1)$.

Proof Apply Corollary 4.12 to $M = \hat{\mathbf{n}} \otimes \hat{\mathbf{n}} + \varepsilon^2 (\mathrm{Id} - \hat{\mathbf{n}} \otimes \hat{\mathbf{n}}) \in \mathrm{S}^{++}(\mathbb{E}_d)$, whose eigenvalues are 1 with eigenvector $\hat{\mathbf{n}}$, and ε^2 with multiplicity $d-1$, thus $\mathrm{Cond}(M) = \varepsilon^{-1}$. □

4.3 Taking Positive Parts of Linear Forms

We conclude in this section the proof of Proposition 2.2. Our main technical result, presented below, shows how to use decompositions of anisotropic symmetric positive definite tensors, as in Corollary 4.13, to build approximations of positive parts of linear forms.

Proposition 4.14 *Let $\hat{\mathbf{n}} \in \mathbb{E}_d^*$ with $\|\hat{\mathbf{n}}\| = 1$, and let $\varepsilon > 0$. Let $\hat{\mathbf{v}}_1, \ldots, \hat{\mathbf{v}}_K \in \mathbb{E}_d^*$ and $\rho_1, \ldots, \rho_K \geq 0$ be such that for all $\dot{\mathbf{p}} \in \mathbb{E}^d$*

$$\sum_{1 \leq k \leq K} \rho_k \langle \hat{\mathbf{v}}_k, \dot{\mathbf{p}} \rangle^2 = \langle \hat{\mathbf{n}}, \dot{\mathbf{p}} \rangle^2 + \varepsilon^2 (\|\dot{\mathbf{p}}\|^2 - \langle \hat{\mathbf{n}}, \dot{\mathbf{p}} \rangle^2). \tag{59}$$

Assume that[5] *$\langle \hat{\mathbf{v}}_k, \hat{\mathbf{n}} \rangle \geq 0$ for each $1 \leq k \leq K$. Then, for all $\dot{\mathbf{p}} \in \mathbb{E}_d$ one has*

$$\langle \hat{\mathbf{n}}, \dot{\mathbf{p}} \rangle_+^2 \leq \sum_{1 \leq k \leq K} \rho_k \langle \hat{\mathbf{v}}_k, \dot{\mathbf{p}} \rangle_+^2 \leq \langle \hat{\mathbf{n}}, \dot{\mathbf{p}} \rangle_+^2 + \varepsilon^2 (\|\dot{\mathbf{p}}\|^2 - \langle \hat{\mathbf{n}}, \dot{\mathbf{p}} \rangle^2). \tag{60}$$

[5] The scalar product $\langle \hat{\mathbf{v}}_k, \hat{\mathbf{n}} \rangle$ makes sense thanks to the Euclidean structure on $\mathbb{E}_d$ and $\mathbb{E}_d^*$.

Proof In this proof, we identify $\mathbb{E}_d$ with its dual $\mathbb{E}_d^*$ thanks to the Euclidean structure, and thus drop the "dot" and "hat" superscripts on vectors and co-vectors for clarity. We assume that $\rho_k = 1$, for all $1 \leq k \leq K$, up to replacing $\mathbf{v}_k$ with $\sqrt{\rho_k} \mathbf{v}_k$.

Denote by $\mathbf{v}_k^* := \mathbf{v}_k - \langle \mathbf{v}_k, \mathbf{n} \rangle \mathbf{n}$ the orthogonal projection of $\mathbf{v}_k$ on the hyperplane orthogonal to $\mathbf{n}$, where $1 \leq k \leq K$. Then, by (59)

$$\sum_{1 \leq k \leq K} \langle \mathbf{n}, \mathbf{v}_k \rangle^2 = 1, \qquad \sum_{1 \leq k \leq K} \mathbf{v}_k^* \otimes \mathbf{v}_k^* = \varepsilon^2 (\mathrm{Id} - \mathbf{n} \otimes \mathbf{n}).$$

The proof of (60) is split into two parts, depending on the sign of $\langle \mathbf{n}, \mathbf{p} \rangle$. If $\langle \mathbf{n}, \mathbf{p} \rangle \leq 0$, then $\langle \mathbf{v}_k, \mathbf{p} \rangle = \langle \mathbf{v}_k, \mathbf{n} \rangle \langle \mathbf{n}, \mathbf{p} \rangle + \langle \mathbf{v}_k^*, \mathbf{p} \rangle \leq \langle \mathbf{v}_k^*, \mathbf{p} \rangle$ for all $1 \leq k \leq K$, thus as announced

$$\begin{aligned} \sum_{1 \leq k \leq K} \langle \mathbf{v}_k, \mathbf{p} \rangle_+^2 &\leq \sum_{1 \leq k \leq K} \langle \mathbf{v}_k^*, \mathbf{p} \rangle_+^2 \\ &\leq \sum_{1 \leq k \leq K} \langle \mathbf{v}_k^*, \mathbf{p} \rangle^2 = \varepsilon^2 (\|\mathbf{p}\|^2 - \langle \mathbf{n}, \mathbf{p} \rangle^2). \end{aligned}$$

In contrary if $\langle \mathbf{n}, \mathbf{p} \rangle \geq 0$, then the second inequality of (60) is immediate. In addition $\langle \mathbf{v}_k, \mathbf{p} \rangle_+^2 \geq \langle \mathbf{v}_k, \mathbf{p} \rangle^2 - \langle \mathbf{v}_k^*, \mathbf{p} \rangle^2$ for any $1 \leq k \leq K$. (Indeed, if $\langle \mathbf{v}_k, \mathbf{p} \rangle \geq 0$, then $\langle \mathbf{v}_k, \mathbf{p} \rangle_+^2 = \langle \mathbf{v}_k, \mathbf{p} \rangle^2 \geq \langle \mathbf{v}_k, \mathbf{p} \rangle^2 - \langle \mathbf{v}_k^*, \mathbf{p} \rangle^2$, and in contrary if $\langle \mathbf{v}_k, \mathbf{p} \rangle \leq 0$, then $0 \geq \langle \mathbf{v}_k, \mathbf{p} \rangle = \langle \mathbf{v}_k, \mathbf{n} \rangle \langle \mathbf{n}, \mathbf{p} \rangle + \langle \mathbf{v}_k^*, \mathbf{p} \rangle \geq \langle \mathbf{v}_k^*, \mathbf{p} \rangle$, thus $\langle \mathbf{v}_k, \mathbf{p} \rangle_+^2 = 0 \geq \langle \mathbf{v}_k, \mathbf{p} \rangle^2 - \langle \mathbf{v}_k^*, \mathbf{p} \rangle^2$.) Hence, we conclude

$$\begin{aligned} \sum_{1 \leq k \leq K} \langle \mathbf{v}_k, \mathbf{p} \rangle_+^2 &\geq \sum_{1 \leq k \leq K} \left(\langle \mathbf{v}_k, \mathbf{p} \rangle^2 - \langle \mathbf{v}_k^*, \mathbf{p} \rangle^2 \right) \\ &= \left(\langle \hat{\mathbf{n}}, \dot{\mathbf{p}} \rangle^2 + \varepsilon^2 \|\mathbf{p}^*\|^2 \right) - \varepsilon^2 \|\mathbf{p}^*\|^2 = \langle \mathbf{n}, \mathbf{p} \rangle^2, \end{aligned}$$

where we denoted $\mathbf{p}^* := \mathbf{p} - \langle \mathbf{p}, \mathbf{n} \rangle \mathbf{n}$, so that $\|\mathbf{p}^*\|^2 = \|\dot{\mathbf{p}}\|^2 - \langle \hat{\mathbf{n}}, \dot{\mathbf{p}} \rangle^2$. □

Combining Corollary 4.13 with Proposition 4.14 we conclude the proof of Proposition 2.2, thanks to the following two remarks. (I) The assumption $\langle \hat{\mathbf{v}}_k, \hat{\mathbf{n}} \rangle \geq 0$ for all $0 \leq k \leq K$ in Proposition 4.14 is not restrictive, since one can always replace $\hat{\mathbf{v}}_k$ with its opposite $-\hat{\mathbf{v}}_k$ without incidence on (59). (II) The roles of $\mathbb{E}_d$ and of its dual $\mathbb{E}_d^*$ are exchanged in Proposition 2.2.

5 Numerical Experiments

This section is devoted to a numerical validation of the proposed PDE schemes, and to an illustration of their potential applications. For validation, compare in Sect. 5.1 the geodesics obtained by solving Hamilton's ODE of geodesics against the results of our PDE discretization. A second validation is presented in Appendix A, and based on numerical

counterparts of the control sets of Fig. 2. We investigate applications to motion planning in Sect. 5.2, and to vessel tracking in simulated medical data in Sect. 5.3. All the test cases presented in this paper are based on synthetic data. Experiments closer to applications and involving real data will be the subject of future work.

Free and open source numerical codes for reproducing (most of) the numerical experiments, as well as additional examples, are available on the author's webpage.[6]

5.1 Comparison with Geodesic Shooting

Consider a model with a smooth Hamiltonian $\mathcal{H}$, such as the reversible Reeds–Shepp model or the Euler–Mumford model. Paths of minimal energy are known to obey[7] the Hamilton equations of geodesics, which read

$$\frac{d\mathbf{p}}{dt} = -\frac{\partial \mathcal{H}}{\partial \hat{\mathbf{p}}}, \qquad \frac{d\hat{\mathbf{p}}}{dt} = \frac{\partial \mathcal{H}}{\partial \mathbf{p}}, \tag{61}$$

where $\mathbf{p}(t)$ and $\hat{\mathbf{p}}(t)$ are, respectively, the state and the co-state of the geodesic at time $t \in [0, 1]$. Given an initial point $\mathbf{p}_0$, and a target point $\mathbf{p}_1$, one can try to adjust the initial co-state $\hat{\mathbf{p}}_0$ so that the solution to (61) starting from $(\mathbf{p}(0), \hat{\mathbf{p}}(0)) = (\mathbf{p}_0, \hat{\mathbf{p}}_0)$ satisfies $\mathbf{p}(1) = \mathbf{p}_1$. We tried this procedure, referred to as geodesic shooting, using a fourth-order Runge–Kutta method for solving (61), and a Newton method for adjusting $\hat{\mathbf{p}}_0$.

Another approach to the computation of geodesics is to numerically solve the PDE (8) and then extract the minimal geodesics as streamlines of the geodesic flow (11). We use a second-order Euler scheme for that latter ODE, together with the following upwind estimate of the geodesic flow direction $\mathrm{d}\mathcal{H}_{\mathbf{p}}(\mathrm{d}u(\mathbf{p}))$, where $\mathbf{p} \in \mathbb{M}$. Assume that the local Hamiltonian $\mathcal{H}_{\mathbf{p}}$ is approximated in the following form

$$H(\hat{\mathbf{p}}) = \frac{1}{2} \sum_{1 \le k \le K} \rho_k \langle \hat{\mathbf{p}}, \dot{\mathbf{e}}_k \rangle_+^2. \tag{62}$$

Differentiating, we obtain the first-order approximation

$$\begin{aligned} \mathrm{d}H(\hat{\mathbf{p}}) &= \sum_{1 \le k \le K} \rho_k \langle \hat{\mathbf{p}}, \dot{\mathbf{e}}_k \rangle_+ \, \dot{\mathbf{e}}_k, \text{ thus } \quad \mathrm{d}\mathcal{H}_{\mathbf{p}}(\mathrm{d}u(\mathbf{p})) \\ &\approx \sum_{1 \le k \le K} \rho_k \left(\frac{u(\mathbf{p}) - u(\mathbf{p} - h\dot{\mathbf{e}}_k)}{h} \right)_+ \dot{\mathbf{e}}_k. \end{aligned}$$

The slightly more general form (15) is handled similarly. Let us mention that our numerical codes also implement a second backtracking method, inspired by the diffuse numerical geodesics described in [5], and which yields similar results. However, we observed that many alternative backtracking methods did (often) fail, in particular with the Dubins model, due to the discontinuity of value function u.

In favorable cases, geodesic shooting is more precise than the PDE and backtracking approach. However, it is also much less general and robust, for the following reasons. (I) Geodesic shooting cannot address the Reeds–Shepp forward and Dubins models, due to their non-twice differentiable Hamiltonians. (More sophisticated shooting methods, based on piecewise smooth paths, can in principle address this issue.) (II) It is incompatible with the presence of obstacles, and with non-smooth cost functions α. (III) It lacks guarantees regarding the global optimality of the extracted geodesics, despite their local optimality.

A comparison of geodesic shooting with the proposed approach is presented in Fig. 5. A similar experiment was presented in [36] for the Reeds–Shepp reversible model, but not for the Euler–Mumford model.

5.2 Motion Planning

Motion planning is a natural field of application for minimal path methods, see for instance [28], and the different models considered in this paper may account for the maneuverability constraints of a number of vehicles. For instance, the reversible Reeds–Shepp model describes wheelchairs or wheelchair-like robots. The forward only variant is appropriate for vehicles of the same type, but which cannot see behind themselves. Minimal paths w.r.t. the Euler–Mumford elastica model have the advantage of being smooth, and their curvature penalization is physically meaningful. The hard upper bound constraint of the Dubins model on the curvature is relevant for the numerous vehicles subject to a minimum turning radius. See [32] for more applications to motion planning of the numerical methods presented in this paper, including two player games where an opponent chooses the obstacles.

Our experiments, presented n Figs. 6, 7, 8 and 9, show that the numerical schemes introduced in this paper can be used to solve complex motion planning problems, on domains involving numerous walls, in CPU time below one second on a standard laptop.[8] Within that time, the PDE (8) is numerically solved on the full domain, here discretized on a $90^2 \times 60$ grid, which yields a complete strategy to reach the given target. Larger grid scales yield more accurate paths, at the price of longer computation times (but still quasi-linear in the number of pixels). Memory usage is dominated by the storage of the value function, namely one floating point number per grid point. Once the PDE is solved, extracting a minimal path from an arbitrary point in the domain has an almost negligible cost.

[6] www.github.com/Mirebeau/HamiltonFastMarching.

[7] Except perhaps *abnormal* geodesics, which we do not discuss here, see [37].

[8] Laptop processor: 2.7GHz Intel®Core i7 using a single core.

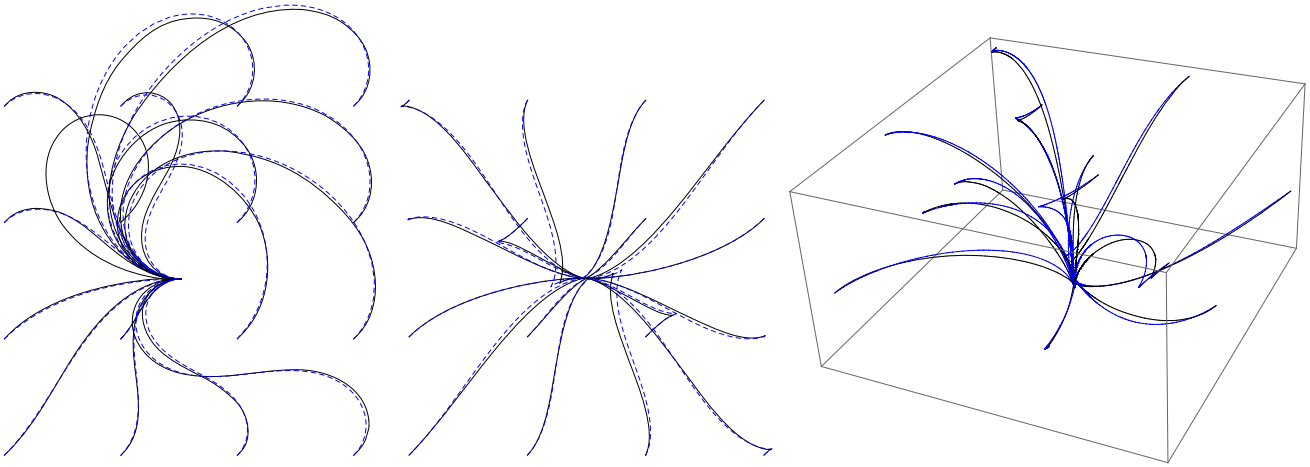

Fig. 5 Comparison of Minimal geodesics obtained by PDE resolution and backtracing (black), or geodesic shooting (blue), for Euler–Mumford (left) and Reeds–Shepp reversible models in 2D (center) or 3D (right) (Color figure online)

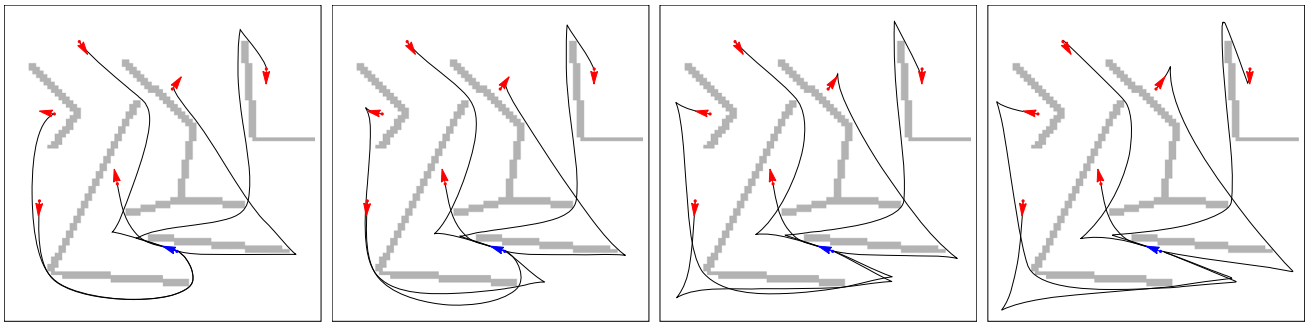

Fig. 6 Reeds–Shepp reversible model, $\xi \in \{0.1, 0.2, 0.4, 0.8\}$. $\varepsilon = 0.1$, CPU time ≈ 0.3 s

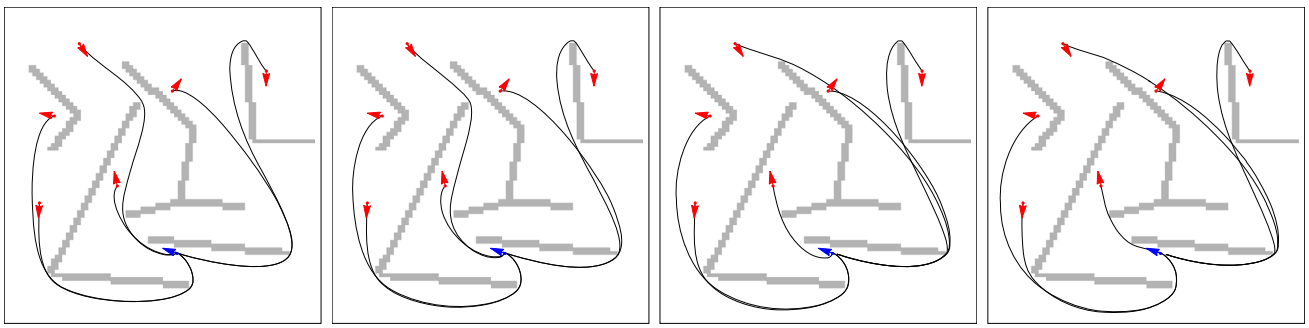

Fig. 7 Reeds–Shepp forward model, $\xi \in \{0.1, 0.2, 0.4, 0.8\}$. $\varepsilon = 0.1$, CPU time ≈ 0.2 s

The chosen domain for this experiment is $[0, 1]^2 \times \mathbb{S}^1$, the relaxation parameter is $\varepsilon = 0.1$, and various values are considered for ξ, which we recall is homogeneous to a radius of curvature. The different qualitative properties of the four models appear clearly, in particular the cusps of the Reeds–Shepp reversible model minimal paths, the in-place rotations of the Reeds–Shepp forward paths, the smoothness of the Euler–Mumford paths, and the lower-bounded radius of curvature of the Dubins paths.

On the rightmost sub-figures of Fig. 9, illustrating the Dubins model, the author acknowledges that two paths fail, in some places, to obey the prescribed lower bound on the radius of curvature. This is due to the approximate nature of the PDE discretization, and to the fact that no path obeying this lower bound seems to exist between these endpoints. These artifacts can easily be eliminated by post-processing.

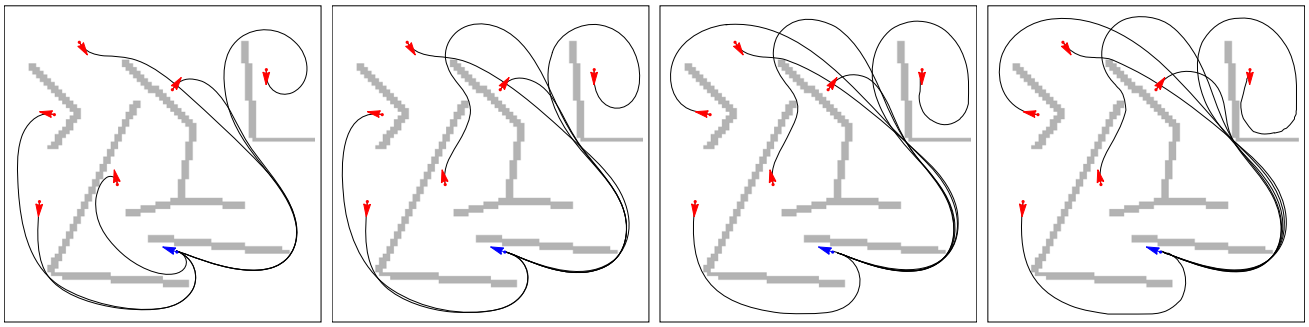

Fig. 8 Euler–Mumford elastica, $\xi \in \{0.1, 0.2, 0.3, 0.4\}$. $\varepsilon = 0.1$, $K = 5$, CPU time ≈ 1.2 s

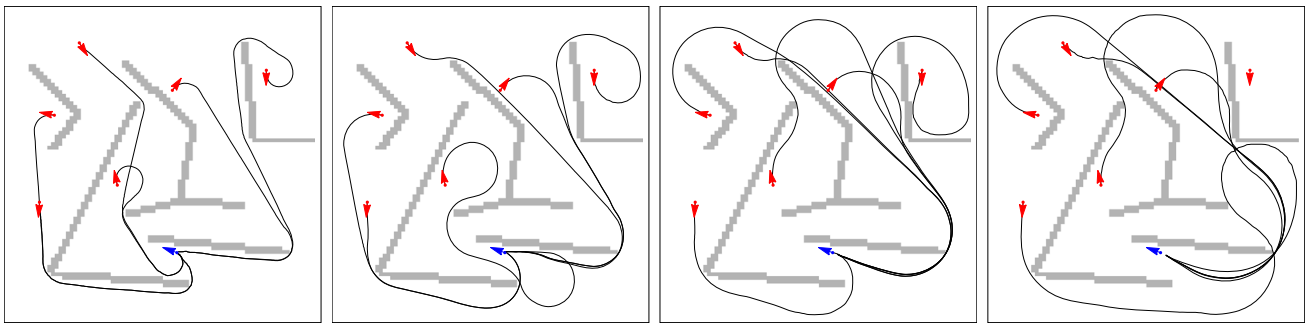

Fig. 9 Dubins model, $\xi \in \{0.05, 0.1, 0.15, 0.2\}$. $\varepsilon = 0.1$, CPU time ≈ 0.6 s

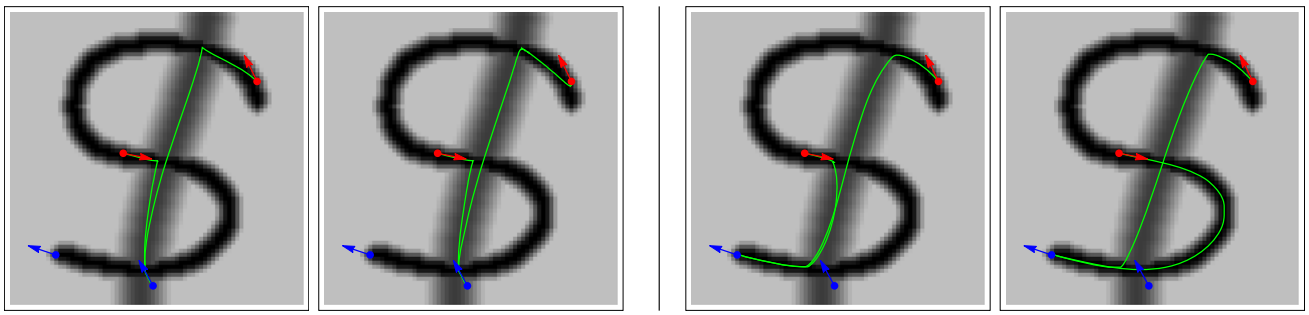

Fig. 10 Tubular segmentation test with the Reeds–Shepp models, reversible (left), and forward (right). First image $\xi = 0.2$, second $\xi = 0.8$. This segmentation test is mostly "failed", on purpose, for different reasons, see Sect. 5.3. CPU time ≈ 0.3 s

5.3 Tubular Structure Segmentation

We present a numerical experiment, based on synthetic data, designed to illustrate the qualitative differences between the four implemented minimal path models in applications to tubular structure segmentation, see the Discussion in Sect. 1.3. Our experiment is illustrated in Figs. 10, 11 and 12. We choose a local cost function $\alpha = \alpha(\mathbf{x})$ taking small values iff $\mathbf{x}$ is close to a vessel, then we extract a minimal path between prescribed endpoints w.r.t. some curvature cost and parameter ξ, see the full description below. Some model/parameter combinations succeed, in the sense that the extracted minimal path goes along the desired vessel, and other fail, as discussed below. We would, however, like to emphasize that our results could be considerably improved by choosing a cost function $\alpha = \alpha(\mathbf{x}, \theta)$ also depending on the orientation θ, see [1,49]. Our "inefficient" choice of cost function α is intended to exacerbate the differences between the different models, by making the problem harder.

As noted by a reviewer, real medical data always contain noise, which is absent from our synthetic test case, see Fig. 11. Due to noise, real applications do not directly define the speed function α as the input image, as we do here. Instead, the data-driven speed function is obtained as the result of a complex pre-processing step, aimed at reducing noise and locally detecting the image features, see the above references on, e.g., tubular structure segmentation. We choose to avoid this complex machinery (thus do not consider noise) so as to keep the experiment as simple, reproducible, and interpretable as possible. Indeed, our objective is not to

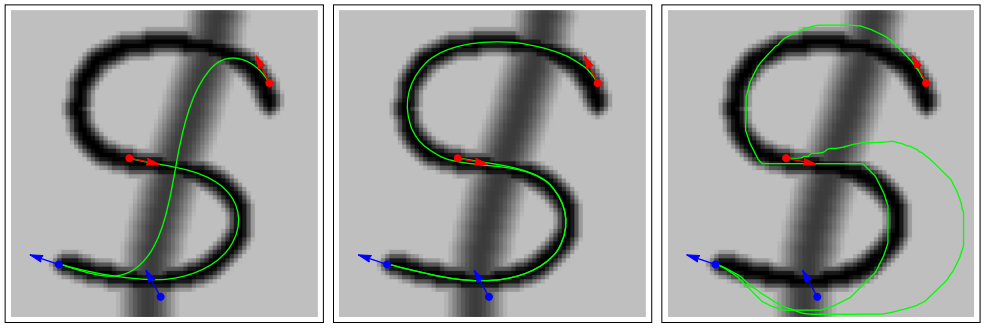

Fig. 11 Tubular segmentation using Euler–Mumford elasticas. Curvature penalization is left: insufficient ($\xi = 0.2$), middle: adequate ($\xi = 0.6$), right: exaggerate ($\xi = 1.5$). CPU time ≈ 1.2 s

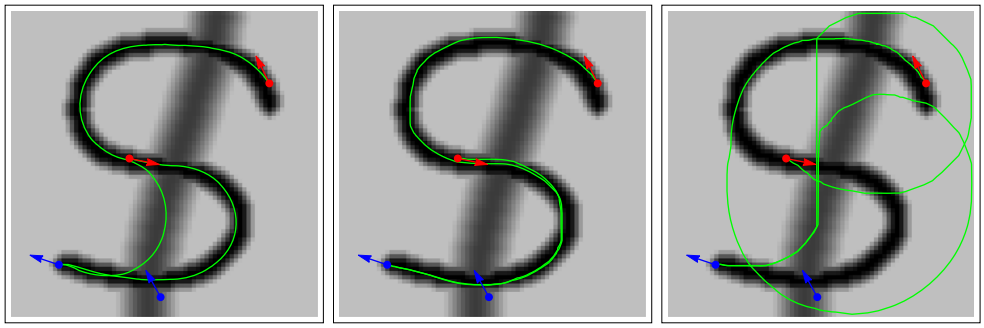

Fig. 12 Tubular segmentation using the Dubins model. Curvature penalization is left: insufficient ($\xi = 0.2$), middle: adequate ($\xi = 0.35$), right: exaggerate ($\xi = 0.5$). CPU time ≈ 0.5 s

address a difficult test case, but to emphasize the qualitative differences between the four implemented path models.

The orientation lifted image domain $\overline{\Omega} = [0, 1]^2 \times \mathbb{S}^1$, is discretized on a $73^2 \times 60$ grid, so that computation times remain within $\approx 1s$. Note that the $\mathcal{O}(N \ln N)$ time complexity and $\mathcal{O}(N)$ space complexity of the proposed numerical method makes it suitable for larger problems as well. The cost function $\alpha = \alpha(\mathbf{x})$, shown in grayscale in Figs. 10, 11 and 12, is set to $\alpha \approx 1/4$ in the neighborhood of the S shaped tubular structure, $\alpha = 1/3$ close to the straight one, and $\alpha = 1$ elsewhere. The HJB PDE (8) is numerically solved, with $u = 0$ at two seed points shown in blue in Fig. 10, and with outflow boundary conditions on $\partial\Omega$. Note that by point we do mean an element of $\mathbb{M} = \mathbb{R}^2 \times \mathbb{S}^1$, displayed as an arrow on the figures. Minimal paths from two points, shown in red, are backtracked. The experiment is called a success if these paths do follow the S tubular structure, and end in the leftmost blue point.

The Reeds–Shepp reversible model fails this test, because the minimal paths shift into reverse gear and thus end at the incorrect blue point. The Reeds–Shepp forward model performs slightly better, ending at the correct endpoint, and correctly extracting the bottom part of the S structure for the larger value of ξ. However, the top part of the S structure is not correctly extracted, because the minimal path intended to do so takes a shortcut through the second straight structure, due to its ability to perform in-place rotations. (Again, let us emphasize that the Reeds–Shepp models can be perfectly suitable for tubular structure segmentation, when contrary to this experiment an orientation dependent cost function $\alpha = \alpha(\mathbf{x}, \theta)$ is provided, see [21].)

The Euler–Mumford model is able to extract the S shaped tubular structure for a large range of parameters ξ, from 0.55 to 1.25. Excessively small values of ξ allow tight turns and therefore shortcuts through the intersecting structure. (Recall that ξ should be interpreted as a radius of curvature) Excessively large values of ξ make it too costly to follow the S structure, and hence the path takes wider turns in the background of the image. We regard the Euler–Mumford model as the best choice among those considered here for image segmentation tasks, in view of our numerical experiments and of the literature [16,39].

The Dubins model is also able to extract the S shaped tubular structure, but for a narrower range of parameters ξ than in the Euler–Mumford case, from 0.25 to 0.38. Excessively small or excessively large choices of ξ lead to symptoms, respectively, shortcuts and excursions in the image background, similar to those observed in the Euler–Mumford case. We expect the Dubins model to be less efficient than the Euler–Mumford model in practical image segmentation tasks, since it requires a finer tuning of the parameter ξ, matching the curvature of the extracted structures.

6 Conclusion

In this paper, we introduced numerical PDE methods for solving a family of non-holonomic optimal control problems, associated with the Reeds–Shepp (reversible or forward only), Euler–Mumford and Dubins models. The design and analysis of these methods uses tools from different branches of mathematics, including (I) an original reformulation of the Euler–Mumford Hamiltonian, (II) a convergence analysis in the setting of discontinuous viscosity solutions to HJB PDEs, and (III) a finite differences scheme based on lattice geometry. The discretized PDEs are solved in a single pass via the dynamic programming principle, which guarantees fast computation times. Synthetic test cases illustrate the potential of our methods in motion planning and image segmentation and can be reproduced using free and open source codes.

Future works include (i) computing three-dimensional[9] Euler–Mumford and Dubins minimal paths, by solving PDEs on $\mathbb{R}^3 \times \mathbb{S}^2$, and addressing other instances of non-holonomic optimal control problems, (ii) implementing GPU accelerations of the solver, in the spirit of [55], (iii) designing mesh-based, instead of cartesian grid based, discretizations of the HJB PDEs considered in this paper, and (iv) developing practical applications of our globally optimal, curvature penalized minimal paths.

Acknowledgements The author thanks Da-Chen(Post-Doctoral researcher at University Paris-Dauphine.), Jorg Portegies(Ph.D. student under the direction of R. Duits at TU/e University, Eindhoven.) and Erik Bekkers(Post-Doctoral researcher at TU/e University, Eindhoven.), for careful testing, bug-fixing, and feedback on the numerical codes.

Appendix A: Local Validation of the Numerical Scheme, via the Control Sets

We present a local validation of our PDE discretization procedure, by comparing the model control sets (4), see also Fig. 2, with some numerical counterparts.

Consider a compact and convex set $\mathcal{B} \subseteq \mathbb{E} = \mathbb{R}^3$, containing the origin, and the corresponding Hamiltonian $\mathcal{H}$. Contrary to the rest of this paper, the possible dependency of $\mathcal{B}$ and $\mathcal{H}$ on some underlying base point $\mathbf{p} \in \mathbb{M}$ is not considered, since the discussion is purely local. Let also H be an approximation of $\mathcal{H}$, for instance of the form (15). Consider the set

$$B := \{\dot{\mathbf{p}} \in \mathbb{E};\ \forall \hat{\mathbf{p}} \in \mathbb{E}^*,\ H(\hat{\mathbf{p}}) \leq 1/2 \Rightarrow \langle \hat{\mathbf{p}}, \dot{\mathbf{p}} \rangle \leq 1\}, \quad (63)$$

and note that $B = \mathcal{B}$ if $H = \mathcal{H}$. We regard the closeness of B and $\mathcal{B}$, inspected visually, as a good witness of the closeness of H and $\mathcal{H}$.

In Fig. 13, left, is illustrated the case where $\mathcal{B}$ is an ellipsoid, with principal axes of length $(1, 0.1, 0.1)$. In that case $\mathcal{H}$ is a quadratic function, and the discrete representation using Corollary 4.13 is exact. One therefore has $H = \mathcal{H}$, thus $B = \mathcal{B}$ as can be observed. This particular case is at the foundation of [36].

In Fig. 13, right, is illustrated the case where $\mathcal{B} = [0, \dot{\mathbf{n}}]$ is a segment, where $\dot{\mathbf{n}} \in \mathbb{E}$ is a unit vector, and therefore $\mathcal{H}(\hat{\mathbf{p}}) = \frac{1}{2}\langle \hat{\mathbf{p}}, \dot{\mathbf{n}} \rangle_+^2$. The discretization is performed using Proposition 2.2 with $\varepsilon = 0.1$, via the basis reduction techniques presented in Sect. 4. As can be observed, the vectors $\dot{\mathbf{e}}_k$, $1 \leq k \leq K$, are almost aligned with $\dot{\mathbf{n}}$, and the set B is close to the segment $\mathcal{B}$ in the Hausdorff distance, although slightly fatter.

Figure 14 is devoted to the models of interest in this paper. The parameters are $\xi = 0.2$ [appearing in the curvature cost (2)], $\theta = \pi/3$ (the current orientation), and $\varepsilon = 0.1$ (tolerance in Proposition 2.2). The offsets $\dot{\mathbf{e}}_k$, $1 \leq k \leq K$, are illustrated in Fig. 4 page 7. Comparing with Fig. 2, we can confirm that the sets B are close to the corresponding ellipse,[10] half ellipse, non-centered ellipse, and triangle $\mathcal{B}$, respectively. However the true control sets $\mathcal{B}$ are flat, with Haussdorff dimension 2, whereas their counterparts B are slightly fatter.

[9] The three-dimensional Reeds–Shepp model is already addressed here and in [21].

[10] The choice $\xi = 1$ in Fig. 2, versus $\xi = 0.2$ in Fig. 14, yields a round disk instead of an ellipse.

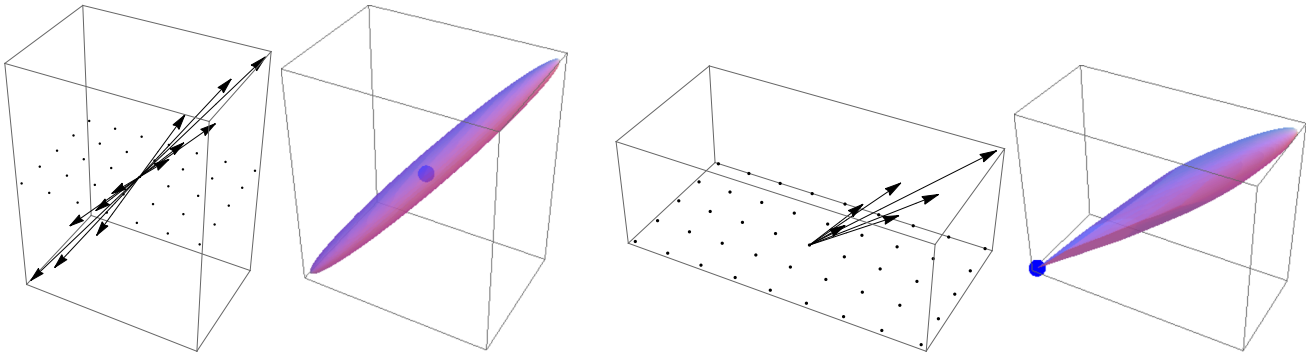

Fig. 13 Illustration of Appendix A. Left: Discretization stencil for a quadratic anisotropic Hamiltonian. The Hamiltonian and control set representation are exact. Right: Discretization stencil of Proposition 2.2, for a Hamiltonian $\mathcal{H}(\hat{\mathbf{p}}) = \frac{1}{2}\langle \hat{\mathbf{p}}, \dot{\mathbf{n}} \rangle_+^2$. The approximate control set (63) is close to the segment $[0, \dot{\mathbf{n}}]$, but slightly fatter

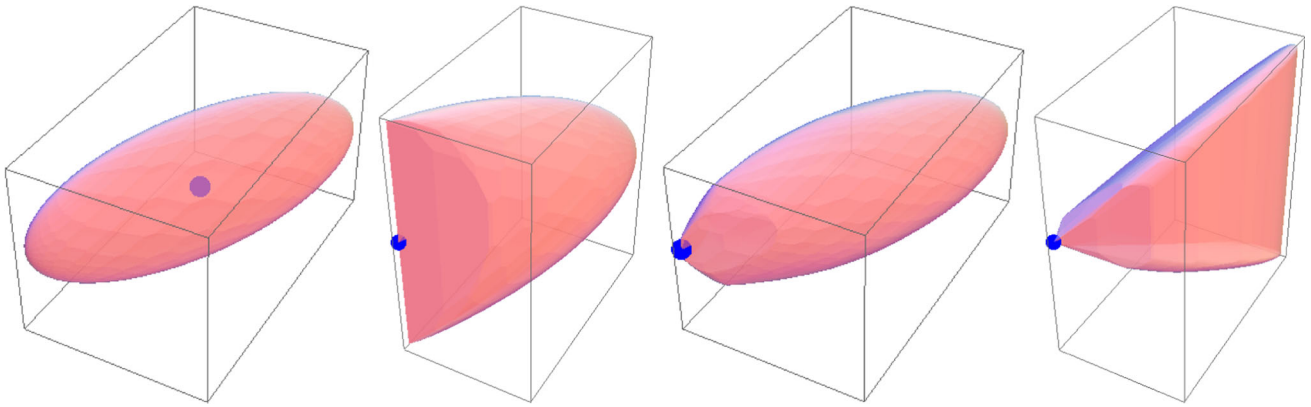

Fig. 14 Approximate control set (63) for the Reeds–Shepp reversible, Reeds–Shepp forward, Euler–Mumford and Dubins models. The shapes of the original control sets, see Fig. 2, are recognizable, elongated due to the model parameter choice $\xi = 0.2$, and slightly fatter due to the effect of discretization, with relaxation parameter $\varepsilon = 0.1$. Orientation $\theta = \pi/3$. Seed Fig. 3 for the corresponding stencils

Appendix B: Convexity of the Metric

We prove in this appendix that the metrics $\mathcal{F}_{\mathbf{p}}^{\mathrm{RS}+}, \mathcal{F}_{\mathbf{p}}^{\mathrm{EM}}, \mathcal{F}_{\mathbf{p}}^{\mathrm{D}} : \mathbb{E} \to [0, \infty]$ are convex, for any fixed $\mathbf{p} \in \Omega$, due to their construction (3) and to the following two results.

Lemma B.1 *Let $\mathcal{C} : \mathbb{R} \to [1, \infty]$ be convex and lower semi-continuous, and let $f :]0, \infty[\times \mathbb{R} \to [0, \infty]$ be defined by $f(n, t) := n\mathcal{C}(t/n)$.*

Then, f is lower semi-continuous, 1-positively homogeneous, everywhere positive, and obeys the triangular inequality.

Proof Lower semi-continuity, homogeneity and positivity are obvious. In addition for any $(n, t), (n', t') \in]0, \infty[\times \mathbb{R}$, one obtains

$$\begin{aligned} \frac{f(n+n', t+t')}{n+n'} &= \mathcal{C}\left(\frac{t}{n}\frac{n}{n+n'} + \frac{t'}{n'}\frac{n'}{n+n}\right) \\ &\leq \frac{n}{n+n'}\mathcal{C}\left(\frac{t}{n}\right) \\ &\quad + \frac{n'}{n+n'}\mathcal{C}\left(\frac{t'}{n'}\right) = \frac{f(n,t) + f(n',t')}{n+n'}. \end{aligned}$$

□

Note that 1-positive homogeneity and the triangular inequality together imply convexity. We recall the notation $\mathbb{E} := \mathbb{R}^2 \times \mathbb{R}$, used in the next result.

Corollary B.2 *Let $\mathcal{C} : \mathbb{R} \to [1, \infty]$ be convex, lower semi-continuous, and such that $l(\varepsilon) := \lim \mathcal{C}(\varepsilon t)/t$ as $t \to \infty$ exists and belongs to $]0, \infty]$, for each $\varepsilon \in \{-1, 1\}$. Let F :*

$\mathbb{E} \to [0, \infty]$ *be defined as* $F(\dot{\mathbf{x}}, \dot{\theta}) := \|\dot{\mathbf{x}}\| \mathcal{C}(\dot{\theta}/\|\dot{\mathbf{x}}\|)$ *for each* $(\dot{\mathbf{x}}, \dot{\theta}) \in \mathbb{E}$ *such that* $\dot{\mathbf{x}} = \|\dot{\mathbf{x}}\|\mathbf{n}$ *and* $\|\dot{\mathbf{x}}\| > 0$*, where* $\mathbf{n} \in \mathbb{S}^{d-1}$ *is a fixed direction. Let also* $F(0, 0) = 0$*,* $F(0, \dot{\theta}) = |\dot{\theta}| l(\dot{\theta}/|\dot{\theta}|)$ *if* $\dot{\theta} \neq 0$*, and* $F(\dot{\mathbf{x}}, \dot{\theta}) := +\infty$ *otherwise. Then,* F *is lower semi-continuous and obeys*

- (1-*positive homogeneity*) $F(\lambda \dot{\mathbf{p}}) = \lambda F(\dot{\mathbf{p}})$*, for all* $\lambda > 0$ *and all* $\dot{\mathbf{p}} \in \mathbb{E}$*.*
- (*Separation*) $F(\dot{\mathbf{p}}) = 0$ *iff* $\dot{\mathbf{p}} = 0$*, for all* $\dot{\mathbf{p}} \in \mathbb{E}$*.*
- (*Triangular inequality*) $F(\dot{\mathbf{p}} + \dot{\mathbf{q}}) \leq F(\dot{\mathbf{p}}) + F(\dot{\mathbf{q}})$*, for all* $\dot{\mathbf{p}}, \dot{\mathbf{q}} \in \mathbb{E}$*.*

Proof By the previous lemma, F obeys the announced properties on the convex set $(]0, \infty[\mathbf{n}) \times \mathbb{R}$. These properties are also satisfied on the closure $([0, \infty[\mathbf{n}) \times \mathbb{R}$ since, clearly, F is extended to it by its lower continuous envelope, and since the limits $l(1)$ and $l(-1)$ are positive (for separation). Finally, the announced properties hold for the trivial extension of F to $\mathbb{R}^2 \times \mathbb{R}$ by $+\infty$ since the subset $([0, \infty[\mathbf{n}) \times \mathbb{R}$ is closed and convex. □

References

1. Benmansour, F., Cohen, L.D.: Tubular structure segmentation based on minimal path method and anisotropic enhancement. Int. J. Comput. Vision **92**(2), 192–210 (2010)
2. Bardi, M., Capuzzo-Dolcetta, I.: Optimal Control and Viscosity Solutions of Hamilton–Jacobi–Bellman Equations. Springer, Berlin (2008)
3. Boissonnat, J.-D., Cérézo, A., Leblond, J.: Shortest paths of bounded curvature in the plane. J. Intell. Robot. Syst. **11**(1–2), 5–20 (1994)
4. Benamou, J.-D., Collino, F., Mirebeau, J.-M.: Monotone and consistent discretization of the Monge–Ampere operator. Math. Comput. **85**(302), 2743–2775 (2016)
5. Benmansour, F., Carlier, G., Peyré, G., Santambrogio, F.: Derivatives with respect to metrics and applications: subgradient marching algorithm. Numer. Math. **116**(3), 357–381 (2010)
6. Bekkers, E.J., Duits, R., Mashtakov, A., Sanguinetti, G.R.: A PDE approach to data-driven sub-Riemannian geodesics in SE (2). SIAM J. Imaging Sci. **8**(4), 2740–2770 (2015)
7. Boscain, U., Duits, R., Rossi, F., Sachkov, Y.: Curve cuspless reconstruction via sub-Riemannian geometry. ESAIM: Control Optim. Calc. Var. **20**(3), 748–770 (2014)
8. Bardi, M., Evans, L.C.: On Hopf's formulas for solutions of Hamilton–Jacobi equations. Nonlinear Anal. Theory Methods Appl. Int. Multidiscip. J. Ser. A Theory Methods **8**(11), 1373–1381 (1984)
9. Bost, J.-B., Künnemann, K.: Hermitian vector bundles and extension groups on arithmetic schemes. I. Geometry of numbers. Adv. Math. **223**(3), 987–1106 (2010)
10. Bonnans, J.F., Ottenwaelter, E., Zidani, H.: A fast algorithm for the two dimensional HJB equation of stochastic control. ESAIM Math. Model. Numer. Anal. **38**(4), 723–735 (2004)
11. Bornemann, F., Rasch, C.: Finite-element discretization of static Hamilton–Jacobi equations based on a local variational principle. Comput. Vis. Sci. **9**(2), 57–69 (2006)
12. Cohen, L.D., Kimmel, R.: Global minimum for active contour models: a minimal path approach. Int. J. Comput. Vis. **24**(1), 57–78 (1997)
13. Chen, D., Mirebeau, J.-M., Cohen, L.D.: Global minimum for curvature penalized minimal path method. In: Xie, X., Jones, M.W., Tam, G.K.L. (eds.) Proceedings of the British Machine Vision Conference (BMVC), pp. 86.1–86.12. BMVA Press (2015)
14. Chen, D., Mirebeau, J.-M., Cohen, L.D.: A new finsler minimal path model with curvature penalization for image segmentation and closed contour detection. In: Computer Vision and Pattern Recognition (CVPR), pp. 355–363 (2016)
15. Chen, D., Mirebeau, J.-M., Cohen, L.D.: Finsler Geodesics Evolution Model for Region based Active Contours. In Wilson, R.C., Hancock, E.R., Smith, W.A.P. (eds.) Proceedings of the British Machine Vision Conference (BMVC), pp. 22.1–22.12. BMVA Press (2016)
16. Chen, D., Mirebeau, J.-M., Cohen, L.D.: Global minimum for a finsler elastica minimal path approach. Int. J. Comput. Vis. **122**(3), 458–483 (2017)
17. Conway, J.H., Sloane, N.J.A.: Low-dimensional lattices. VI. Voronoi reduction of three-dimensional lattices. Proc. R. Soc. A Math. Phys. Eng. Sci. **436**(1896), 55–68 (1992)
18. Campbell, J.S.W., Siddiqi, K., Rymar, V.V., Sadikot, A.F., Pike, G.B.: Flow-based fiber tracking with diffusion tensor and q-ball data: validation and comparison to principal diffusion direction techniques. NeuroImage **27**(4), 725–736 (2005)
19. Chan, T.F., Vese, L.A.: Active contours without edges. IEEE Trans. Image Process. **10**(2), 266–277 (2001)
20. Duits, R., Boscain, U., Rossi, F., Sachkov, Y.: Association fields via cuspless sub-Riemannian geodesics in SE(2). J. Math. Imaging Vis. **49**(2), 384–417 (2013)
21. Duits, R., Meesters, S.P.L., Mirebeau, J.-M., Portegies, J.M.: Optimal Paths for Variants of the 2D and 3D Reeds–Shepp Car with Applications in Image Analysis (2016). arXiv:1612.06137
22. Dubins, L.E.: On curves of minimal length with a constraint on average curvature, and with prescribed initial and terminal positions and tangents. Am. J. Math. **79**, 497–516 (1957)
23. Euler, L.: Methodus inveniendi Lineas curvas maximi minive proprietate gaudentes. Lausanne: Bousquet (1744)
24. Fuster, A., Haije, T.D., Tristán-Vega, A., Plantinga, B., Westin, C.-F., Florack, L.: Adjugate diffusion tensors for geodesic tractography in white matter. J. Math. Imaging Vis. **54**(1), 1–14 (2016)
25. Féjer, L.: On the infinite sequences arising in the theories of harmonic analysis, of interpolation, and of mechanical quadratures. Bull. Am. Math. Soc. **39**(8), 521–534 (1933)
26. Fehrenbach, J., Mirebeau, J.-M.: Sparse non-negative stencils for anisotropic diffusion. J. Math. Imaging Vis. **49**(1), 123–147 (2014)
27. Jbabdi, S., Bellec, P., Toro, R., Daunizeau, J., Pélégrini-Issac, M., Benali, H.: Accurate anisotropic fast marching for diffusion-based geodesic tractography. J. Biomed. Imaging **2008**(1–2), 2–12 (2008)
28. Kimmel, R., Kiryati, N., Bruckstein, A.M.: Multivalued distance maps for motion planning on surfaces with moving obstacles. IEEE Trans. Robot. Autom. **14**(3), 427–436 (1998)
29. Kass, M., Witkin, A., Terzopoulos, D.: Snakes: active contour models. Int. J. Comput. Vis. **1**(4), 321–331 (1988)
30. Liao, W., Rohr, K., Wörz, S.: Globally optimal curvature-regularized fast marching for vessel segmentation. In: Medical Image Computing and Computer-Assisted Intervention-MICCAI 2013. Springer, Berlin, Heidelberg, pp. 550–557 (2013)
31. Li, H., Yezzi, A.: Vessels as 4-D curves: global minimal 4-D paths to extract 3-D tubular surfaces and centerlines. IEEE Trans. Med. Imaging **26**(9), 1213–1223 (2007)
32. Mirebeau, J.-M., Dreo, J.: Automatic differentiation of non-holonomic fast marching for computing most threatening trajectories under sensors surveillance. In: Nielsen, F., Barbaresco, F.

(eds.) Proceedings of Third International Conference on Geometric Science of Information (GSI). Paris, France (2017)
33. Mirebeau, J.-M.: Anisotropic fast-marching on cartesian grids using lattice basis reduction. SIAM J. Numer. Anal. **52**(4), 1573–1599 (2014)
34. Mirebeau, J.-M.: Efficient fast marching with Finsler metrics. Numer. Math. **126**(3), 515–557 (2014)
35. Mirebeau, J.-M.: Minimal stencils for discretizations of anisotropic PDEs preserving causality or the maximum principle. SIAM J. Numer. Anal. **54**(3), 1582–1611 (2016)
36. Mirebeau, J.-M.: Anisotropic fast-marching on cartesian grids using Voronoi's first reduction of quadratic forms. HAL (Preprint), April (2017)
37. Montgomery, R.: A Tour of Subriemannian Geometries, Their Geodesics and Applications. American Mathematical Soc, Providence (2006)
38. Melonakos, J., Pichon, E., Angenent, S., Tannenbaum, A.: Finsler active contours. IEEE Trans. Pattern Anal. Mach. Intell. **30**(3), 412–423 (2008)
39. Mumford, D.: Elastica and computer vision. In: Bajaj, C.L. (ed.) Algebraic Geometry and its Applications, pp. 491–506. Springer, Berlin (1994)
40. Nguyen, P.Q., Stehlé, D.: Low-dimensional lattice basis reduction revisited. In: Buell, D. (ed.) ANTS, pp. 338–357. Springer, Berlin (2004)
41. Oberman, A.M.: Convergent difference schemes for degenerate elliptic and parabolic equations: Hamilton–Jacobi equations and free boundary problems. SIAM J. Numer. Anal. **44**(2), 879–895 (2006)
42. Pechaud, M., Keriven, R., Peyré, G.: Extraction of tubular structures over an orientation domain. In: 2009 IEEE Computer Society Conference on Computer Vision and Pattern Recognition Workshops (CVPR Workshops), pp. 336–342. IEEE (2009)
43. Peyré, G., Pechaud, M., Keriven, R.: Geodesic methods in computer vision and graphics. Found. Trends® Comput. Graph. Vis. **5**(3–4), 197–397 (2010)
44. Parker, G.J.M., Wheeler-Kingshott, C.A.M., Barker, G.J.: Estimating distributed anatomical connectivity using fast marching methods and diffusion tensor imaging. IEEE Trans. Med. Imaging **21**(5), 505–512 (2002)
45. Randers, G.: On an asymmetrical metric in the four-space of general relativity. Phys. Rev. **59**(2), 195–199 (1941)
46. Reeds, J.A., Shepp, L.A.: Optimal paths for a car that goes both forwards and backwards. Pac. J. Math. **145**(2), 367–393 (1990)
47. Rouy, E., Tourin, A.: A viscosity solutions approach to shape-from-shading. SIAM J. Numer. Anal. **29**(3), 867–884 (1992)
48. Sachkov, Y.L.: Cut locus and optimal synthesis in the sub-Riemannian problem on the group of motions of a plane. ESAIM Control Optim. Calc. Var. **17**(2), 293–321 (2011)
49. Sanguinetti, G., Bekkers, E., Duits, R., Janssen, M.H.J., Mashtakov, A., Mirebeau, J.-M.: Sub-Riemannian fast marching in SE (2). In: Pardo, A., Kittler, J. (eds.) Iberoamerican Congress on Pattern Recognition, pp. 366–374. Springer, Cham (2015)
50. Schürmann, A.: Computational geometry of positive definite quadratic forms. Polyhedral reduction theories, algorithms, and applications. In: University Lecture Series, vol. 48, pp. xvi+162. American Mathematical Society, Providence, RI (2009)
51. Selling, E.: Ueber die binären und ternären quadratischen Formen. J. Reine Angew. Math. **77**, 143–229 (1874)
52. Schober, M., Kasenburg, N., Feragen, A., Hennig, P., Hauberg, S.: Probabilistic shortest path tractography in DTI using gaussian process ode solvers. In: Medical image computing and computer-assisted intervention—MICCAI 2014, pp. 265–272. Springer, Cham, September (2014)
53. Strandmark, P., Ulen, J., Kahl, F., Grady, L.: Shortest paths with curvature and torsion. In: 2013 IEEE International Conference on Computer Vision (ICCV), pp. 2024–2031. IEEE (2013)
54. Tsitsiklis, J.N.: Efficient algorithms for globally optimal trajectories. IEEE Trans. Autom. Control **40**(9), 1528–1538 (1995)
55. Weber, O., Devir, Y.S., Bronstein, A.M., Bronstein, M.M., Kimmel, R.: Parallel algorithms for approximation of distance maps on parametric surfaces. ACM Trans. Graph.: TOG **27**(4), 104–116 (2008)
56. Zach, C., Shan, L., Niethammer, M.: Globally optimal finsler active contours. In: Hutchison, D., Kanade, T., Kittler, J., Kleinberg, J.M., Mattern, F., Mitchell, J.C., Naor, M., Nierstrasz, O., Rangan, C.P., Steffen, B., Sudan, M., Terzopoulos, D., Tygar, D., Vardi, M.Y., Weikum, G., Denzler, J., Notni, G., Süße, H. (eds) DAGM-Symposium, pp. 552–561. Springer, Berlin (2009)

Jean-Marie Mirebeau is a researcher in applied mathematics from the French CNRS (National Center for Scientific Research), working in Department of Mathematics of University Paris-Sud, University Paris-Saclay. His main subject of research is the numerical analysis of PDEs, focusing on difficulties related to strong anisotropies, which are addressed using tools from discrete geometry. He also studies PDE-based image analysis, and distributes open source numerical codes of his work. He defended his Ph.D. at University Pierre et Marie Curie in 2010, prepared under the supervision of Pr Albert Cohen, and is a former student of the Ecole Normale Supérieure of Paris. Jean-Marie Marie Mirebeau received in 2016 the 9th Popov prize, which is an international prize awarded every three years for contributions in approximation theory.